Tampere University

Joonas Kuisma

SCALING PROPERTIES OF HEART RATE VARIABILITY IN ASSESSMENT OF ATHLETIC PERFORMANCE

Master of Science Thesis
Faculty of Engineering and Natural Sciences
Examiners: Esa Räsänen
Antti Vehkaoja
November 2023

ABSTRACT

Joonas Kuisma: Scaling properties of heart rate variability in assessment of athletic performance
Master of Science Thesis
Tampere University
Science and Engineering, MSc
November 2023

In sports physiology, the key concepts of aerobic and anaerobic threshold are necessary to assess an athlete's performance and individual exercise strain, as well as to optimize the training load. Traditionally, these thresholds for a three-zone exercise model are determined either by invasive blood lactate samples taken from the fingertip or by monitoring changes in respiratory gas variables in laboratory conditions. A combination of these methods is also possible. The development of computational methods and the proliferation of electronics available to consumers, such as sports watches and heart rate monitors, creates an interesting alternative to these traditional threshold determination methods.

It has long been known that heart rate variability (HRV), i.e. the time between successive beats of the heart, varies in a complex way. In this thesis, a recently developed method, dynamical detrended fluctuation analysis (DDFA) is used to analyze HRV. This method examines the dependence of correlations in a time series as functions of scale and time. The thesis studies and compares the scalability results provided by DDFA with the thresholds measured using conventional methods including lactate and ventilation measurements. In addition, the effect of raw data filtering on the operation of the DDFA method is tested. The aim of this thesis is to demonstrate the qualitative link between HRV and thresholds.

The material for the experimental part of the thesis consists of 15 direct tests of maximum oxygen uptake on bicycle ergometers and 9 tests on a treadmill. The tests were carried out under laboratory conditions, in which both respiratory gas variables and blood lactate concentrations were used to determine individual thresholds for each volunteer subject. The intervals between consecutive heartbeats (RR intervals, RRIs) during the test were also recorded and this RRI time series was analyzed using the DDFA.

As indicated by previous studies, the results show clear changes in HRV during exercise. Despite individual differences, these changes are systematic, allowing them to be utilized in the assessment of thresholds as well. In addition, adequate filtering of data prior to the calculation of DDFA is shown to be necessary. On the other hand, even excessive filtering does not significantly reduce the quality of the results. In conclusion, it is possible to use the results of DDFA to define predictions of thresholds without tedious lactate measurements and/or gas tests. Forecasts and indicators will be developed in further research.

Keywords: computational analysis, heart rate variability, dynamical detrended fluctuation analysis, exercise physiology, metabolic thresholds

TIIVISTELMÄ

Joonas Kuisma: Sykevälivaihtelun skaalautuvuus urheilijan suorituskyvyn arvionnissa
Diplomityö
Tampereen yliopisto
Teknis-luonnontieteellinen, DI
Marraskuu 2023

Urheilufysiologiassa keskeiset käsitteet aerobinen ja anaerobinen kynnys ovat tarpeen urheilijan suorituskyvyn ja yksittäisen harjoituksen rasittavuuden arvioinnissa sekä harjoituskuorman optimoinnissa. Perinteisesti nämä kolmiportaisen harjoittelumallin kynnykset määritetään joko invasiivisesti sormenpäästä otetuista veren laktaattinäytteistä tai laboratorio-olosuhteissa hengityskaasujen pitoisuuksissa tapahtuvia muutoksia seuraamalla. Myös näiden menetelmien yhdistelmä on mahdollinen. Laskennallisten menetelmien kehittyminen sekä kuluttajien saatavilla olevan elektroniikan, kuten urheilukellojen ja sykemittareiden, yleistyminen luo mielenkiintoisen vaihtoehdon näille perinteisille kynnysten määritysmenetelmille.

Jo pitkään on ollut ollut tiedossa, että sykevälivaihtelu (HRV, Heart Rate Variability) eli sydämen peräkkäisten lyöntien välinen aika vaihtelee monimutkaisella tavalla. Tässä työssä HRV:n analysoinnissa käytetään tuoretta dynaamista trendit poistavaa fluktuaatioanalyysia (DDFA, Dynamical Detrended Fluctuation Analysis). Kyseisellä menetelmällä tutkitaan aikasarjassa esiintyvien korrelaatioiden riippuvuutta ajan ja skaalan eli mittakaavan funktiona. Työssä tarkastellaan ja vertaillaan DDFA:n antamia skaalautuvuustuloksia suhteessa perinteisillä menetelmillä mitattuihin kynnysarvoihin. Lisäksi testataan sykevälidatan suodatuksen vaikutusta DDFA-menetelmän toimintaan. Tämän opinnäytetyön tavoitteena on osoittaa HRV:n ja kynnysarvojen välinen laadullinen yhteys.

Työn kokeellisen osuuden aineisto koostuu 15:sta polkupyöräergometrillä sekä 9:stä juoksumatolla laboratorio-olosuhteissa tehdystä suorasta maksimaalisen hapenottokyvyn testistä. Testit tehtiin labaratorio-olosuhteissa, joissa sekä hengityskaasumuuttujien että veren laktaattipitoisuuksien avulla määritettiin jokaiselle vapaaehtoiselle koehenkilölle yksilölliset kynnysarvot. Myös testin aikainen sykevälidata (RRIs, RR intervals) tallennettiin ja tätä RRI-aikasarjaa analysoitiin DDFA-menetelmällä.

Tuloksissa havaitaan aikaisempien tutkimusten mukaiset selkeät rasituksenaikaiset muutokset sykevälivaihtelussa. Yksilöllisistä eroista huolimatta nämä muutokset ovat systemaattisia, mikä mahdollistaa niiden hyödyntämisen myös kynnysten arvionnissa. Lisäksi datan riittävän suodattamisen ennen DDFA:n laskentaa osoitetaan olevan välttämätöntä, Toisaalta liiallinenkaan suodattaminen ei merkittävästi heikennä tulosten laatua. Johtopäätöksenä todetaan, että DDFA:n tulosten avulla on mahdollista määritellä ennusteita kynnysarvoista ilman vaivalloisia laktaattimittauksia ja/tai kaasutestejä. Ennusteita ja mittareita kehitetään jatkotutkimuksessa.

Avainsanat: laskennallinen analyysi, sykevälivaihtelu, dynaaminen trendit poistava fluktuaatioanalyysi, liikuntafysiologia, metaboliset kynnykset

PREFACE

Once again, it was great to get into the wonderful world of heart rate variability and sports physiology. As you can see, the topic of this thesis is almost a direct continuation of my bachelor's thesis [1], but the writing language changed from Finnish to English. While in my bachelor's thesis I mainly familiarized myself with the subject matter and methods, this time I was able to deepen my knowledge and do actual research. Along the way, especially when coding with Python and visualizing data, important skills developed that are sure to be of use later in working life. For an active and passionate endurance athlete, the subject of the thesis was again excellent, as I was able to connect the know-how accumulated in studies with the sports world in a very interesting way. It was also great to get involved in writing a scientific article together with the research group [2]. As the title "Estimation of physiological exercise thresholds based on dynamical correlation properties of heart rate variability" might suggest, the same subject matter is discussed.

Even though this thesis is my own individual performance, this would not have been created without the help of other people. Thank you for close relatives and friends who have been supportive in the writing process. Thank you for my employer for the flexibility, which greatly facilitated the writing of this thesis. Special thanks to the Kauppi Sports Coaching Oy and Master of Sport Science Kimmo Lajunen for delivering the data used in this thesis. A great one also to the thesis supervisors, examiners and entire research group for all their help, especially in the calculation and visualization of the results, as well as for their expert advice when writing the thesis. Thank you all for your patience waiting for this long marathon-type project to be completed. Without all of you, this thesis would not have succeeded!

Pirkkala, 19th November 2023

Joonas Kuisma

CONTENTS

LIST OF FIGURES

List of Figures in Appendices is given at the beginning Appendix A and B, respectively.

LIST OF TABLES

LIST OF SYMBOLS AND ABBREVIATIONS

$\langle B \rangle$	arithmetic mean of B
$\lfloor x \rfloor$	floor of x
α	DFA scaling exponent
$B(i)$	interbeat time series
$F(s)$	fluctuation function
$F_s^2(v)$	variance in DFA calculations
H	Hurst exponent
h_+	logarithmic forward difference
h_-	logarithmic backward difference
i	beat index
$\log$	base-10 logarithm
$l(s)$	segment lengths in DDFA calculations
N	order of DDFA
$p_v(k)$	vth segment fitting polynomial in DFA calculations
s	DFA scale
t	time
v	segment in DFA calculations
$y(k)$	integrated time series
$y_s(k)$	values of linear fits in DFA calculations
AeT	aerobic threshold
ANS	autonomic nervous system
AnT	anaerobic threshold
ApEn	approximate entropy
AV	atrioventricular
BLa	blood lactate concentration
BMI	body mass index
BPM	beats per minute

CCS	cardiac conduction system
CPET	cardiopulmonary exercise testing
D_2	correlation dimension
DDFA	dynamical detrended fluctuation analysis
DFA	detrended fluctuation analysis
ECG	electrocardiogram
EDR	ECG-derived respiration frequency
HF	high frequency
HR	heart rate
HR_{max}	maximal heart rate
HR_{min}	minimal heart rate during test
HR_{norm}	normalized heart rate
HR_{rel}	relative heart rate
HRM	heart rate monitor
HRV	heart rate variability
HRVI	HRV triangular index
IQR	inter-quartile range
LF	low frequency
LT	lactate threshold
MLSS	maximal lactate steady state
NN	normal-to-normal
PNS	parasympathetic nervous system
PPG	photoplethysmogram
PRV	pulse rate variability
PSD	power spectral density
RMSSD	square root of the mean squared differences of successive NN intervals
RP	recurrence plot
RRI	RR interval
RSA	respiratory sinus arrhythmia
SA	sinoatrial
SampEn	sample entropy

SDANN	standard deviation of the average NN intervals calculated over the 5-min segments
SDNN	standard deviation of the NN intervals
SNS	sympathetic nervous system
TID	training intensity distribution
TL	training load
VLF	very low frequency
$VO_{2,max}$	maximal oxygen uptake
VO_2	oxygen uptake
VO_2/kg	weight-proportional oxygen uptake
VT	ventilation threshold

1. INTRODUCTION

The human heart is a complex organ that beats continuously throughout a person's lifetime [3]. However, the healthy heart is not a metronome, as the time between successive heartbeats fluctuates in a complex manner, including randomness and short and long-range correlations [4]. This phenomenon is known as heart rate variability (HRV) and it is regulated by the autonomic nervous system (ANS), whose function is to maintain homeostasis [5]. This homeostasis refers to the effort to keep the internal environment of the body stable despite changes in external conditions [6].

Measuring HRV involves analyzing the time between successive heartbeats, that is RR intervals (RRIs) and various methods have been developed to quantify the complexity and variability of RRIs [5]. These measures can provide insights into the activity of the sympathetic (SNS) and parasympathetic (PNS) branches of the ANS, which respectively regulate the "fight or flight" response and the "rest and digest" response. HRV has become an increasingly popular area of research in recent years, as it has been shown to provide valuable information about the health and functioning of the ANS. Various factors, such as stress, exercise, and disease, can affect HRV, making it a useful tool for assessing autonomic function and overall health.

Fractal properties of heart rate (HR) refer to the self-similar or repeating patterns in HRV across different time scales [7]. This means that the fluctuations in heart rate (HR) at shorter time scales are similar to those at longer time scales, and that the pattern repeats itself over time. Fractal analysis of HRV has revealed several important features of this phenomenon. One such feature is the presence of long-range correlations, meaning that changes in HR at one point in time are related to changes at much later points in time. This suggests that the regulation of HR is a highly integrated and coordinated process, involving both short- and long-term feedback mechanisms. Another important feature of fractal HRV is its sensitivity to changes in physiological and psychological states. For example, decreased fractal complexity has been associated with aging, disease, and stress, while increased complexity has been linked to physical fitness and healthy aging.

In this thesis, the analysis of HRV uses a recently developed method, dynamical detrended fluctuation analysis (DDFA). This method examines the dependence of correlations in a time series as functions of time scale and time. The thesis studies and compares the results provided by the DDFA in relation to the thresholds measured using traditional methods including blood lactate concentration (BLa) and ventilation gas variables measurements. For DDFA, no similar research has been done before, but for other HRV methods it has. Especially in recent studies, detrended fluctuation analysis (DFA), on which the DDFA is based, has been used to determine these thresholds. In addition, the effect of raw data filtering on the operation of the DDFA method is tested. The purpose of this thesis is to demonstrate the qualitative connection between HRV and the thresholds and to consider various factors that affect them. The thesis aims to provide a basis for further research and the development of more accurate mathematical models, for example, by studying the effect of filtering on DDFA results.

This thesis is organized as follows. Chapter 2 gives background to physiology of the heart, HRV phenomenon and estimating cardiac load under exercise. This is followed by a more detailed description of the mathematical methods used to analyse HRV in Ch. 3. Chapter 4 focuses on describing the dataset and pre-prosessing used in this thesis. In Ch. 5 the calculated results are presented and described. Finally, Ch. 6 summarizes the thesis by briefly discussing the results and providing further prospects and opportunities.

2. CARDIAC ACTIVITY

This chapter describes the physiology of the heart and thus opens the background for understanding HRV. It is complicated phenomenon and there are multiple factors affecting it as will be discussed in Sec. 2.2. Especially for a endurance athlete, the heart is subjected to heavy stress and load during exercises and competitions. Section 2.3 explains how HR and HRV are used to estimate the amount of cardiac load. In addition, from the point of view of sport physiology, it considers the optimal training strategy. Thus, to maximise sport performance, it justifies the importance of measurement of body's biosignals.

2.1 Anatomy and physiology of the heart

The heart is a muscular organ responsible for pumping blood throughout the body via circulatory system. It is located in the chest and is about the size of a closed fist. This organ beats continuously, approximately 100 000 times each day [3]. The heart is made up of four chambers: the right atrium, right ventricle, left atrium, and left ventricle. The right atrium receives deoxygenated blood from the body and pumps it to the right ventricle. The right ventricle then pumps the blood to the lungs, where it receives oxygen and gets rid of carbon dioxide. The oxygenated blood then returns to the heart's left atrium, which pumps it to the left ventricle. The left ventricle then pumps the oxygenated blood to the rest of the body via the aorta. Since the heart is a organ, so like all other organs and cells in the body, it also needs oxygen, nutrients and a way of removing metabolic wastes to maintain its function. Coronary circulation on the surface of the heart is responsible for this.

The heart also has valves that prevent blood from flowing back into the chambers it has already left. The atriovencticular valves, which one is known as tricuspid valve, separates the right atrium from the right ventricle, and the second one know as mitral valve separates the left atrium from the left ventricle. The semilunar valves such as pulmonary valve and aortic valve separates the right ventricle from the pulmonary artery and the left ventricle from the aorta respectively. The anatomical structure of the heart and the main components are shown in Fig. 2.1.

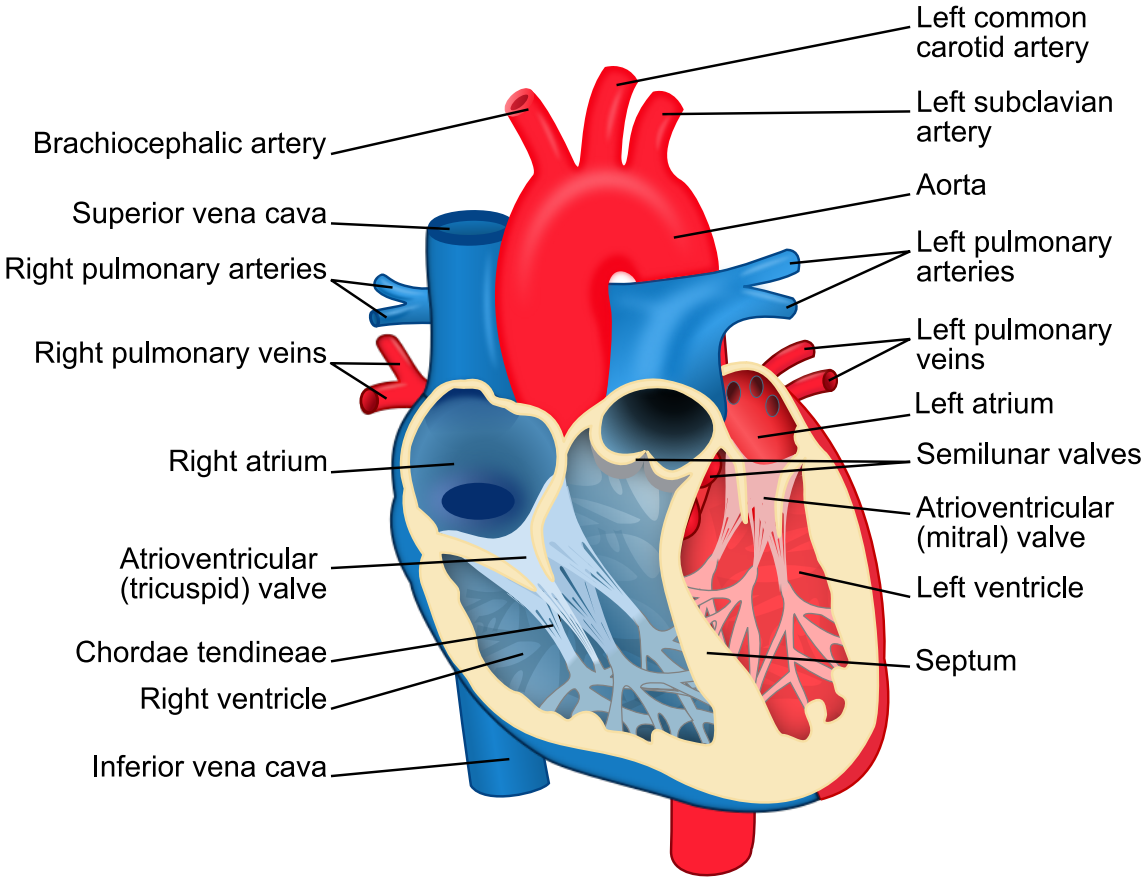

Figure 2.1. *Heart diagram with its main components. Blue components indicate deoxygenated blood pathways and red components indicate oxygenated blood pathways. Figure adopted from Ref. [8].*

The coordinated contraction and relaxation of the heart's chambers are essential for maintaining adequate blood flow and delivering oxygen and nutrients to the body's tissues. The rotation of these contraction and relaxation periods, called as systole and diastole respectively, is referred as the cardiac cycle. This cycle correlates with an electrical signal measured on the skin surface via an electrocardiography. Thus obtained electrocardiogram (ECG) describes voltage as a function of time. A healthy human ECG curve consists of different waves designated in alphabetical order starting from P. The P wave represents the electrical activity that causes the atria to contract and pump blood into the ventricles, i.e. atrial systole. The QRS complex, which consist of three waves or spikes actually, indicates ventricles contraction (ventricular systole) when they pump blood out of the heart into the arteries. The T wave corresponds the repolarization and relaxation of the ventricles (ventricular diastole), which prepares them for the next heartbeat. Atrial diastole or repolarization is usually not visible in the ECG as it falls under the QRS complex. The cardiac cycle and its connection to ECG is shown in Fig. 2.2.

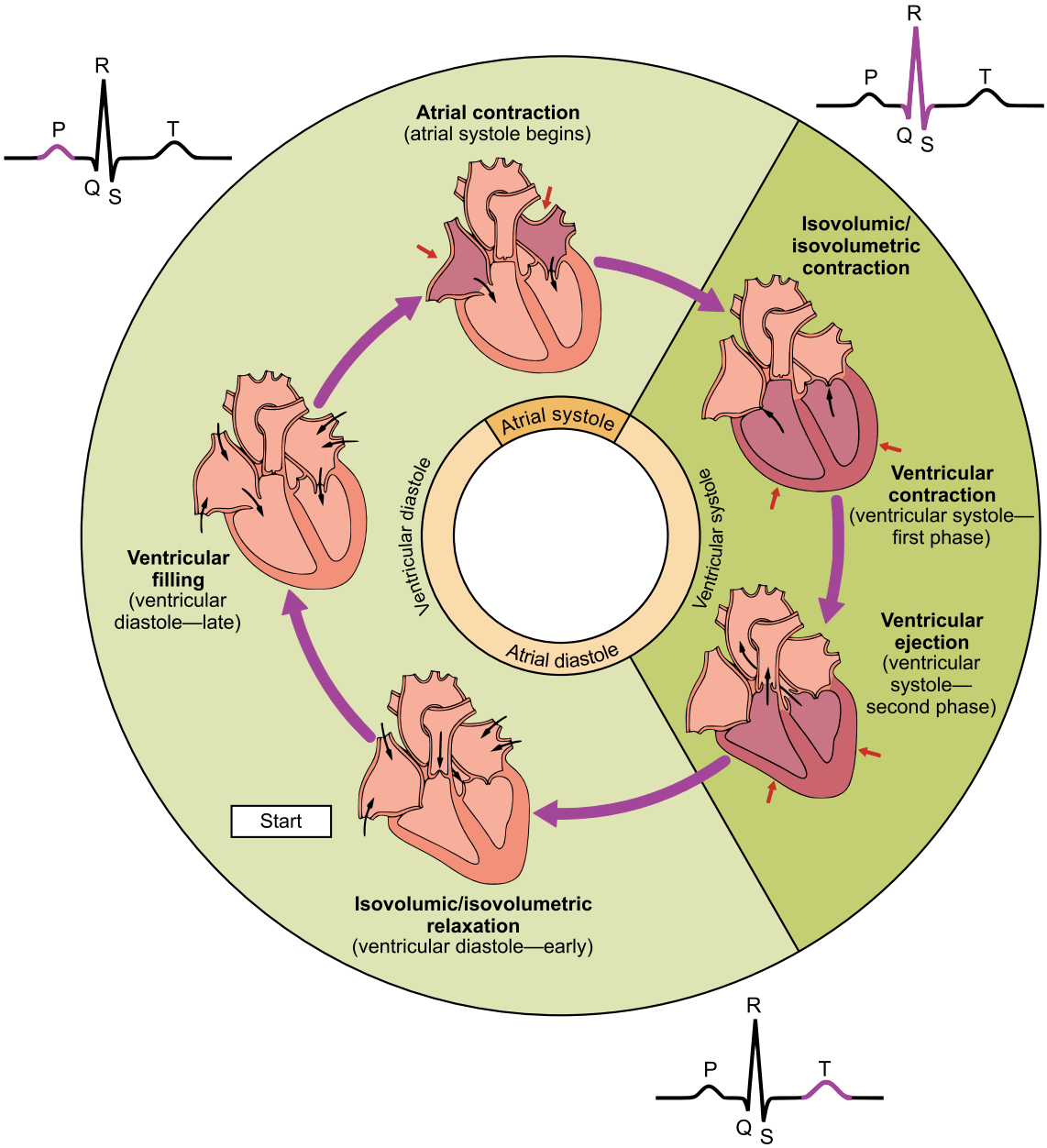

Figure 2.2. *Diagram describing the phases of the human cardiac cycle and their correlation between ECG. P, QRS and T waves of ECG are shown in highlighted purple color next to the corresponding heart phases. Figure adopted from Ref. [9].*

The above-mentioned cardiac cycle has to be initiated and orchestrated very precisely. Therefore the heart has a complex electrical system that controls its beating, called as cardiac conduction system (CCS) [11] , which is shown in Fig. 2.3. This system controls the timing and sequence of the heart's contractions, which is necessary for it to pump blood effectively. The heart's electrical system consists of specialized cells that generate and transmit electrical impulses throughout the heart.

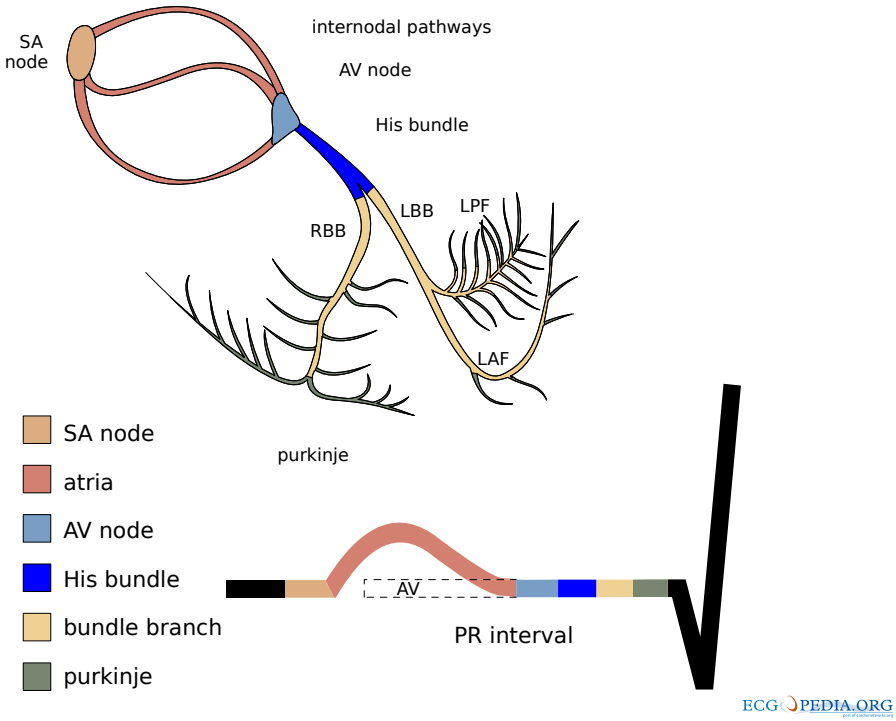

Figure 2.3. *Heart's electrical conduction system called also as cardiac conduction system (CCS). PQ segment divided into parts corresponding to the location in CSS. Figure adopted from Ref. [10].*

The primary pacemaker of the healthy heart is the sinoatrial (SA) node, which is located in the upper part of the right atrium. The SA node generates electrical impulses called cardiac action potential that spread across both atria, causing them to contract. This contraction helps push blood into the ventricles.

From the SA node, the electrical impulses travel through a pathway of specialized muscle fibers called the atrioventricular (AV) node, which is located in the lower part of the right atrium. The AV node acts as a gatekeeper, slowing down the electrical impulses and allowing time for the atria to contract fully and for the ventricles to fill with blood.

After passing through the AV node, the electrical impulses travel through a bundle of specialized fibers called the bundle of His, which divides into two branches: the left and right bundle branches. These branches extend down the ventricular walls and transmit the electrical impulses to the Purkinje fibers. The Purkinje fibers rapidly conduct the electrical impulses throughout the ventricles, causing them to contract forcefully and push blood out of the heart and into the circulation.

Although the SA node is responsible for controlling normal healthy heart rhythm, called sinus rhythm, other parts of the cardiac conduction system, and even the heart muscle itself, are also able to create activation potentials to cause heart beats when necessary or mandatory. However, disruptions in the CCS can lead to arrhythmias or abnormal heart rhythms, which can affect the heart's ability to pump blood effectively and thus lead to serious health problems.

The SA node itself generates a rhythm of approximately 100 beats per minute (BPM), but the heart must constantly adjust its beating rate based on various factors and prevailing circumstances. The primary factors influencing HR are autonomous nervous system (ANS) function and hormonal regulation. The ANS has two divisions, with the sympathetic nervous system (SNS) primarily activated during stress and physical activity, leading to an increase in HR. On the other hand, the parasympathetic nervous system (PNS) is activated during periods of rest, reducing HR via vagus nerve. In addition, certain hormones, such as adrenaline and noradrenaline in plasma, play a significant role in this process by accelerating the activation potential triggering rate.

2.2 Heart rate variability

As mentioned in Ch. 1, HRV is a physiological phenomenon of complex variation in the time interval between heartbeats, which includes randomness and both short and long-range correlations [4]. Measuring HRV involves analyzing the time between successive heartbeats, but first it is important to identify the RRIs as accurately as possible. The most used method for this is the analysis of the ECG signal, whose the mechanism by which it is generated in heart, is described in Sec. 2.1. In particular, the location of the signal R-peak is quite easy to identify by mathematical algorithms such as those in Refs. [12–14] even from a noisy signal.

However, since in the case of HRV, we are generally interested in the rhythms produced by the SA node with the influence of ANS, so in theory, in order to avoid any variation in intra-cardiac electrical signal conduction, it would be best to use the P-wave instead, but determining its exact location is not as simple [14, 15]. Therefore, the HRV is measured between the R-peaks, i.e. RRIs. Another frequently used term instead of RRI is NN interval (normal-to-normal) [16]. This highlights the fact that it is a question of analysing the normal heartbeats produced only by SA node, so in other words, the ectopic beats and arrhythmic events are often excluded from HRV analysis [16].

In addition to the ECG as the golden standard, the growing popularity of commercial devices such as smart watches has also brought an attractive opportunity to measure HRV via photoplethysmography (PPG) [17]. PPG measures blood flow volume changes within the vasculature, for example from the wrist, arm or fingertip, using light absorption. However, PPG does not directly measure heart and thus HRV, but in fact rather pulse rate variability (PRV) [18]. This thesis focuses on the use of ECG to determine HRV.

When RRI or NN intervals are defined, various HRV methods have been developed to quantify the complexity and variability of these intervals [5]. These methods are described in Ch. 3. They provide insights into the activity of the sympathetic and parasympathetic branches of the ANS.However, there are several other factors that influence HRV, such as subject-dependent age [19], gender [19], heart rate [20] and health status [5]. As mentioned in Sec. 2.1, several hormones affect the function of ANS. Hormone levels, in turn, are affected by various physiological and psychological factors, such as stress, state of alertness, posture, movement, recency of physical activity and different cognitive tasks [5, 21]. In addition, two main sources of regular fluctuations have been identified in HRV: respiratory sinus arrhythmia RSA [22] and Mayer waves [23, 24]. RSA refers to the respiration-driven speeding and slowing of the heart via the vagus nerve [5, 22]. Mayer waves are cyclic changes in arterial blood pressure brought about by oscillations in baroreceptor and chemoreceptor reflex control systems [23, 24]. These are both therefore related to the complex regulation of functions of body, in this case breathing and blood pressure regulation. This entirety makes HRV, on the one hand, a very complex research subject with a huge variety of variables, but on the other hand, a very diverse one, as HRV can be studied in connection with very different matters. However, this thesis focuses on the study of HRV during sport.

HRV has been used in sports primarily to analyze rest and post-exercise recovery [25]. For example, Kaikkonen et. al. suggests that a 2-minute HRV measurement after the exercise is sufficient as a measure of training load (TL) in field conditions, as the higher intensity or longer duration of the exercise immediately reduces HRV recovery [26]. There are fewer research results like and basketball players [27] on the measurement of HRV during exercise due to more unstable conditions and the fact that many of the HRV methods presented in Ch. 3 are not suitable for such situations. On the other hand, Gronwald et al. have obtained promising results from the use of nonlinear methods during exercise [28–35]. In more detail, these recent results are presented in Sec. 3.2.

2.3 Cardiac load under exercise

It should be clear that in endurance training, the heart and circulation of the body in particular play a major role. The heart rate monitor (HRM) is a familiar tool for endurance athletes to measure HR [36]. In general, all kinds of measuring and predicting results often fascinate endurance athletes. For example, mathematical models have been developed to predict the end time of a marathon run based on exercises [37]. But how to practice optimally and what are the cornerstones on which endurance training is based? Endurance training is done on a very wide scale, from long and light exercises to short intervals of a few seconds. The frequency, power (or intensity) and duration of the exercises therefore vary greatly. It is relevant to quantify how they are distributed when looking at the training in its entirety. This is described as training intensity distribution (TID).

Endurance exercise and training programs are broadly based on the three-area TID model presented in the literature. Zone 1 describes a low-intensity exercise that occurs below the first ventilation (VT1) or lactate threshold (LT1). This threshold is also referred to as the aerobic threshold (AeT). That name suggests that up to that intensity, the body is able to maintain its energy production mainly aerobically, i.e. using oxygen to convert fat and carbohydrates into energy. After this, as the intensity increases, the body has to start producing energy also anaerobically, i.e. without oxygen. As a result of such metabolism, lactate begins to accumulate in the body and blood. More specifically, lactate accumulates in the muscles even at rest, but it can be removed. It is therefore a question of a balance between the yield of the lactate and the rate at which it is removed. As the yield of the lactate increases, the rate of removal also increases, so BLa only gradually increases.

When the intensity grows so high that the lactate can no longer be removed at the same rate, BLa begins to grow exponentially. This point is called an anaerobic threshold (AnT). AnT can be used to split higher intensity training into two parts, so that TID zone 2 falls between AeT and AnT and zone 3 is the area of intensity above AnT. For the determination of the thresholds, a incremental test to voluntary exhaustion is conventionally used, either for the BLa or breath gas measurements, or a combination of these two. Whichever measurement method was used, there are several mathematical ways to determine the thresholds from the measurement results [38, 39]. The method used may have some effect on the results and there is always a certain degree of uncertainty when determining the thresholds. In general, the threshold can be misleading as the term, since physiological changes in the body's energy production do not occur suddenly, but rather smoothly as intensity increases [39].

However, the AnT in particular could be determined very accurately by several measurements. By definition, as explained above, AnT is a balance where the yield of the lactate and the rate of removal match and in this case the BLa does not rise even under long load. This is also referred to by the descriptive term maximal lactate steady state (MLSS),

which is often used instead of AnT. The threshold determined by the first test could be verified by a test in which the subject moves at the constant power or speed specified by MLSS over a long period of time and the values of the BLa are monitored. If the MLSS is correct, the lactate remains constant during performance and if it goes up, the MLSS is set too high. In this case, the test should be performed again until a correct limit is found. As it may sound, such an iterative method, with its potentially multiple check measurements, is very laborious and in practice therefore very difficult to implement in studies. In addition, it should be noted that there is no corresponding exact definition or method of measurement for AeT.

AnT is also often referred to on the basis of the method of determination. When using BLa, the measurement is often referred to as the second lactate threshold (LT2) and, respectively, the second ventilation threshold (VT2) for breathing gases. In this thesis, both BLa and breathing gas measurements are used. However, the more precise method of determining the thresholds is not further elaborated, and no distinction is made between lactate and ventilation thresholds. Defined thresholds are introduced as reference values defined by a professional. Therefore, when talking about thresholds, the abbreviations AeT and AnT are used instead of LT1, VT1, LT2, VT2 and MLSS from now on.

When it comes to endurance training, there is no consensus on what kind of TID is best [40, 41]. However, the most common, i.e., so-called polarized (zone 1 > zone 3 > zone 2) and pyramid model (zone 1 > zone 2 > zone 3), are based on a large zone 1 share. In other words, a large portion, up to 80% of the total amount of training, should be very low-intensity in endurance training. However, especially for novice endurance athletes, this is not often the case, as the exercises are typically done at too high a intensity compared to their own fitness level. A recent extensive study found that for people who are not physically active this can happen even as a result of daily activity, i.e. taking the stairs during the day etc. causes a bias in TID (zone 1 is not clearly the smallest) [42]. It would therefore be necessary to know the thresholds and evaluate TL for people with various fitness levels, and it would be a significant advantage if this can be done in a fast, cheap, reliable and uninvasive way. Since current HRMs and smart watches are likely to be able to measure body biosignals, such as PPG and ECG, very accurately, this thesis will consider the suitability of HRV as a TL indicator and as a determination of thresholds.

3. METHODS FOR ANALYZING HEART RATE VARIABILITY

This chapter introduces the mathematical methods used in HRV research. All conventional and commonly used methods are mentioned and briefly presented, but a more accurate review is given in the references. The main focus is on the presentation of the methods used in this thesis. Section 3.1 provides a brief description of the conventional time-domain and frequency-domain HRV methods which, however, were not used in this work. Section 3.2 introduces detrended fluctuation analysis (DFA) method, which is essential for this thesis. A brief introduction on other non-linear analysis methods is also given. Section 3.3 introduces dynamical detrended fluctuation analysis (DDFA), which has been further developed on the basis of the DFA.

3.1 Time-domain and frequency-domain analysis

Time-domain analysis of HRV quantifies the amount of variability in the RRI time series during monitoring periods that may range from < 1 min to > 24 h [5]. There are numerous statistical as well as geometrical time-domain methods, but Task Force of the European Society of Cardiology and The North American Society of Pacing and Electrophysiology [43] recommends using the following four methods for HRV analysis in different situations:

1. Standard deviation of the NN intervals (SDNN), that is, the square root of variance. SDNN is suitable when estimating the overall HRV.
2. HRV triangular index (HRVI) is geometric measure, which is obtained as the integral of the histogram (i.e. total number of RRIs) divided by the height of the histogram which depends on the selected bin width (recommended bin width is 1/128 s). HRVI is also estimate of overall HRV, but only allows casual pre-processing of the ECG signal, when compared to SDNN.
3. Standard deviation of the average NN intervals calculated over the 5-min segments (SDANN), which estimates the long-term components of HRV.
4. Square root of the mean squared differences of successive NN intervals (RMSSD), used as an estimate of short-term components of HRV.

The advantage of time-domain methods is that they are simple to calculate, but on the other hand, they produce only one quantity from the entire time series. In addition, it is often misleading to compare values calculated from recordings of different lengths [43].

Frequency-domain or power spectral density (PSD) analysis provides the basic information of how power (variance) distributes as a function of frequency [43]. In these methods, a spectrum estimate is calculated usually by first converting the RRI series to equidistantly sampled series by cubic spline interpolation [44]. Then the spectrum estimate is divided into very low frequency (VLF), low frequency (LF), and high frequency (HF) bands, whose limits are usually 0-0.04 Hz, 0.04-0.15 Hz and 0.15-0.4 Hz, respectively. The measured values used in HRV analysis include peak frequencies (i.e., the frequency values corresponding to maximum power within VLF, LF and HF bands), absolute and relative powers (calculated by integrating the spectrum estimate over VLF, LF and HF bands), normalized powers (for LF and HF), LF/HF power ratio, and the total spectral power [44].

3.2 Non-linear and detrended fluctuation analysis

As explained in Sec. 2.1, the control system of the heart is complex. Therefore, it is presumable that HRV cannot be fully described by using only linear methods [44]. As a result, a number of non-linear methods have been developed, including Poincaré plot [45], approximate entropy (ApEn) [46], sample entropy (SampEn) [46], correlation dimension (D_2) [47], recurrence plot (RP) analysis [48] and DFA [49]. All of these methods mentioned so far in Sec. 3.1 and Sec. 3.2 can be easily calculated with several software developed for the analysis of HRV, such as Kubios [44]. Since these HRV methods have already been extensively used in sports analytics, the focus in this thesis will be on the latest methods, such as DDFA. First, the DFA, on which the DDFA is based, is presented in more detail.

The DFA is well-established method for the detecting of long-range correlations in time series with non-stationarities [50]. It was developed by Peng et al. [51] and first demonstrated for the analysis of DNA sequences. Since then, the DFA method has been used to analyse time series in several fields of science. It has been applied, for example, to the climate [52], quantum and statistical physics [53, 54] and even music [55].

As mentioned, the DFA has been used often especially for the analysis of HRV. Of particular interest has been the identification of heart diseases [56–58]. In addition, wakefulness, sleep and even its phases can be detected by the method [59, 60]. In sports physiology, DFA was used to measure changes in running frequency and gait as a result of training [61], and to examine the dynamics of HRV for endurance athletes of various sports [33, 62].

For the reliable detection of long-range correlations, it is essential to distinguish trends from intrinsic long-range fluctuations in the data, because strong trends in the data can lead to a false detection of long-range correlations [50]. Trends are caused by external effects – in the case of HRV during physical activity – and they are usually supposed to have a smooth and monotonous behaviour. The advantage of the DFA is that it can systematically eliminate trends of different order and thus provides an opportunity to study the scaling behavior of the natural variability in the considered time series [50].

The algorithm for calculating DFA for interbeat time series $B(i)$ of length N consist of the following steps [50]:

1. Integrate the time series $B(i)$ into series

$$y(k) = \sum_{i=1}^{k} (B(i) - \langle B \rangle), \tag{3.1}$$

   where $\langle B \rangle$ is the mean value of original time series $B(i)$. Note that the subtraction of the average is not in fact mandatory, as the later detrending step 3 will remove it in any case [50].

2. Split the integrated time series $y(k)$ from the previous step into non-overlapping segments of equal length s. A short part of the end of the recording may be omitted, because the length of the recording does not have to be a multiple of the considered time scale s. The number of segments N_s is thus obtained from

$$N_s = \lfloor N/s \rfloor . \tag{3.2}$$

   However, in order not to ignore the end of the recording, the same procedure is repeated starting this time from the end of the recording. Thus, $2N_s$ segments are obtained together.

3. Calculate the local trend for each segments v by fitting the m-degree polynomial with the method of least-squares and denote this vth segment fitting polynomial as $p_v(k)$. The degree of fitting polynomials is expressed as DFA-m. Conventionally [49], linear first degree polynomial $m = 1$ is used. Hence, usually "DFA" refers to DFA-1 by default.

   Next we calculate the difference between integrated time series $y(k)$ and the local trends as

$$y_s(k) = y(k) - p_v(k). \tag{3.3}$$

4. Calculate the squared fluctuations $F_s^2(v)$ as the variance from local trend for each $2N_s$ segments with the equation

$$F_s^2(v) = \left\langle y_s^2(k) \right\rangle = \frac{1}{s} \sum_{k=1}^{s} y_s^2 \left[(v-1)\, s + k \right], \tag{3.4}$$

   where v is segment index.

5. Finally, all the squared fluctuation functions calculated in the segments are averaged, and the square root is calculated from the result, giving a scale-dependent fluctuation function

$$F(s) = \left[\frac{1}{2N_s} \sum_{v=1}^{2N_s} F_s^2(v) \right]^{1/2}. \tag{3.5}$$

The scale dependence of the fluctuation function enables estimating the nature of the noise in the time series. This is done with the help of the so-called scaling exponent α. There is a power-law relation between the fluctuation function $F(s)$ and the scale s

$$F(s) \sim s^{\alpha}, \tag{3.6}$$

where α is the scaling exponent. If the fluctuation function is plotted as a function of a scale with both axes being logarithms, the scaling exponent is determined by the slope of this line.

The scaling exponent determined by the DFA can be interpreted as a generalized Hurst exponent (H). These interpretations for α are presented in Table 3.1 [63]. In this table, anti-correlation refers to intra-series anti-correlation. This means that a positive change in the time series follows most likely a negative change and vice versa. White noise, on the other hand, means a signal which has the same power of each frequency in the power spectrum. The values of white noise signal do not depend on each other.

Brownian noise (or Brownian motion) can be produced by integrating white noise, making the differences between successive values independent of each other. The power spectrum of Brownian noise follows the $1/f^2$ ratio. Physically, it corresponds to the random movement of particles in a medium such as gas or liquid. In the power spectrum between Brownian noise and white noise, there is so-called pink noise, which power spectrum follows $1/f$ proportionality.

In the case of HRV, the scaling exponent is conventionally calculated in two different areas: so-called short-range α_1 (4–16 beats) and long-range α_2 (16–64 beats). This division is convenient because on the logarithmic scale the ranges correspond to $[2^2, 2^4]$ and $[2^4, 2^6]$. Scales larger than 64 are unnecessarily long and often describe fluctuations in daily activity, visible in HR trends due to movement, instead of the actual HRV.

Table 3.1. *Interpretation of the DFA scaling exponent α [63].*

Scaling exponent	Interpretation	Stationarity
$0 < \alpha < 0.5$	anti-correlated	stationary
$\alpha = 0.5$	white noise	
$0.5 < \alpha < 1$	correlated	
$\alpha = 1$	$1/f$ (pink) noise	
$1 < \alpha < 1.5$	anti-correlated increments	nonstationary, stationary increments
$\alpha = 1.5$	Brownian noise	
$1.5 < \alpha < 2$	correlated increments	

The short-scale α_1 of DFA-1 has proven useful in recent years, especially during both low and high intensity training [28]. For example, Gronwald et al. have proposed using α_1 as a new biomarker for TID [29]. The same group has also used α_1 to provide an assessment first for AeT [30] and later for AnT [31, 32]. This was based on an earlier observation that α_1 increases from rest to light intensity and in turn decreases almost linearly under high intensity during incremental cycling exercise [33]. The method has been tested in real time as a field study with a former olympic-level triathlete [34]. However, while the results have been promising, the individual differences and deviations are large. To address this, a recent study [35] was able to improve accuracy by combining HRV-based α_1 thresholds with thresholds determined by ECG-derived respiration frequency (EDR), which is introduced in Ref. [64].

3.3 Dynamical detrended fluctuation analysis

The DFA scaling exponent describes the whole time series. If the scaling features change as a function of another variable, e.g., time, DFA may provide insufficient information. For example, in the case of HRV and sport, the intensity of the training may change significantly. Therefore, α_1 and α_2 calculated from the whole exercise do not provide sufficient information about the events during the exercise. Of course, it is possible to divide the time series into smaller parts for calculating α, but this may cause bias.

To solve this problem, DDFA has been developed to examine the local variations of the scaling exponent. In addition to the HRV in different situations, such as running and driving [63, 65, 66], the DDFA method has also recently been applied in the field of physics to the determination of the roughness exponent of elastic interfaces [67] and in the field of environmental technology to optimization of wastewater treatment processes [68]. Next we introduce the main steps of DDFA following Ref. [63].

The first step is the dynamic segmentation of the time series. The segmentation is performed by a function that describes the length of the segment as a function of scale s. In this thesis we use a linear function

$$l(s) = as, \tag{3.7}$$

where a is constant. This simple function has been found to be working well in different situations. The possible values of constant a are limited on the one hand by the largest scale in which the fluctuation functions are calculated in the segments, i.e., $s + 1$, and on the other hand, the length of the time series, as the segment cannot be longer than the length of the time series. The smaller the constant a, the more detailed the analysis of the time series can be, but at the same time the noise is increasing. For example, a value of $a = 5$ has previously been found to be suitable for HRV analysis [63], but smaller values can be used to make the analysis as local as possible [67]. In this thesis we resort to $a = 5$.

After selecting $l(s)$, the time series is divided for each scale into s segments. Let us denote these segments by notation $S_{s,t}$, where t is the segment index. Thus, formed segments may overlap, resulting in smoother results. For example, the segment index may be the average time index of the segment. If some other data are available for the segment, they can also be used as the segment index. Such indexing allows the scaling exponent to be viewed as a function of any parameter, which makes DDFA an effective method [63]. In the case of this thesis and HRV analysis, HR is a very useful parameter instead of time. In addition, interpolation also allows the scaling exponent to be viewed as a function of lactate values or ventilation parameters.

After segmentation, the logarithmic fluctuation function is calculated on each segment of scales $\{s - 1, s, s + 1\}$ and the results are denoted as $F_t(s - 1)$, $F_t(s)$ and $F_t(s + 1)$. After the calculation of logarithmic fluctuation functions, a *dynamical scaling exponent* $\alpha(t, s)$ of each segment is determined by finite difference approximation

$$\alpha(t, s) \approx \frac{h_-^2 F_t(s + 1) + (h_+^2 - h_-^2)F_t(s) - h_+^2 F_t(s - 1)}{h_- h_+ (h_+ + h_-)}, \tag{3.8}$$

where $h_- = \log(s) - \log(s - 1)$ and $h_+ = \log(s + 1) - \log(s)$ are the logarithmic backward and forward differences. The use of a difference approximation is justified because it has been found that the fluctuation functions calculated in the maximally overlapping segments are sufficiently smooth [63]. The interpretation of the DDFA scaling exponent corresponds to the interpretation of the DFA scaling exponent. Hence, Table 3.1 is also valid for examining the DDFA results.

Similarly to DFA, the detrending order of DDFA can be determined. As can be seen in Eq. (3.8), the calculation of $\alpha(t, s)$ also needs the fluctuation function from scale $s - 1$. Increasing the order of DDFA affects only to the fitting polynomial. For example, the fitting of the straight line requires two points and the parabola three, respectively. There is therefore a lower limit for the calculation of DDFA, which can be expressed as N + 3, where N is the order of DDFA. Here we have tested orders from N = 1 to N = 4.

In this thesis, the DDFA results were calculated using Python with an efficient implementation. In practice, an increase in the order of DDFA has no significant effect on the calculation time.

4. RESEARCH METHODOLOGY AND MATERIAL

This chapter presents the subjects of the thesis and their background information in Sec. 4.1. Then Sec. 4.2 describes test protocol used in the study, as well as used measuring devices. Finally, Sec. 4.3 presents the methods of data pre-processing, which were performed prior to the calculation of the final results.

4.1 Participants

The data used in this thesis consists of 9 tests on a treadmill as well as 15 tests with a cyclo-ergometer. All 24 participants were voluntary and healthy adults (aged 22–44), who gave a written consent to the use of their data for scientific research. Background information for the subjects is given in Tables 4.1 and 4.2. These tables contain information on gender, age, height, weight and body mass index (BMI = weight / height^2). Below, tests performed on the treadmill are denoted by letter "R" (running) and, accordingly, the bicycle ergometer tests by letter "C" (cycling). Before the test, the participants filled out a form that charted, e.g., medical risk factors, exercise background and training goals. In addition, subjects were instructed to eat only lightly and not to consume caffeine for a few hours and alcohol for a few days before the test. The approval of the study was given by the Tampere University Hospital Ethics Committee, and the principles of the Declaration of Helsinki were followed.

4.2 Test protocol and instrumentation

In both running and bicycle tests, the protocol was a direct test of maximum oxygen uptake ($VO_{2,max}$) with both gas and lactate measurements. This refers to a incremental test, which is carried out all the way up to voluntary exhaustion, where the maximum oxygen uptake capacity is measured directly from the breathing gases. The test was started with a 5-minute warm-up period. The appropriate starting load for the test was then selected based on the subject's training background and fitness level.

Table 4.1. *Background information of cycling test subjects including the gender (male = M, female = F), age, height, weight and body mass index (BMI).*

Subject	Gender	Age (years)	Height (cm)	Weight (kg)	BMI (kg/m^2)
C2	M	33	177	77.3	24.7
C5	M	36	189	84.0	23.5
C8	M	44	184	87.4	25.8
C9	M	37	173	71.4	23.9
C11	F	27	172	55.7	18.8
C12	M	31	183	104.2	31.1
C13	F	35	169	81.2	28.4
C14	F	41	170	61.4	21.2
C17	F	22	166	72.8	26.4
C21	F	34	160	69.3	27.1
C22	F	30	174	79.0	26.1
C23	F	35	171	64.4	22.0
C24	F	42	166	68.5	24.9
C25	M	42	173	89.6	29.9
C26	M	27	180	80.9	25.0
mean ($\pm$ std)	M=7, F=8	34 ($\pm$ 6)	174 ($\pm$ 8)	76.5 ($\pm$ 12.3)	25.3 ($\pm$ 3.2)

Table 4.2. *Background information of running test subjects including the gender (male = M, female = F), age, height, weight and body mass index (BMI).*

Subject	Gender	Age (years)	Height (cm)	Weight (kg)	BMI (kg/m^2)
R1	M	28	190	78.5	21.7
R2	F	40	165	59.2	21.7
R4	F	25	169	66.5	23.3
R5	M	36	180	80.3	24.8
R7	F	40	172	66.4	22.4
R8	M	39	178	83.2	26.3
R10	M	36	177	75.5	24.1
R27	M	28	180	71.9	22.2
R28	M	38	185	79.9	23.3
mean ($\pm$ std)	M=6, F=3	34 ($\pm$ 6)	177 ($\pm$ 8)	73.5 ($\pm$ 8.0)	23.3 ($\pm$ 1.5)

In the treadmill 0, 0.5 or 0.6 degree slope of the treadmill was used to compensate for, e.g. the air resistance compared to running outdoors. In accordance with Finnish testing practice [69], the speed of the treadmill was always increased by 1 km/h every 3 minutes until the test subject could no longer run the required speed or wanted to interrupt the test. For safety reasons, the subject was attached to a harness hanging from the ceiling for the duration of the test to avoid falling and injury. The used treadmill was Rodby RL2700E X 1000 (Rodby Innovation AB, Sweden), whose speed deviation is $\pm$1 % and elevation deviation $\pm$0,2 % according to manufacturer.

Correspondingly, in the cyclo-ergometer test, the starting load was 40–120 W and every 3 minutes the load was increased by 20–30 W depending on the individual background and fitness level. The test was continued until the subject was no longer able to maintain the required power level. Test was done by using Monark LC4 cyclo-ergometer (Monark Exercise AB, Sweden).

In both test protocols, after each 3-minute load and before the next load, a blood sample was taken from the subject's fingertip to determine lactate levels. The blood sample was also taken at the end of the test and analyzed using Biosen C-Line Clinic glucose-lactate analyzer (EKF Diagnostic GmbH, Germany). The ventilatory gas exchange was measured constantly with Cosmed Quark CPET respiratory gas analyzer (Cosmed s.r.l., Italy) by using breath-by-breath measurement mode.

During the test, the RR intervals were measured with Polar Pro chest strap and Polar H10 heart rate sensor (Polar Electro Oy, Finland), which has been shown to be highly reliable for RR interval determination, especially during intense physical exercise [70, 71]. Polar H10 was connected Polar M430 (Polar Electro Oy, Finland) watch for data storage. The test was used to determine individual performance values for each subject, such as maximum heart rate (HR_{max}), maximum oxygen uptake ($VO_{2,max}$), and thresholds (AeT and AnT). These values can be read from the figures in Appendices A and B for each subject.

All tests were carried out in the Valmennus- ja Testauskeskus Kauppi[1], Tampere, Finland by experienced professional (Master of Sport Science). He also defined individual thresholds for each subject, i.e., aerobic threshold (AeT) and anareobic threshold (AnT). In accordance with Finnish testing practice, the thresholds are based on the LT1 and LT2 thresholds determined from lactate values, which can be fine-tuned when needed using the VT1 and VT2 indicated by the subject's breathing gas variables [69].

[1] Nowadays called as Kunnon testaus

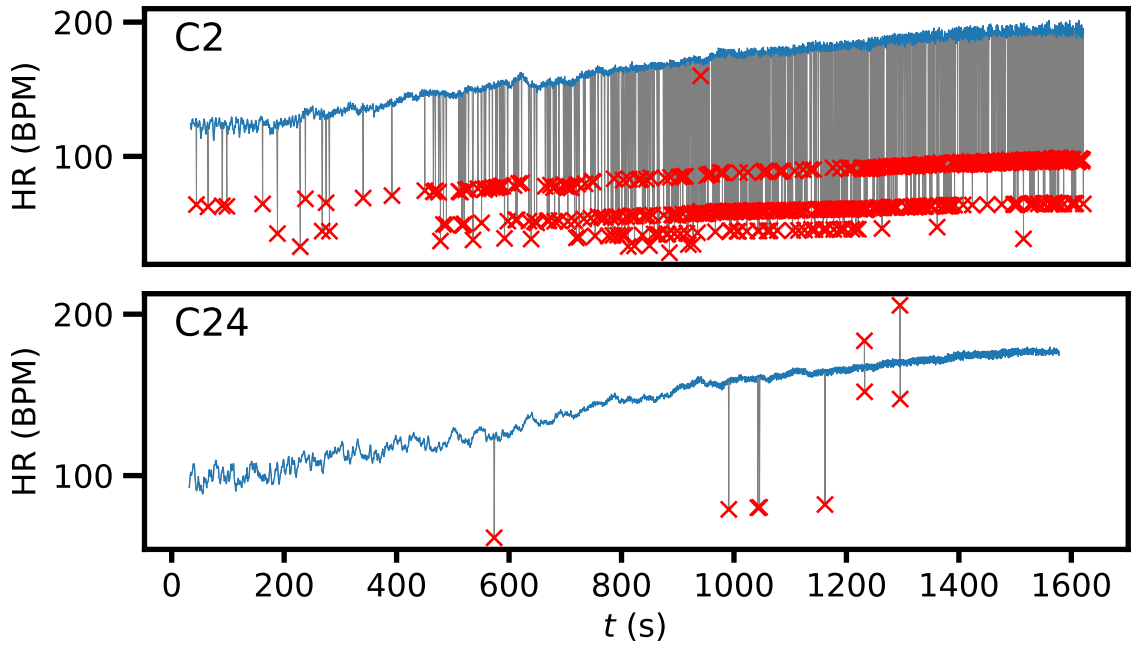

Figure 4.1. *Example of data filtering. The instantaneous heart rate (HR) calculated directly from the RR intervals during the test with two subjects C2 and C24 is shown with a thin grey line in the background as a function of time t, the erroneous RR intervals omitted from the data analysis are shown as red crosses, and the final heart rate used for calculating the results is shown as a blue line. Figures A.1, A.2, A.3, B.1 and B.2 in the Appendices show also the filtered heart rate (corresponding the blue curve) as a function of the time for all the subjects.*

Although lactate and raw data from breath gas measurements were available in this work, determining thresholds using them is not straightforward. Various computational methods for detecting these thresholds have been developed, but the interpretation and verification of results often requires professional know-how. In addition, the computational determination of thresholds was beyond the scope of this thesis. Therefore, this thesis uses thresholds specified by the tester.

4.3 Data pre-processing

Data pre-processing was started by combining an Excel table with breath gas variables and lactate values with a table with RR intervals. Both measurements had been started at the same moment, but the breath gas variables were reported as a 30 second moving average, and the values were updated approximately every 10 seconds. Therefore, the first breath gas values were not received until 30 s, so the RRI time series was limited to starting from the same moment. For this reason, Fig. 4.1, for example, does not start from time 0 s when viewed closely. In addition, the recording of the breath gas variables was stopped at the end of the test, i.e., immediately after the maximum load, but the recording

Table 4.3. *RR Interval filtering values of bicycle ergometer test with their means and standard deviations. The filtering parameters are described in Sec. 4.3. Automatically deleted values were used as a basis for visual inspection.*

Subject	RRIs (pcs)	Automatic (pcs)	Automatic (%)	Visual (pcs)	Visual (%)
C2	3456	524	15.2	520	15.0
C5	4183	4	0.10	9	0.22
C8	3993	21	0.53	24	0.60
C9	4426	0	0	0	0
C11	4723	0	0	0	0
C12	4240	2	0.05	0	0
C13	3479	1	0.03	3	0.09
C14	3180	0	0	0	0
C17	4291	0	0	0	0
C21	3716	2	0.05	2	0.05
C22	4693	1	0.02	4	0.09
C23	2821	135	4.79	152	5.39
C24	3659	8	0.22	9	0.25
C25	3601	2	0.06	2	0.06
C26	4564	2	0.04	2	0.04
mean	3935	47	1.40	48	1.45
($\pm$ std)	($\pm$ 573)	($\pm$ 136)	($\pm$ 4.00)	($\pm$ 136)	($\pm$ 4.00)

Table 4.4. *RR Interval filtering values of treadmill test with their means and standard deviations. The filtering parameters are described in Sec. 4.3. Automatically deleted values were used as a basis for visual inspection.*

Subject	RRIs (pcs)	Automatic (pcs)	Automatic (%)	Visual (pcs)	Visual (%)
R1	3902	4	0.10	7	0.18
R2	4916	36	0.73	37	0.75
R4	3875	17	0.44	28	0.72
R5	4437	2	0.05	6	0.14
R7	3906	1	0.03	1	0.03
R8	3702	0	0	0	0
R10	3982	18	0.45	20	0.50
R27	4462	2	0.04	2	0.04
R28	4678	13	0.28	24	0.51
mean	4207	10	0.24	14	0.32
($\pm$ std)	($\pm$ 425)	($\pm$ 12)	($\pm$ 0.26)	($\pm$ 14)	($\pm$ 0.30)

of the HR and RRI could continue for some time afterwards. Thus, the RRI data was also limited from the top to the value of the last recorded breath gas variables. As a result, the RRI series were comparable with each other, containing only the values during the actual test.

The method described above also made it possible to present data reliably using parameters other than time after the data was interpolated. Thus, it was possible to present on the x-axis, for example, an aggregate heart rate, lactate, or some breath gas variable such as VO_2, so that the values during and after the test itself were not mixed. For example, at some point in the test the HR might have been 150 BPM and the moment after the end of the test the same, but the situation was completely different from the point of view of HRV and lactate values.

The RRI data range was determined to be 200–2000 ms, or correspondingly 30–300 BPM and values not belonging to this range were removed first. Automatic filtering was then performed by calculating windowed median filter with kernel size of 7 RRIs and the data was allowed to deviate by 10% from this trend curve. In HRV measurements data filtering is a commonly known problem [72], and it is challenging to create a robust and universal filtering algorithm that works well in every situation. After automatic filtering, the data was checked and corrected by visual inspection.

Since the ECG signal or raw voltage signal was not in use, there is no complete assurance whether the R peaks were correctly determined in all the cases. Visually made corrections were mainly a few probably incorrectly defined R peaks, that cause abnormal RRIs in the time series. Of course, these abnormalities can also be a sign of real arrhythmia, but in terms of DDFA analysis, the effect on the results is the same. Automatic filtering did not detect some of these cases. In addition, a few RR intervals were deleted incorrectly by automatic filtering, so they were included in the final calculation of the results.

Nevertheless, the number of corrections made by visual inspection was very small and in most cases the quality of the data was excellent as shown in Tables 4.3 and 4.4. These tables also show the difference between the number of deletions after automatic and visual filtering. The parameters of the automatic filtering were intentionally adjusted to be loose, so that the algorithm would not delete anything by mistake, and more difficult cases were then processed manually. With the exception of two subjects out of a total of 24, the final removal rate after visual inspection was 0.75% or less, in many subjects even zero. Only samples C2 and C23 contained a significant number of missed beats.

In addition, Fig. 4.1 shows data from subject C24, which represents a typical test subject in terms of data quality. For C24, 5 missed beats have been removed (at about 1100 s, two almost overlap each other) as well as two incorrectly defined R peaks, which appear as long-short pairs between 1200–1400 s and thus cause 4 RRs to deviate from the trend. So in total, there are 9 of these deleted RRIs as shown in Table 4.3.

5. RESULTS AND ANALYSIS

This chapter is divided into two parts. Section 5.1 focuses on testing the DDFA method for the effect of raw RRI data filtering. In addition, it justifies the order of the DDFA used in this work. Section 5.2 contains a comparison of the DDFA results with the thresholds determined by traditional lactate and breathing gas methods.

5.1 Testing the DDFA method

It is first useful to take a look at the functionality and necessity of the filtering. Figure 5.1 shows how filtering and removing RR intervals that clearly deviate from the trend affect the results. The data of subject C24 shown in Fig. 4.1 is used as an example. Figure 5.1A shows the DDFA results according to the raw unfiltered RRI time series and 5.1B shows the filtered one. The black curve on the secondary y-axis represents the instantaneous HR calculated directly from the RRIs.

The color map shows the value of the DDFA scaling exponent α locally as functions of time and scale. In this thesis, 20 logarithmically evenly distributed values between $[(\mathrm{N}+3), 64]$, where N is the order of DDFA, rounded to the nearest integer, were used as the scale.

Figure 5.1A shows vertical "bands" for the points of the deviating RR intervals. They naturally hinder the interpretation and interfere with the results, especially when α is presented as a function of a variable other than time, e.g., as a function of HR. Then the values in these bands are mixed with the true values of α at the same HR. Therefore, it is necessary to filter RRI data before calculating the DDFA scaling exponent.

As Table 4.3 shows, for subjects C2 and C23 the filtering percentage is high, even above 15 %, so it is appropriate to consider its effect on the results. This was done by taking subject C17 as a reference. In accordance with Table 4.3, 0% of RRIs had been removed from this data. Thus, it is a good starting point for an artificial and systematic study of the effect of RRI removal. The effect of random removal of RRIs on the DDFA α color map is shown in Fig. 5.2. Removals were carried out in such a way that the interval removed once remained removed with increasing percentage.

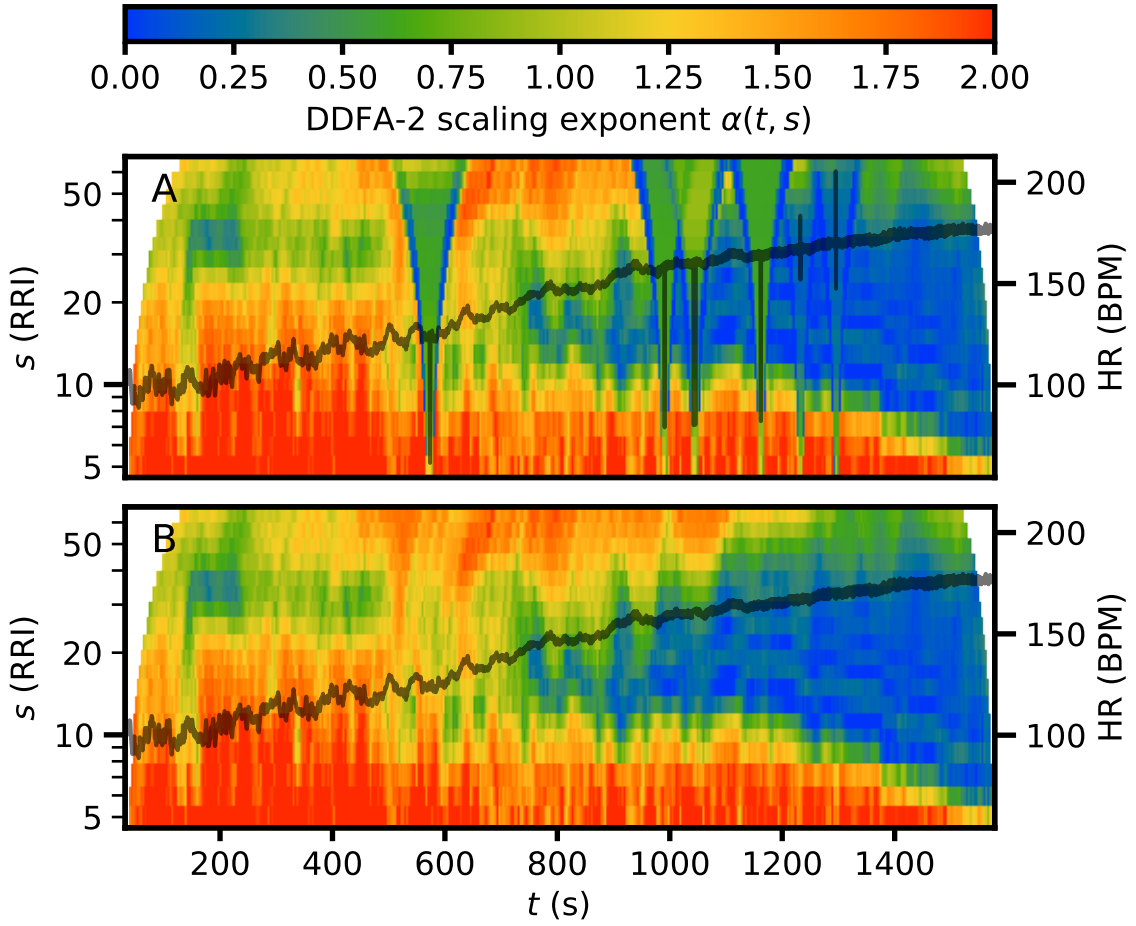

Figure 5.1. *DDFA-2 scaling exponents for subject C24 as functions of time t and scale s calculated for both raw (A) and filtered (B) time series. The black curve shows the instantaneous heart rate (HR) calculated directly from the RR intervals.*

At first glance, all the graphs in Fig. 5.2 look similar.This shows that filtering does not significantly reduce the quality of the results. When comparing Figs. 5.1A and 5.2 it is found that in terms of DDFA results, a few RRIs that are clearly different from the trend causes deviations. On the other hand, even a large number of removals does not significantly affect the values of α. In case of doubt, it may be better to remove the incorrect appearance of intervals as a precaution than to leave them in place.

However, by carefully examining the Fig. 5.2 deviations are detected. For example, the distinctive anticorrelations (in blue) are slightly reduced as the filtration percentage increases. In addition, there are large differences in the smallest scales. They are clearly visible in a zoomed presentation in Fig. 5.3, showing beat indices 3500–3700. On the smallest scales, the red areas of the 0% graph slowly disappear, but even with the remaining 15% they still stand out clearly. Figure 5.3 also shows how the HR curve changes visually due to removals. For example, when comparing 0% and 30% situations, it is seen that in a 0% situation, the HR actually bounces up-and-down almost alternately, forming

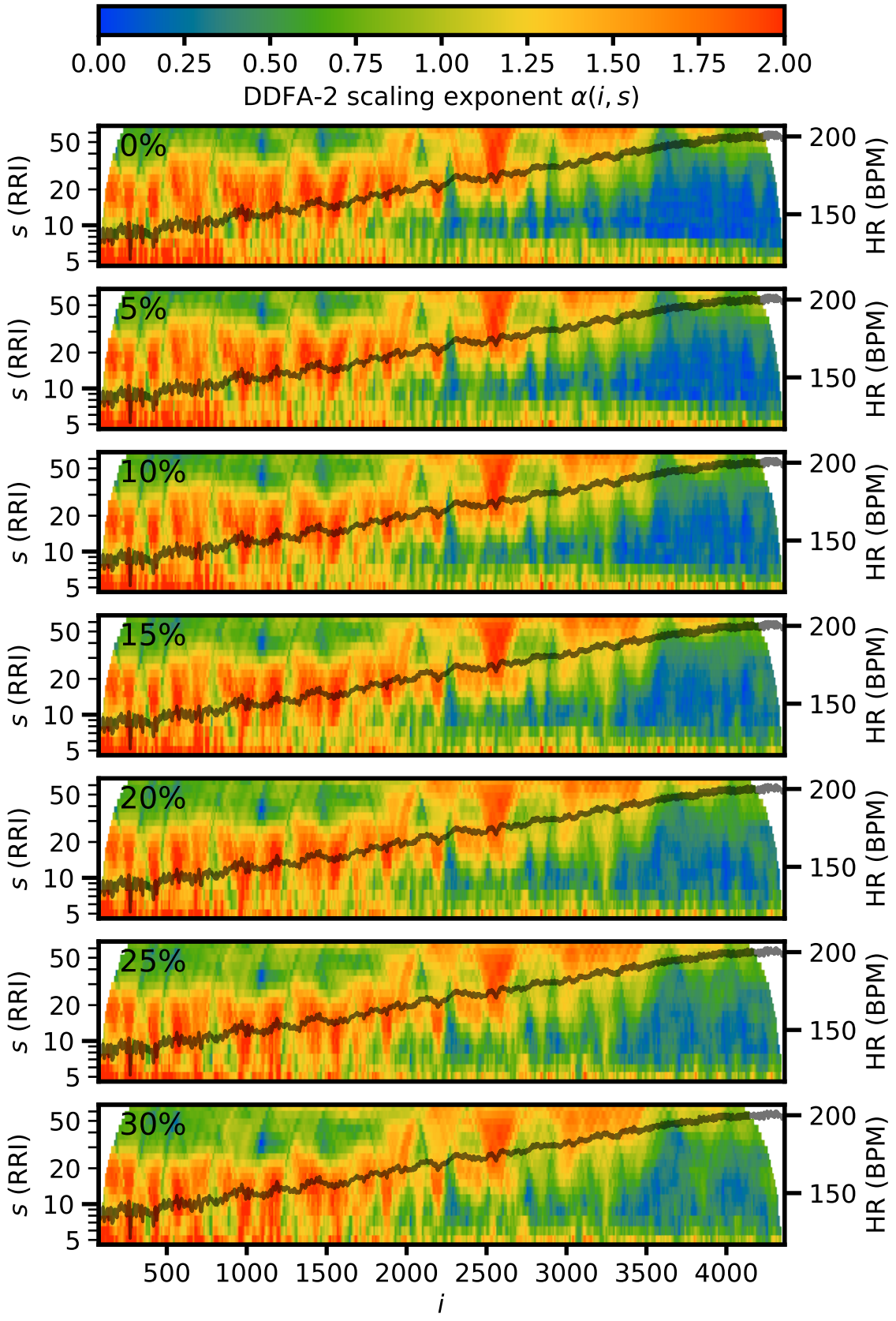

Figure 5.2. *DDFA-2 scaling exponents for subject C17 as a functions of the beat index i and scale s with different total filtering percentages. The number of RR intervals corresponding to the percentage was removed randomly, but in such way that the removed intervals remain removed as the percentage increases.*

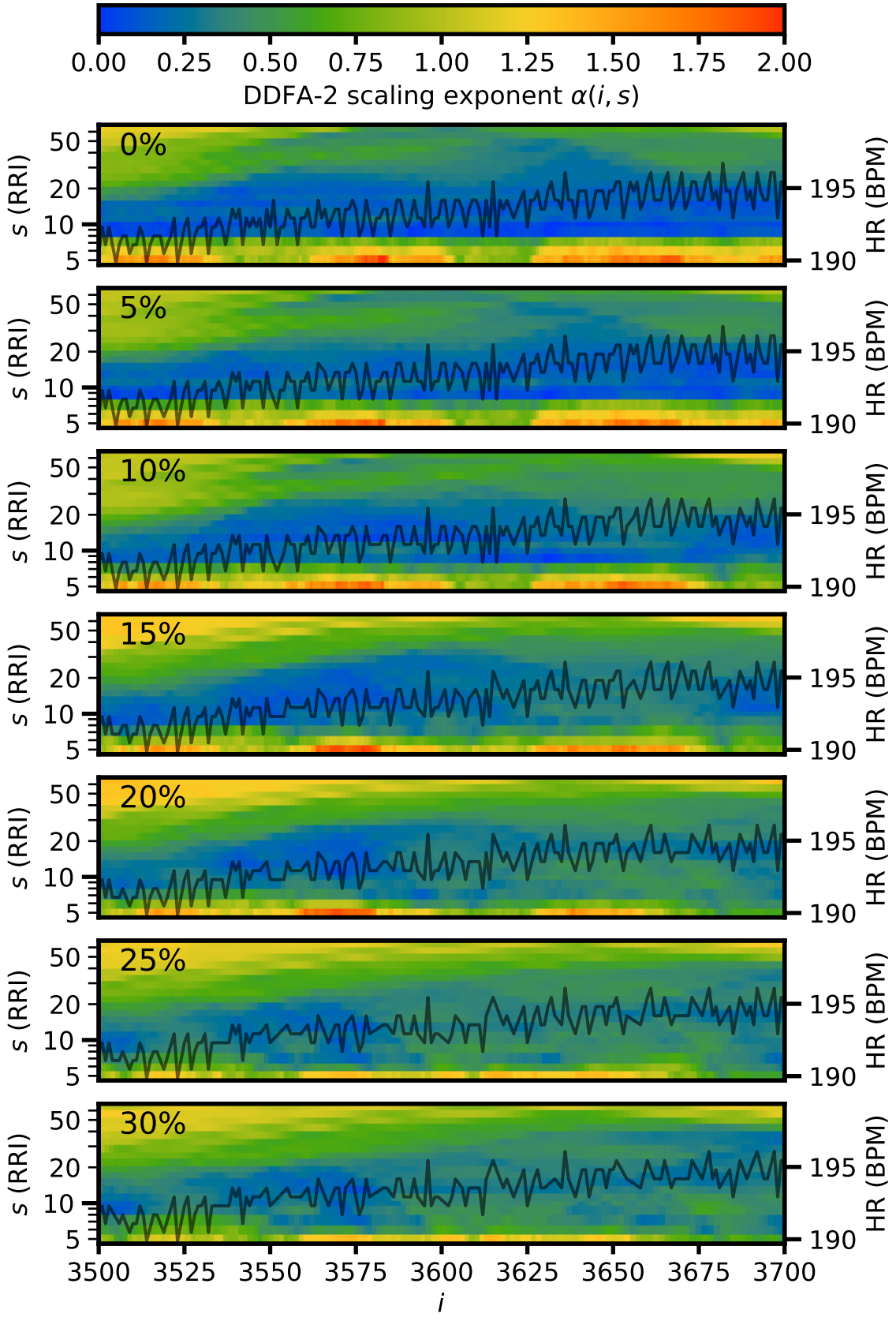

Figure 5.3. *Subject C17 data from Fig. 5.2 zoomed between beat indices 3500–3700.*

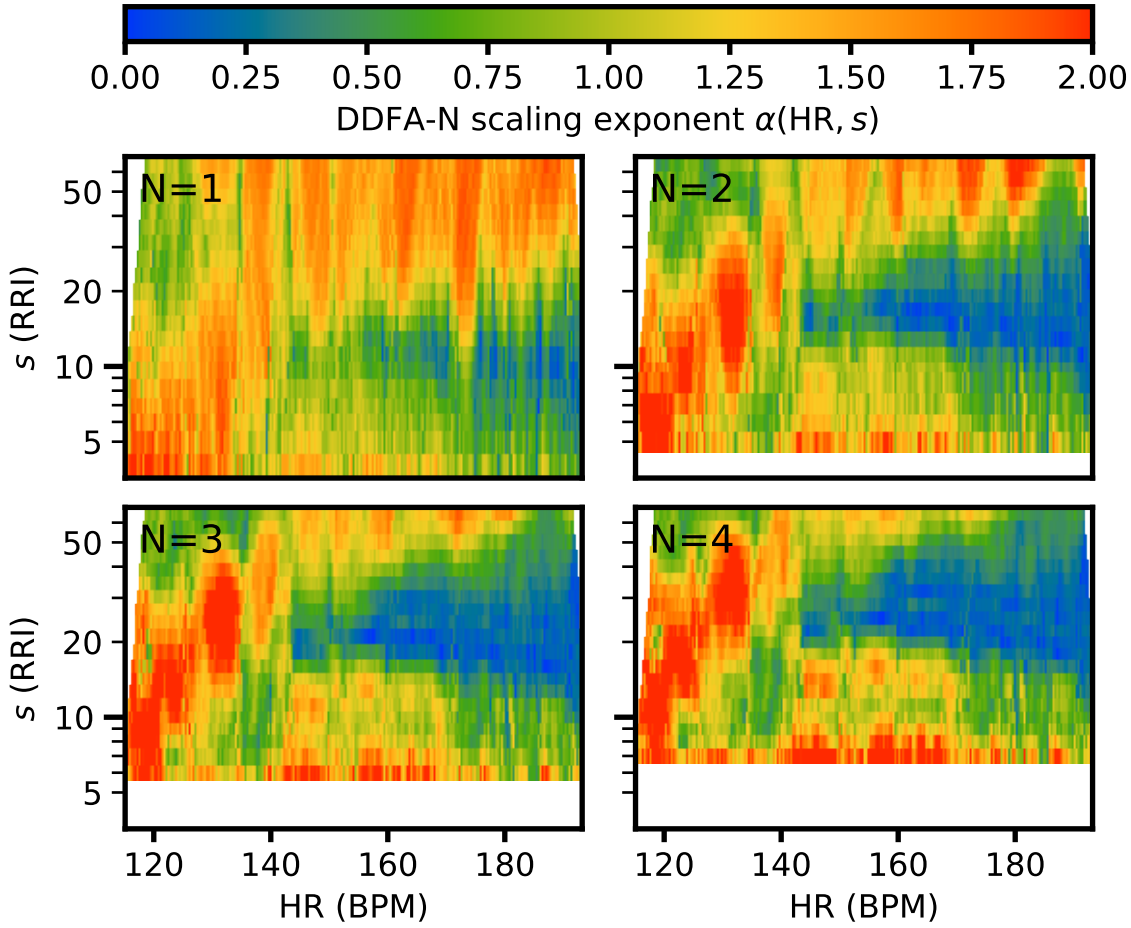

Figure 5.4. *Comparison of the DDFA orders. The figure shows DDFA scaling exponents as a function of the heart rate (HR) and scale s from the subject C5, calculated with different DDFA orders (N = 1, 2, 3 and 4). The DDFA-2 plot from the subject C5 is also presented in Fig. A.4 with thresholds.*

a fairly regular and serrated curve. This kind of long-short variation is very strong, which manifests itself in the value of α indicating anticorrelations. Similarly, in a 30% situation, such a small variation is much less frequent and irregular, which is reflected in the increasing value of α.

In conclusion, the removal of clearly incorrect RRIs is necessary, but even substantial filtering is not a major problem in terms of DDFA results. Of course, the more data is deleted, the more information is lost. For example, in the case of missed beats, it is not possible to say for sure whether they would have an effect on the results if determined correctly. More accurate and detailed testing and examination of filtering functionality is beyond the scope of this thesis.

In all the DDFA figures presented so far we have used order of N = 2. The effect of the DDFA order on the results is presented in Fig. 5.4. This time the scaling exponent α is presented as functions of HR and scale. When the degree of the polynomial is increased, the information on the lowest scales is completely lost, since the smallest scale on which DDFA can be calculated is N + 3. When comparing the graphs, it is found that increasing the order increases the contrast, i.e., the extremes in the values of α are stronger.

In addition, looking at the scales, it can be seen that increasing the order, moves the areas of different colors upwards. For example, in N = 1, the strongest blue range is around scale 10, in N = 2 it is between 10–20, in N = 3 around 20 and in N = 4 at 20–30. It seems that the absence of low scales (white area) thus raises the whole picture upwards. Increasing the order means that more fluctuations are eliminated, especially on larger scales. In the case of HRV, N = 2 appears as a good compromise to eliminate trivial trends but to retain the relevant fluctuations, so it was chosen for the rest of this thesis. Superior resolution of orders beyond linear detrending (N = 2 or N = 3) has also been demonstrated in studying the HRV of long QT syndrome patients [58].

5.2 Comparing HRV results to thresholds

This section presents the HRV results calculated using DDFA and compares them to aerobic and anaerobic thresholds determined using lactates as well as breathing gases. The individual figures of all cycling subjects in relation to different variables are shown in Appendix A and corresponding figures for running subjects can be found in Appendix B. The variables used on the x-axis are time, HR, relative heart rate (HR_{rel}), normalized heart rate (HR_{norm}), weight-proportional oxygen uptake (VO_2/kg) and blood lactate concentration (BLa). The individual thresholds have been added to each figure with a black vertical dotted line.

Originally, the thresholds were determined and reported as either bicycle ergometer resistance power (W) or treadmill speed (km/h). Thresholds were determined either at the end of each 3-minute load, i.e., the point of the lactate measurement, or at the centre of the load if the threshold was not found to coincide directly with any of the lactate samples. These power or speed thresholds were changed so that if the threshold hit a lactate sample, the mean value for all other variables was used for the lactate sample site and the preceding 30s. If the threshold was between the lactate points, the mean values for both the points before and after the threshold were calculated in the same way, and the mean value was calculated from these two mean values. Another option would have been to read directly the corresponding values at the midpoint of the lactate measurements. Especially for HR, which is probably the most interesting and essential value for the thresholds, there was little difference between these two methods. It is worth noting that the threshold conversion method may affect the results, especially in the case of VO_2.

5.2.1 Cycling results

Figure 5.5 shows an aggregate plot of $\alpha(\mathrm{HR}, s)$ for all subjects (upper panel) together with the thresholds (lower panel) as a function of HR. The graph is thus a summary of all 15 cycling subjects whose individual α color maps are shown in Figs. A.4, A.5 and A.6. This upper panel was composed by calculating 50 even HR bins for each scale. The black vertical dashes represent the thresholds, this time the average of all 15 samples. The lower panel displays AeT and AnT distribution as a box plot. The box shows the quartiles of the dataset, while the whiskers extend to show the rest of the distribution, except for points that are determined to be outliers using a method that is a function of the inter-quartile range (IQR). In this thesis, the maximum length of the whisker was 1.5 x IQR.

Figure 5.5 shows that changes in α values occur as functions of both HR and scale. For example, on scales 5–20 and at HR < 140 BPM, which is approximately the average of AeT, α receives values between 1.25 and 2. In accordance with Table 3.1, this corresponds to highly correlated data. Similarly, when HR is greater than the average of AnT, i.e., > 170 BPM, α has small values in the range 0–0.5. This, in turn, means that the time series is anticorrelated. This behavior is clearly visible in the HR curve of Fig. 5.3.

By looking at Fig. 5.5 by horizontal rows, i.e., scales, it seems that the best resolution, i.e., the greatest change in α values, is achieved by limiting the scale range to 8–30. This range is particularly interesting and useful when trying to determine thresholds with the help of HRV. For example, Gronwald et al. [28–35] have focused on using the conventional α_1, with a scale range of 4–16. In addition, the first-order detrending was used by Gronwald et al. Based on this thesis, it seems that by using the second-order detrending, as well as slightly shifting the scale range upwards, even more accurate results could be achieved when predicting thresholds. Similar results were found previously in Ref. [63]. In particular, the observed anticorrelations appear on short scales (a few beats) at low to moderate exercise intensities. As the intensity is increased, the anticorrelations increase in magnitude and span to longer scales (up to 20–30 beats).

The same observations can also be made in the individual graphs of the subjects, presented in Figs. A.4, A.5 and A.6. However, it should be noted that the individual differences in α behavior are large. By studying the location of AeT and AnT and the ratio of α values, for example, it can be observed that the anticorrelated blue areas in subjects C9, C11, C13, C14 and C17 begin at the AnT. In contrast, for subjects with C5, C12, C24 and C26 this regime is clearly visible already between AeT and AnT. For C2, C21 and C22, this regime exists even below AeT, actually even from the very beginning of the test. In any case, for all the 15 subjects, the anticorrelations are intensified towards the end of the test, both in magnitude and scale.

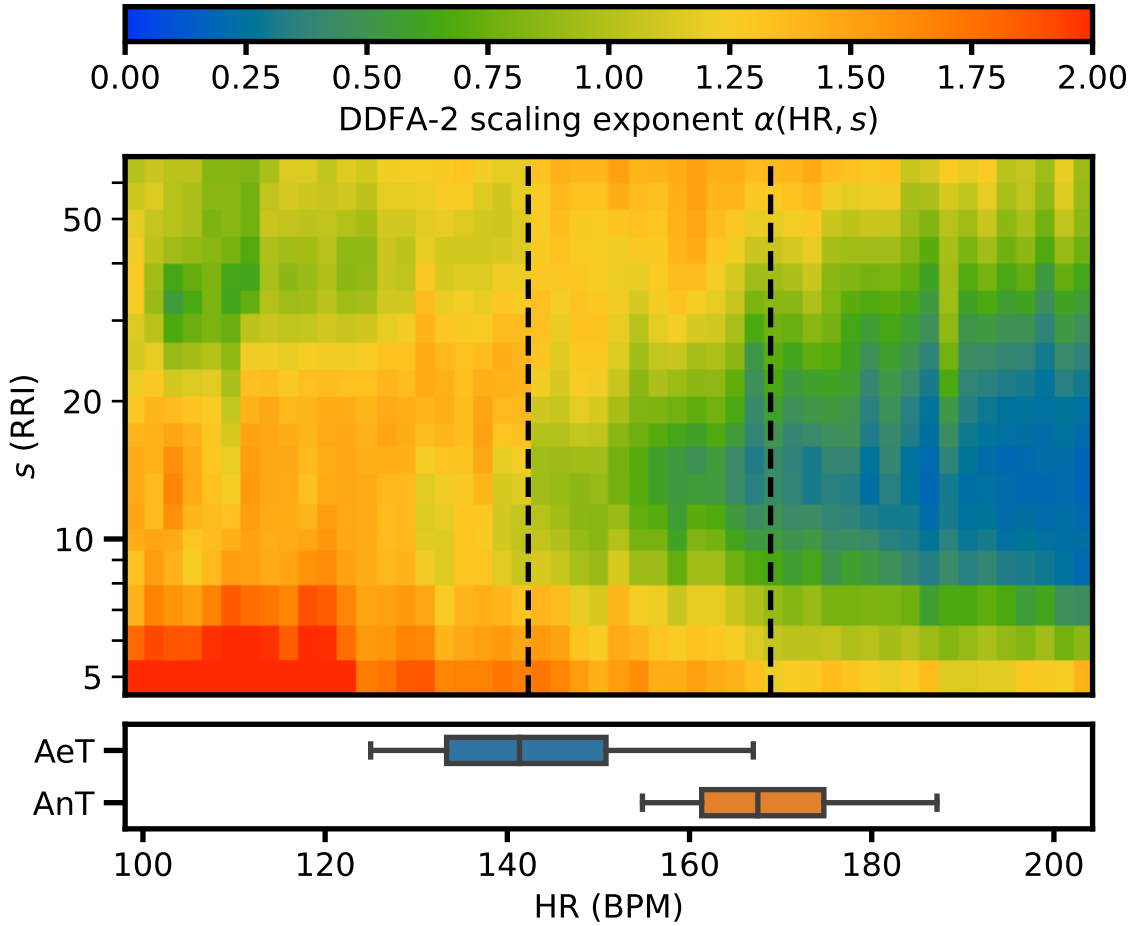

Figure 5.5. *Aggregate plot of the DDFA-2 scaling exponents for all cycling subjects as a function of the heart rate (HR). The mean values of the aerobic and anaerobic thresholds are shown as vertical dashed lines and the box plots show the distribution of these threshold values. The corresponding individual data of the subjects are presented in Figs. A.4, A.5 and A.6.*

Because HR is individual measurement, the absolute HR value is not the best measure when the thresholds are compared to each other. For example HR_{max} depends on, among other things, the age of the person. As Fig. 5.5 shows, some subjects have a higher AeT than others have an AnT. Therefore, when thresholds are compared between different subjects, it is often customary to use the relative HR (HR_{rel}), which is calculated as HR/HR_{max} [73]. Figure 5.6 shows the results as a function of HR_{rel}. Now, the thresholds are more consistent. However, exercise is known to have a great effect on the location of thresholds in the HR_{rel}. For example, experienced athletes often have thresholds closer to the HR_{max} than those with less training. On the other hand, overload or wrong kind of training can appear as exceptionally low relative thresholds.

The problem with Fig. 5.6 is the fact that the lower limit of HR_{rel} is not the same for all subjects. This is seen in detail in Figs. A.7, A.8 and A.9. For example, for the subject C12, the lowest HR during the test is about 45% of the maximum, while for C17 it is almost 70%. As a result, aggregated plot in Fig. 5.6 consists of only a few subjects

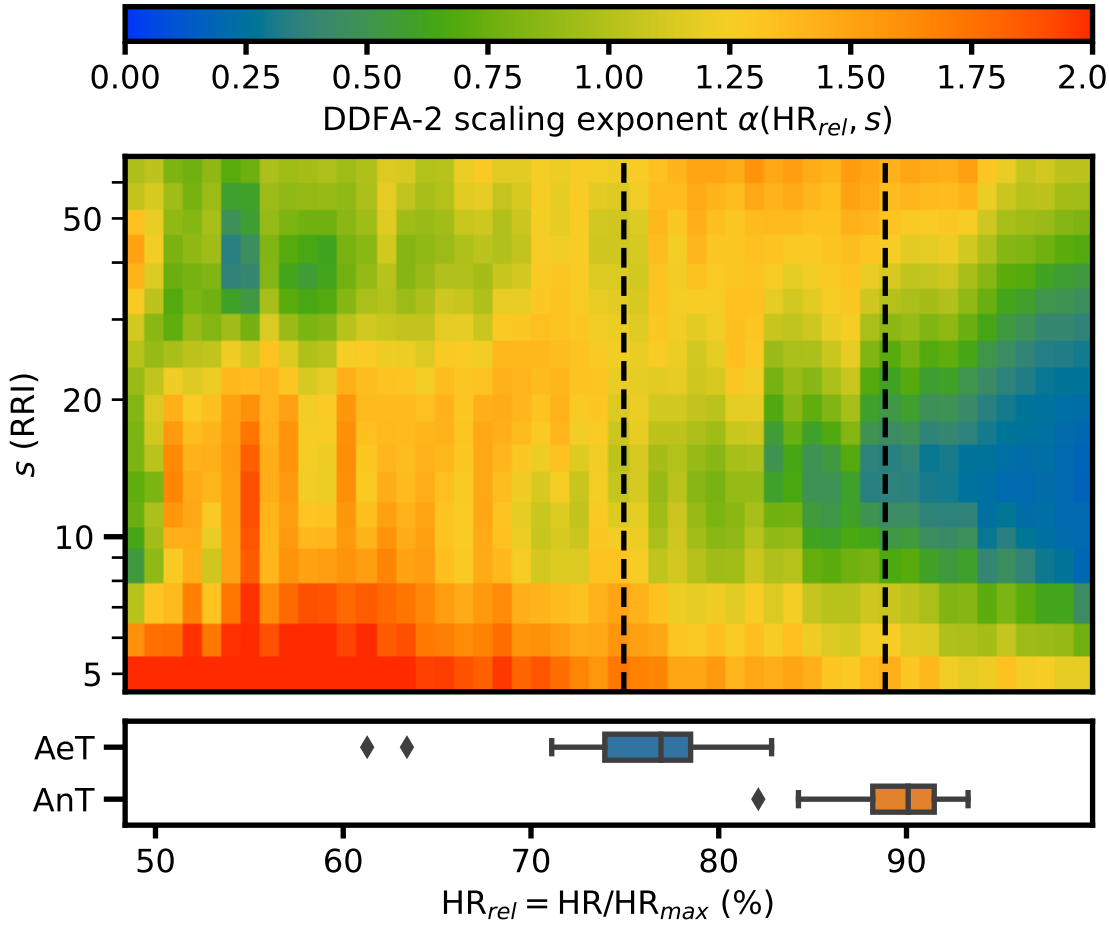

Figure 5.6. *Aggregate plot of the DDFA-2 scaling exponents for all cycling subjects as a function of the relative heart rate (HR_{rel}). The mean values of the aerobic and anaerobic thresholds are shown as vertical dashed lines and the box plots show the distribution of these threshold values. The corresponding individual data of the subjects are presented in Figs. A.7, A.8 and A.9.*

with small HR_{rel} values. The same problem also applies to Fig. 5.5 with both high and low HR values. To solve this, it is best to normalize the HR between 0 and 1 for all the subjects.The rescaling is done using min-max normalization

$$x' = a + \frac{(x - \min(x))(b - a)}{\max(x) - \min(x)}, \tag{5.1}$$

where x' is the normalized value, x is the original value and $[a, b]$ is the min-max range. In this case, interval $[0, 1]$ was used, so Eq. (5.1) can be written as

$$x' = \frac{x - \mathrm{HR}_{\min}}{\mathrm{HR}_{\max} - \mathrm{HR}_{\min}}. \tag{5.2}$$

The results for normalized HR are shown in Fig. 5.7 (aggregate) and Figs. A.10, A.11 and A.12 (individuals). The advantage of normalization is the fact that the thresholds are clearly separated from each other.

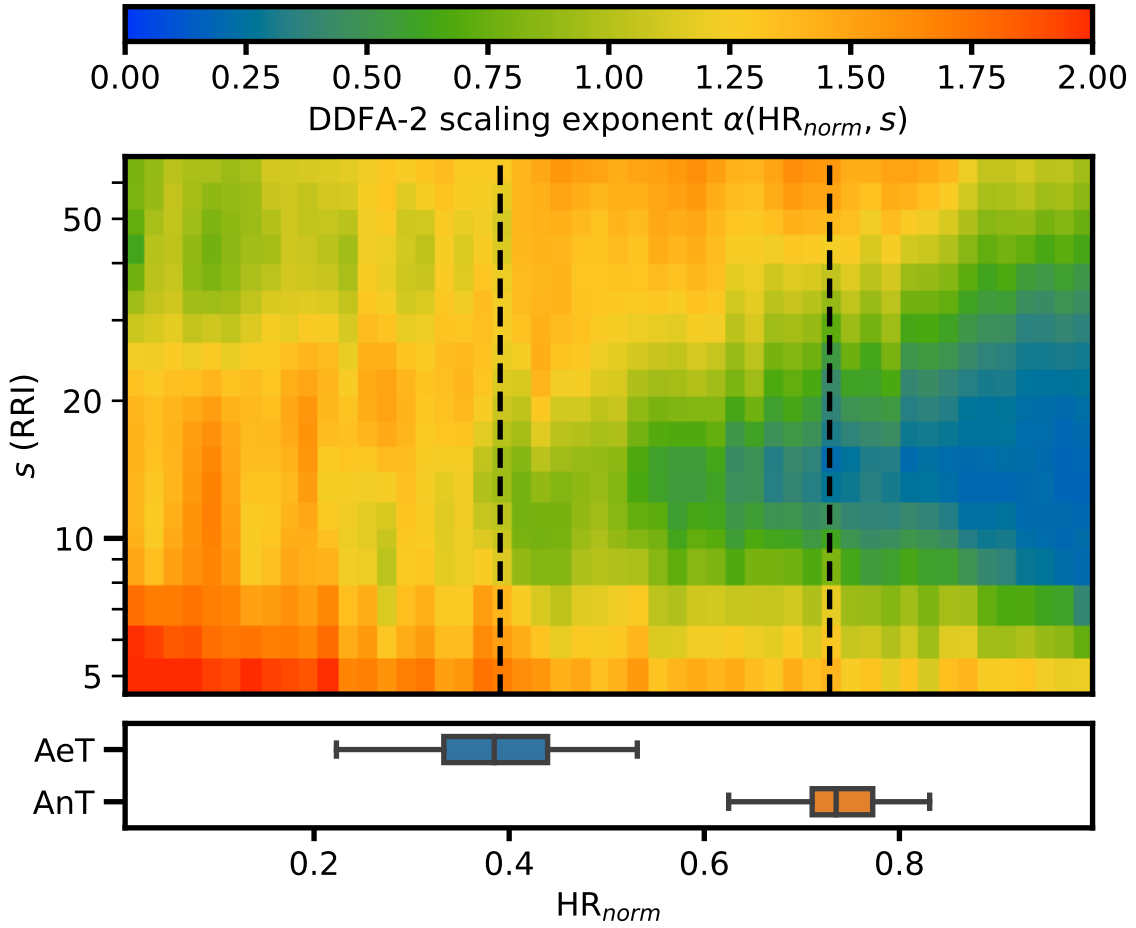

Figure 5.7. *Aggregate plot of the DDFA-2 scaling exponents for all cycling subjects as a function of the normalized heart rate (HR_{norm}). The mean values of the aerobic and anaerobic thresholds are shown as vertical dashed lines and the box plots show the distribution of these threshold values. The corresponding individual data of the subjects are presented in Figs. A.10, A.11 and A.12.*

However, it is important to remember that HR_{min} is not as accurate as HR_{max}. For example, if the starting load of the test had been chosen to be lower, it is likely that the HR at the beginning of the test would also be lower, even if the HR_{max} lactate values and thus the thresholds would have been the same.

By comparing Figs. 5.5, 5.6 and 5.7 it is found that there are no major differences in the color maps themselves or in the locations of the thresholds relative to the color map. Of course, this is entirely in line with expectations, as all three figures basically describe the same phenomenon. It can be concluded that it is necessary to delineate the scale range between about 8–30. Based on the results, it is therefore possible to propose using this range to examine the effects of increasing exercise intensity on the scaling exponent.

5.2.2 Running results

In the same way as in subsection 5.2.1 for cycling, Figs. 5.8, 5.9 and 5.10 show the corresponding aggregate plots for all subjects who completed the test on the treadmill. In general, the idea and results are the same, i.e., the value of α decreases as the HR increases, especially in the scale range between 8 and 30. However, when comparing cycling and running figures, i.e., Figs. 5.7 and 5.10, it is noticed that in cycling the values of α have greater differences. The explanation is that although the test protocol was the same, the treadmill had to be stopped for each lactate sampling for a few seconds. This led to HR reduction. When looking at α as a function of time, these "recovery periods" are clearly observed every 3 minutes. As a result, HRV changes momentarily. In Figs. B.1 and B.2, which are drawn as a function of time, the existence of these "recovery periods" is clearly observed. The analysis of the results is straightforward as a function of time. However, as a function of HR the α values during the recovery period are mixed with other values at the same HR. The problem is therefore similar to that of the "bands" of the unfiltered RRIs in Sec. 5.1. A solution could be to remove, for example, 1 min sections from the data immediately after taking the blood sample and only examine the remaining 2 min sections, corresponding to a constant state in terms of HR. Such a removal was not carried out in this thesis, as the aim was to examine the use of HRV as a whole during the test. Interval exercise data is best analyzed as a function of time so that rapid changes in HRV can be detected.

5.3 Limitations of research and future directions

This thesis does not directly provide a threshold prediction model based on HRV, but such predictions and indicators will be developed in further research [2]. However, the results above demonstrate the need for individual baseline consideration. It is essential to monitor how the values of α change *from the baseline* during the test. Of course, this also applies to lactate and respiration gas values, because individual differences can be large in them as well. The sample size of this thesis was quite small, although typical for sports physiological studies. Therefore, more data and research will be needed in the future to better understand the phenomenon and create and validate a mathematical threshold model based on HRV.

Essential questions for future research are, in particular, whether the individual differences that have emerged in the study are characteristic for each test subject, i.e., whether they will be repeated if the subject retakes the test later. If so, we could speak of an individual "α fingerprint" that would provide an accurate, reliable and reproducible basis for the HRV threshold model.

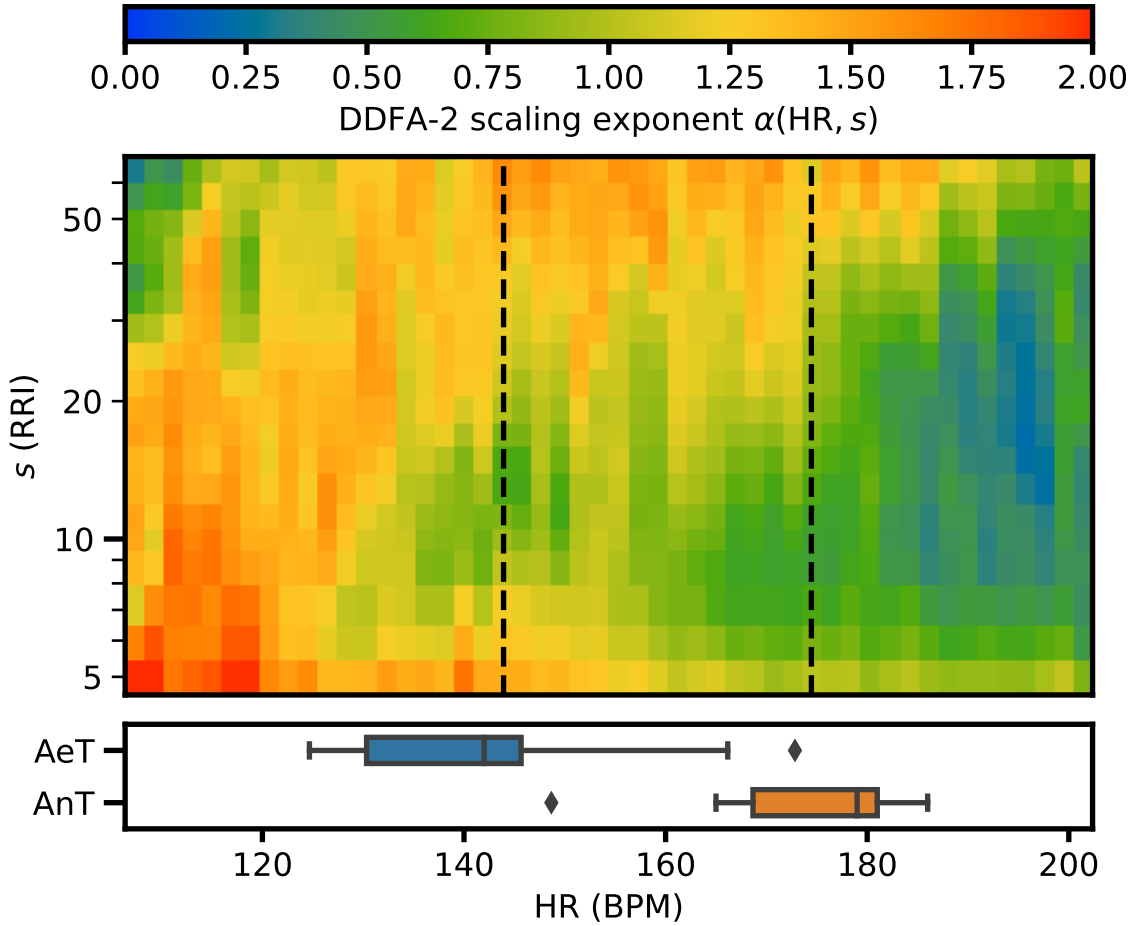

Figure 5.8. *Aggregate plot of the DDFA-2 scaling exponents for all running subjects as a function of the heart rate (HR). The mean values of the aerobic and anaerobic thresholds are shown as vertical dashed lines. In addition, the box plots show the distribution of these threshold values. The corresponding individual data of the subjects are presented in Figs. B.3 and B.4.*

Another key question is whether the behavior of α will change if the test protocol is different. In other words, if a mathematical model is developed using direct maximal oxygen uptake test as a source, the question would be whether it can be applied even in ordinary and very different types of exercises. It might be possible for a HRV to provide an estimate of the thresholds after at least certain types of high-intensity interval exercises. This would allow the athlete to check their threshold levels without tedious lactate or ventilation measurements.

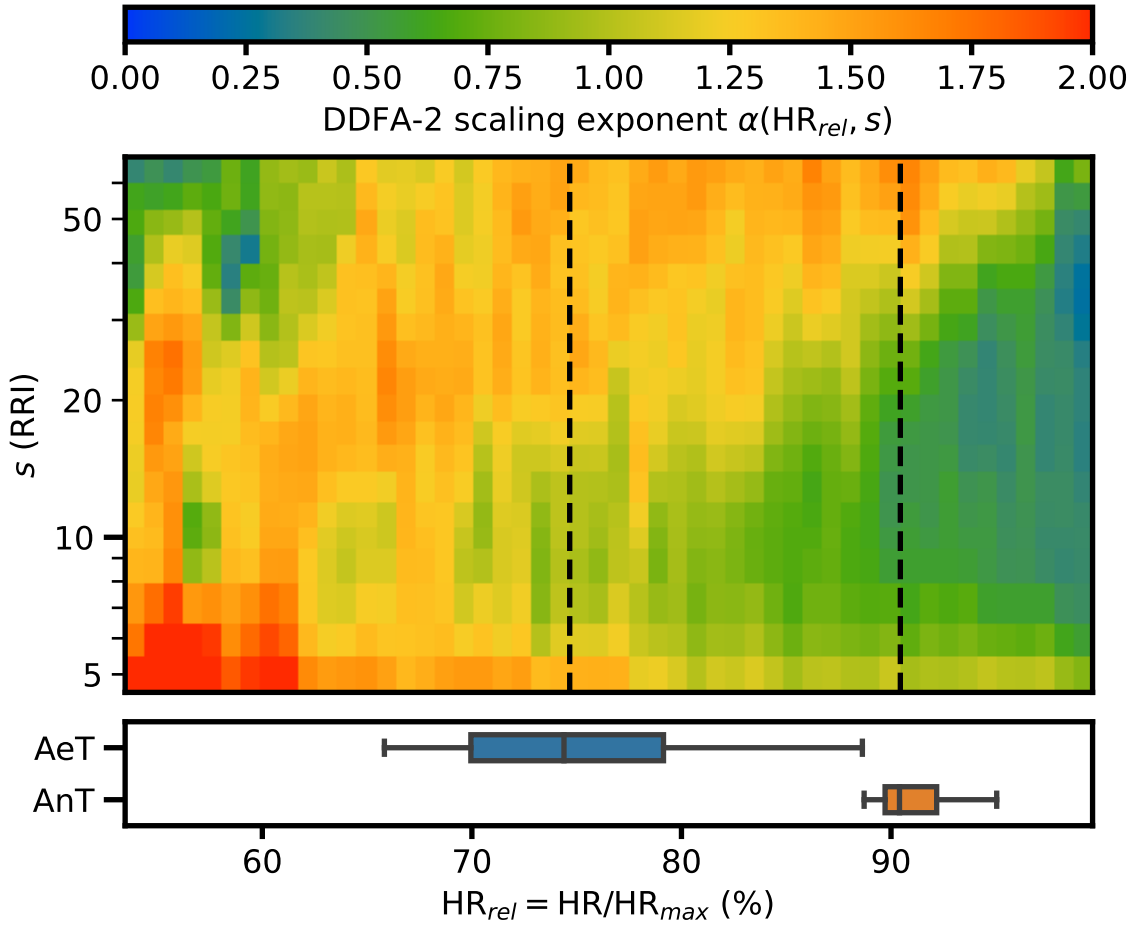

Figure 5.9. *Aggregate plot of the DDFA-2 scaling exponents for all running subjects as a function of the relative heart rate (HR_{rel}). The mean values of the aerobic and anaerobic thresholds are shown as vertical dashed lines and the box plots show the distribution of these threshold values. The corresponding individual data of the subjects are presented in Figs. B.5 and B.6.*

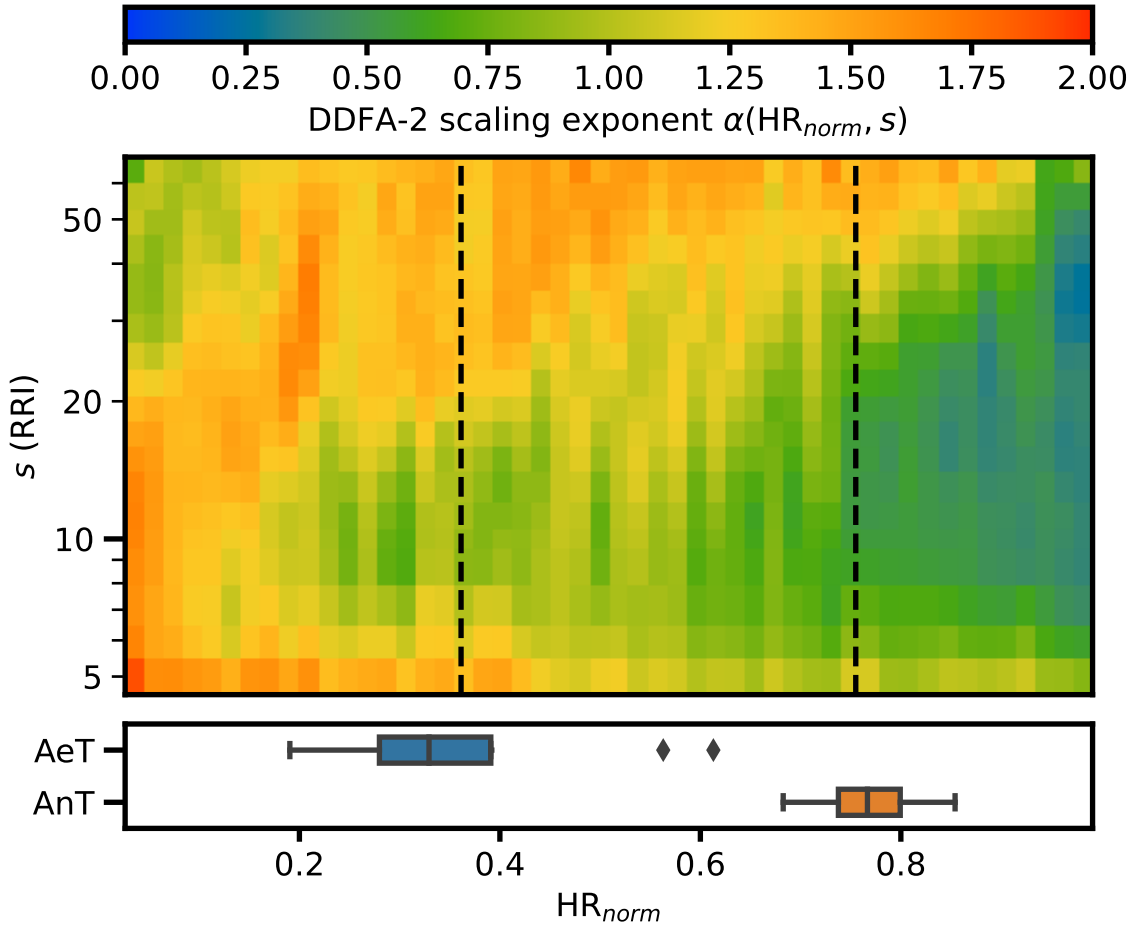

Figure 5.10. *Aggregate plot of the DDFA-2 scaling exponents for all running subjects as a function of the normalized heart rate (HR_{norm}). The mean values of the aerobic and anaerobic thresholds are shown as vertical dashed lines and the box plots show the distribution of these threshold values. The corresponding individual data of the subjects are presented in Figs. B.7 and B.8.*

6. CONCLUSIONS

The aim of this thesis was to demonstrate the qualitative link between heart rate variability (HRV) and conventional thresholds based on lactate and ventilation measurements. The thesis used the advanced time series analysis method dynamical detrended fluctuation analysis (DDFA) to systematically study HRV during increasing exercise. This method makes it possible to study the scaling exponents as functions of both scale and time, thus providing more detailed information about the scaling properties of HRV.

A total of 24 volunteers were used to perform a direct maximal oxygen uptake test using both lactate and breath gas measurements. 15 tests were performed on a bicycle ergometer and 9 on a treadmill. The lactate values, ventilation parameters and the RRI time series of consecutive heartbeats during the tests were recorded. An experienced sport scientist performed the determination of the metabolic thresholds. These aerobic and anaerobic thresholds (AeT and AnT, respectively), which are unique to each subject, were compared to results calculated from RRI with DDFA. In addition, the functionality of the DDFA method and the effect of filtering raw RRI data on the results were studied.

The results demonstrated specifically the usefulness of the second order of DDFA (DDFA-2) for the analysis of HRV data. As a method, DDFA was shown to be sensitive to clearly incorrectly defined RR intervals or completely missed strokes. Therefore, adequate filtering of RRI data was necessary. However, even significantly excessive filtering did not substantially affect the quality of the DDFA *overall* representation, as changes in the scaling exponents were clearly detected despite the fact that much of the data was filtered out unnecessarily. Of course, there were still small local differences in the scaling exponents when the results were examined in detail.

A clear and common trend for all subjects was that the value of the DDFA scaling exponent α decreases during exercise. This decrease in α values occurred throughout the whole scale range 5–64, which was used. In particular, when the HR was above AnT, the value of α was very low and the behavior of the time series was strongly anticorrelated for all the subjects. However, in some test subjects, anticorrelations did occur even before the AeT, but even then they intensified and/or spread over a wider scale range as the HR increased.

As a conclusion, scaling properties of RRIs provide a suitable basis for the development of predictions and indicators about training intensity. The results of this thesis can be used as a basis for various models in which HRV is used to estimate aerobic and/or anaerobic thresholds [2].

REFERENCES

[1] Kuisma, J., Sykevälivaihtelun skaalautumisominaisuuksien hyödyntäminen urheiluanalytiikassa, Bachelor of Science Thesis (Tampere University, 2020).

[2] Kanniainen, M., Pukkila, T., Kuisma, J., Molkkari, M., Lajunen, K. and Räsänen, E., Estimation of physiological exercise thresholds based on dynamical correlation properties of heart rate variability, submitted (2023).

[3] Shaffer, F., McCraty, R. and Zerr, C. L., A healthy heart is not a metronome: an integrative review of the heart's anatomy and heart rate variability, Frontiers in Psychology **5**, 1040–1040 (2014).

[4] Peng, C. K., Havlin, S., Hausdorff, J. M., Mietus, J. E., Stanley, H. E. and Goldberger, A. L., Fractal mechanisms and heart rate dynamics. long-range correlations and their breakdown with disease, Journal of Electrocardiology **28 Suppl**, 59–64 (1995).

[5] Shaffer, F. and Ginsberg, J., An overview of heart rate variability metrics and norms, Frontiers in Public Health **5**, 258–258 (2017).

[6] Acharya, U. R., Joseph, K. P., Kannathal, N., Lim, C. M. and Suri, J. S., Heart rate variability: a review, Medical & Biological Engineering & Computing **44**, 1031–1051 (2006).

[7] Ivanov, P. C., Amaral, L. A., Goldberger, A. L., Havlin, S., Rosenblum, M. G., Struzik, Z. R. and Stanley, H. E., Multifractality in human heartbeat dynamics, Nature (London) **399**, 461–465 (1999).

[8] ZooFari, *Heart diagram-en.svg*, License: CC BY-SA 3.0, via Wikimedia Commons, Mar. 1, 2014 (visited on 04/08/2023).

[9] Usien6, *Phases of the cardiac cycle.svg*, License: CC BY-SA 4.0, via Wikimedia Commons, July 4, 2017 (visited on 04/09/2023).

[10] ecgpedia, *Heart electrical conduction system (PQ segment).svg*, License: CC BY-SA 3.0, via Wikimedia Commons, May 17, 2022 (visited on 04/12/2023).

[11] Kennedy, A., Finlay, D. D., Guldenring, D., Bond, R., Moran, K. and McLaughlin, J., The cardiac conduction system: generation and conduction of the cardiac impulse, Critical Care Nursing Clinics of North America **28**, 269–279 (2016).

[12] Pan, J. and Tompkins, W. J., A real-time qrs detection algorithm, IEEE Transactions on Biomedical Engineering **BME-32**, 230–236 (1985).

[13] Manikandan, M. and Soman, K., A novel method for detecting r-peaks in electrocardiogram (ecg) signal, Biomedical Signal Processing and Control **7**, 118–128 (2012).

[14] Hossain, B., Bashar, S. K., Walkey, A. J., McManus, D. D. and Chon, K. H., An accurate qrs complex and p wave detection in ecg signals using complete ensemble empirical mode decomposition approach, IEEE Access **7**, 128869–128880 (2019).

[15] Jarm, T., Cvetkoska, A., Mahnič-Kalamiza, S. and Miklavcic, D., Heart rate variability calculation using heart periods measured between consecutive ponset points, *8th European Medical and Biological Engineering Conference*, Vol. 80, IFMBE Proceedings (Springer International Publishing AG, Switzerland, 2020), pp. 613–621.

[16] Malik, M., Camm, A., Bigger Jr, J., Breithardt, G., Cerutti, S., Cohen, R., Coumel, P., Fallen, E., Kennedy, H., Kleiger, R., Lombardi, F., Malliani, A., Moss, A., Rottman, J., Schmidt, G., Schwartz, P. and Singer, D., Heart rate variability. standards of measurement, physiological interpretation, and clinical use, European Heart Journal **17**, 354–381 (1996).

[17] Lam, E., Aratia, S., Wang, J. and Tung, J., Measuring heart rate variability in free-living conditions using consumer-grade photoplethysmography: validation study, JMIR Biomedical Engineering **5**, e17355 (2020).

[18] Schäfer, A. and Vagedes, J., How accurate is pulse rate variability as an estimate of heart rate variability?: a review on studies comparing photoplethysmographic technology with an electrocardiogram, International Journal of Cardiology **166**, 15–29 (2013).

[19] Ryan, S. M., Goldberger, A. L., Pincus, S. M., Mietus, J. and Lipsitz, L. A., Gender- and age-related differences in heart rate dynamics: are women more complex than men?, Journal of the American College of Cardiology **24**, 1700–1707 (1994).

[20] Billman, G. E., The effect of heart rate on the heart rate variability response to autonomic interventions, Frontiers in Physiology **4**, 222–222 (2013).

[21] Pham, T., Lau, Z. J., Chen, S. H. A. and Makowski, D., Heart rate variability in psychology: a review of hrv indices and an analysis tutorial, Sensors (Basel, Switzerland) **21**, 3998 (2021).

[22] Garcia, A. J., Koschnitzky, J. E., Dashevskiy, T. and Ramirez, J.-M., Cardiorespiratory coupling in health and disease, Autonomic Neuroscience **175**, 26–37 (2013).

[23] Julien, C., The enigma of mayer waves: facts and models, Cardiovascular Research **70**, 12–21 (2006).

[24] Julien, C., An update on the enigma of mayer waves, Cardiovascular Research **116**, e210–e211 (2020).

[25] Michael, S., Graham, K. S. and Oam, G. M. D., Cardiac autonomic responses during exercise and post-exercise recovery using heart rate variability and systolic time intervals-a review, Frontiers in Physiology **8**, 301–301 (2017).

[26] Kaikkonen, P., Hynynen, E., Mann, T., Rusko, H. and Nummela, A., Can hrv be used to evaluate training load in constant load exercises?, European Journal of Applied Physiology **108**, 435–442 (2010).

[27] Ramos-Campo, D. J., Rubio-Arias, J. A., Ávila-Gandía, V., Marín-Pagán, C., Luque, A. and Alcaraz, P. E., Heart rate variability to assess ventilatory thresholds in professional basketball players, Journal of Sport and Health Science **6**, 468–473 (2017).

[28] Gronwald, T. and Hoos, O., Correlation properties of heart rate variability during endurance exercise: a systematic review, Annals of Noninvasive Electrocardiology **25**, e12697 (2020).

[29] Gronwald, T., Rogers, B. and Hoos, O., Fractal correlation properties of heart rate variability: a new biomarker for intensity distribution in endurance exercise and training prescription?, Frontiers in Physiology **11**, 1152 (2020).

[30] Rogers, B., Giles, D., Draper, N., Hoos, O. and Gronwald, T., A new detection method defining the aerobic threshold for endurance exercise and training prescription based on fractal correlation properties of heart rate variability, Frontiers in Physiology **11**, 1806 (2021).

[31] Rogers, B., Giles, D., Draper, N., Mourot, L. and Gronwald, T., Detection of the anaerobic threshold in endurance sports: validation of a new method using correlation properties of heart rate variability, Journal of Functional Morphology and Kinesiology **6**, 38 (2021).

[32] Rogers, B. and Gronwald, T., Fractal correlation properties of heart rate variability as a biomarker for intensity distribution and training prescription in endurance exercise: an update, Frontiers in Physiology **13**, 879071–879071 (2022).

[33] Gronwald, T., Hoos, O., Ludyga, S. and Hottenrott, K., Non-linear dynamics of heart rate variability during incremental cycling exercise, Research in Sports Medicine **27**, 88–98 (2019).

[34] Gronwald, T., Berk, S., Altini, M., Mourot, L., Hoos, O. and Rogers, B., Real-time estimation of aerobic threshold and exercise intensity distribution using fractal correlation properties of heart rate variability: a single-case field application in a former olympic triathlete, Frontiers in Sports and Active Living **3**, 148 (2021).

[35] Rogers, B., Schaffarczyk, M. and Gronwald, T., Improved estimation of exercise intensity thresholds by combining dual non-invasive biomarker concepts: correlation properties of heart rate variability and respiratory frequency, Sensors (Basel, Switzerland) **23**, 1973 (2023).

[36] Borresen, J. and Lambert, M. I., The quantification of training load, the training response and the effect on performance, Sports Medicine (Auckland) **39**, 779–795 (2009).

[37] Emig, T. and Peltonen, J., Human running performance from real-world big data, Nature Communications **11**, 4936–4936 (2020).

[38] Gaskill, S., Ruby, B., Walker, A., Sanchez, O., Serfass, R. and Leon, A., Validity and reliability of combining three methods to determine ventilatory threshold, Medicine and Science in Sports and Exercise **33**, 1841–1848 (2001).

[39] Faude, O., Kindermann, W. and Meyer, T., Lactate threshold concepts: how valid are they?, Sports Medicine (Auckland) **39**, 469–490 (2009).

[40] Seiler, K. S. and Kjerland, G. Ø., Quantifying training intensity distribution in elite endurance athletes: is there evidence for an "optimal" distribution?, Scandinavian Journal of Medicine & Science in Sports **16**, 49–56 (2006).

[41] Stöggl, T. and Sperlich, B., Polarized training has greater impact on key endurance variables than threshold, high intensity, or high volume training, Frontiers in Physiology **5**, 33–33 (2014).

[42] Vähä-Ypyä, H., Sievänen, H., Husu, P., Tokola, K. and Vasankari, T., Intensity paradox–low-fit people are physically most active in terms of their fitness, Sensors (Basel, Switzerland) **21**, 2063 (2021).

[43] Task Force of the European Society of Cardiology and the North American Society of Pacing and Electrophysiology, Heart rate variability: standards of measurement, physiological interpretation and clinical use., Circulation (New York, N.Y.) **93**, 1043–1065 (1996).

[44] Tarvainen, M. P., Niskanen, J.-P., Lipponen, J. A., Ranta-aho, P. O. and Karjalainen, P. A., Kubios hrv – heart rate variability analysis software, Computer Methods and Programs in Biomedicine **113**, 210–220 (2014).

[45] Brennan, M., Palaniswami, M. and Kamen, P., Do existing measures of poincare plot geometry reflect nonlinear features of heart rate variability?, IEEE Transactions on Biomedical Engineering **48**, 1342–1347 (2001).

[46] Richman, J. S. and Moorman, J. R., Physiological time-series analysis using approximate entropy and sample entropy, American Journal of Physiology. Heart and Circulatory Physiology **278**, H2039–H2049 (2000).

[47] Guzzetti, S., Signorini, M. G., Cogliati, C., Mezzetti, S., Porta, A., Cerutti, S. and Malliani, A., Non-linear dynamics and chaotic indices in heart rate variability of normal subjects and heart-transplanted patients, Cardiovascular Research **31**, 441–446 (1996).

[48] Webber C. L., J. and Zbilut, J. P., Dynamical assessment of physiological systems and states using recurrence plot strategies, Journal of Applied Physiology **76**, 965–973 (1994).

[49] Peng, C. K., Havlin, S., Stanley, H. E. and Goldberger, A. L., Quantification of scaling exponents and crossover phenomena in nonstationary heartbeat time series, Chaos (Woodbury, N.Y.) **5**, 82–87 (1995).

[50] Kantelhardt, J. W., Koscielny-Bunde, E., Rego, H. H., Havlin, S. and Bunde, A., Detecting long-range correlations with detrended fluctuation analysis, Physica A: Statistical Mechanics and its Applications **295**, 441–454 (2001).

[51] Peng, C. K., Buldyrev, S. V., Havlin, S., Simons, M., Stanley, H. E. and Goldberger, A. L., Mosaic organization of dna nucleotides, Physical Review E **49**, 1685–1689 (1994).

[52] Orun, M. and Koçak, K., Applicatıon of detrended fluctuation analysis to temperature data from turkey, International Journal of Climatology **29**, 2130–2136 (2009).

[53] Santhanam, M., Bandyopadhyay, J. and Angom, D., Quantum spectrum as a time series : fluctuation measures, Physical Review E **73**, 015201 (2006).

[54] Varotsos, P. A., Sarlis, N. V. and Skordas, E. S., Detrended fluctuation analysis of the magnetic and electric field variations that precede rupture, Chaos (Woodbury, N.Y.) **19**, 023114–023114 (2009).

[55] Räsänen, E., Pulkkinen, O., Virtanen, T., Zollner, M. and Hennig, H., Fluctuations of hi-hat timing and dynamics in a virtuoso drum track of a popular music recording, PLoS ONE **10**, e0127902 (2015).

[56] Goldberger, A., Amaral, L., Hausdorff, J., Ivanov, P., Peng, C.-K. and Stanley, H., Fractal dynamics in physiology: alterations with disease and aging, Proceedings of the National Academy of Sciences of the United States of America **99**, 2466–2472 (2002).

[57] Havlin, S., Amaral, L., Ashkenazy, Y., Goldberger, A., Ivanov, P., Peng, C.-K. and Stanley, H., Application of statistical physics to heartbeat diagnosis, Physica A: Statistical Mechanics and its Applications **274**, 99–110 (1999).

[58] Pukkila, T., Molkkari, M., Kim, J. and Räsänen, E., Reduced rr interval correlations of long qt syndrome patients, 2022 Computing in Cardiology (CinC) (2022).

[59] Ivanov, P. C., Bunde, A., Amaral, L. A. N., Havlin, S., Fritsch-Yelle, J., Baevsky, R. M., Stanley, H. E. and Goldberger, A. L., Sleep-wake differences in scaling behavior of the human heartbeat: analysis of terrestrial and long-term space flight data, Europhysics Letters **48**, 594–600 (1999).

[60] Kantelhardt, J. W., Ashkenazy, Y., Ivanov, P. C., Bunde, A., Havlin, S., Penzel, T., Peter, J.-H. and Eugene Stanley, H., Characterization of sleep stages by correlations in the magnitude and sign of heartbeat increments, Physical Review E **65**, 051908 (2002).

[61] Bellenger, C. R., Arnold, J. B., Buckley, J. D., Thewlis, D. and Fuller, J. T., Detrended fluctuation analysis detects altered coordination of running gait in athletes following a heavy period of training, Journal of Science and Medicine in Sport **22**, 294–299 (2019).

[62] Platisa, M. M. and Gal, V., Correlation properties of heartbeat dynamics, European Biophysics Journal **37**, 1247–1252 (2008).

[63] Molkkari, M., Angelotti, G., Emig, T. and Rasanen, E., Dynamical heart beat correlations during running, Scientific Reports **10**, 13627–13627 (2020).

[64] Cross, T. J., Morris, N. R., Schneider, D. A. and Sabapathy, S., Evidence of breakpoints in breathing pattern at the gas-exchange thresholds during incremental cycling in young, healthy subjects, European Journal of Applied Physiology **112**, 1067–1076 (2012).

[65] Molkkari, M., Advanced methods in detrended fluctuation analysis with applications in computational cardiology, Master of Science Thesis (Tampere University, 2019).

[66] Pukkila, T., Molkkari, M. and Rasanen, E., Dynamical heart beat correlations during complex tasks - a case study in automobile driving, 2021 Computing in Cardiology (CinC) (2021).

[67] Toivonen, E., Molkkari, M., Räsänen, E. and Laurson, L., Asymmetric roughness of elastic interfaces at the depinning threshold, Physical Review Letters **129**, 175701–175701 (2022).

[68] Toivonen, E., Paperitehtaan jätevesien aikasarja-analyysi ja vedenkäsittelyprosessien optimointi, Master of Science Thesis (Tampere University, 2023).

[69] Keskinen, K. L., Häkkinen, K., Kallinen, M. and Aho, J., *Kuntotestauksen käsikirja* (Liikuntatieteellinen seura, Helsinki, 2007).

[70] Gilgen-Ammann, R., Schweizer, T. and Wyss, T., Rr interval signal quality of a heart rate monitor and an ecg holter at rest and during exercise, European Journal of Applied Physiology **119**, 1525–1532 (2019).

[71] Schaffarczyk, M., Rogers, B., Reer, R. and Gronwald, T., Validity of the polar h10 sensor for heart rate variability analysis during resting state and incremental exercise in recreational men and women, Sensors (Basel, Switzerland) **22**, 6536 (2022).

[72] dos Santos, L., Barroso, J. J., Macau, E. E. and de Godoy, M. F., Application of an automatic adaptive filter for heart rate variability analysis, Medical Engineering & Physics **35**, 1778–1785 (2013).

[73] Mann, T., Lamberts, R. P. and Lambert, M. I., Methods of prescribing relative exercise intensity: physiological and practical considerations, Sports Medicine (Auckland) **43**, 613–625 (2013).

APPENDIX A: CYCLING FIGURES

This appendix contains additional pictures of all the subjects who took the test on the cyclo-ergometer.

List of Figures in Appendix A

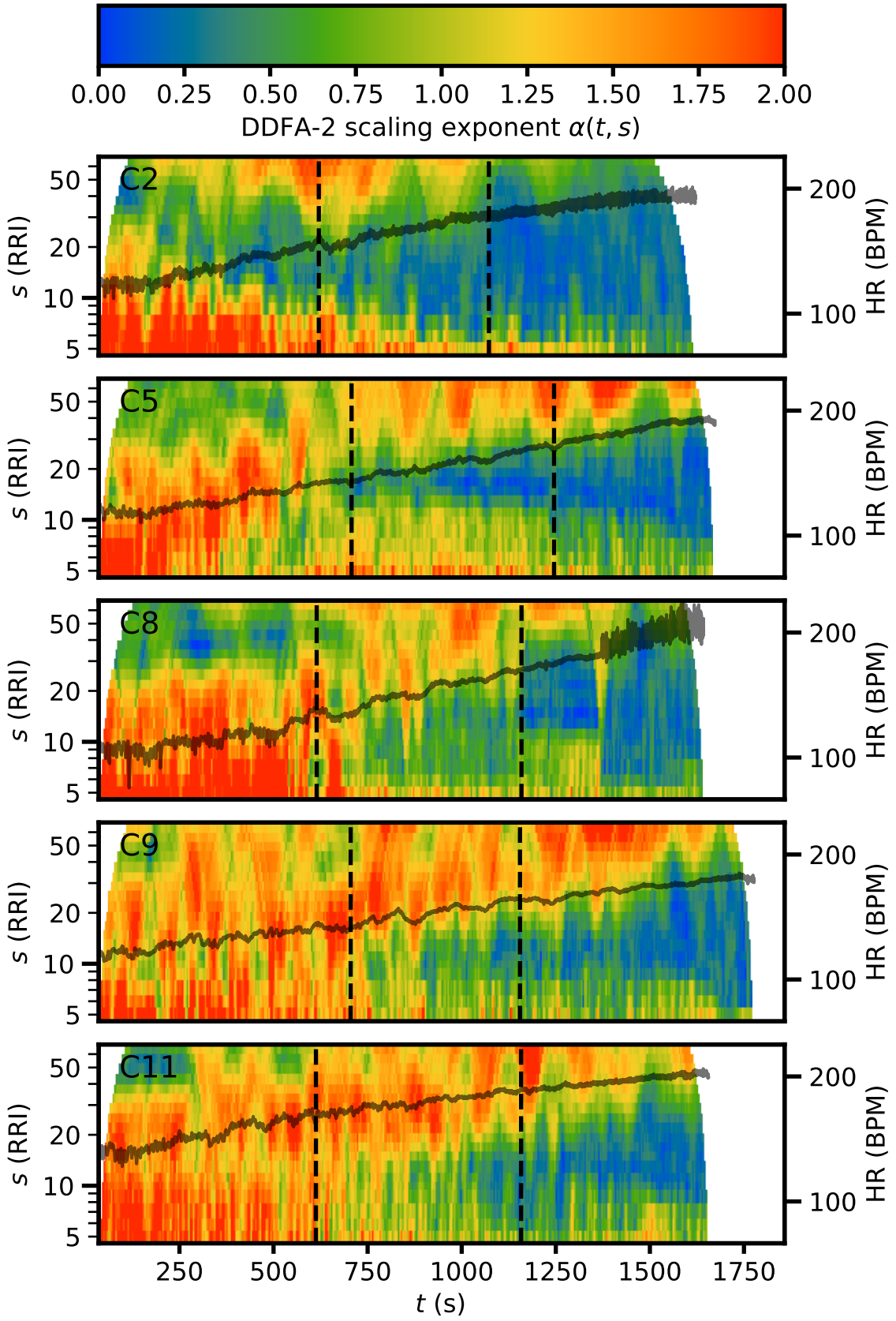

Figure A.1. *DDFA-2 scaling exponents and the heart rate (HR) for cycling subjects C2–C11 as a function of the time t. The aerobic and anaerobic thresholds are shown as vertical dashed lines.*

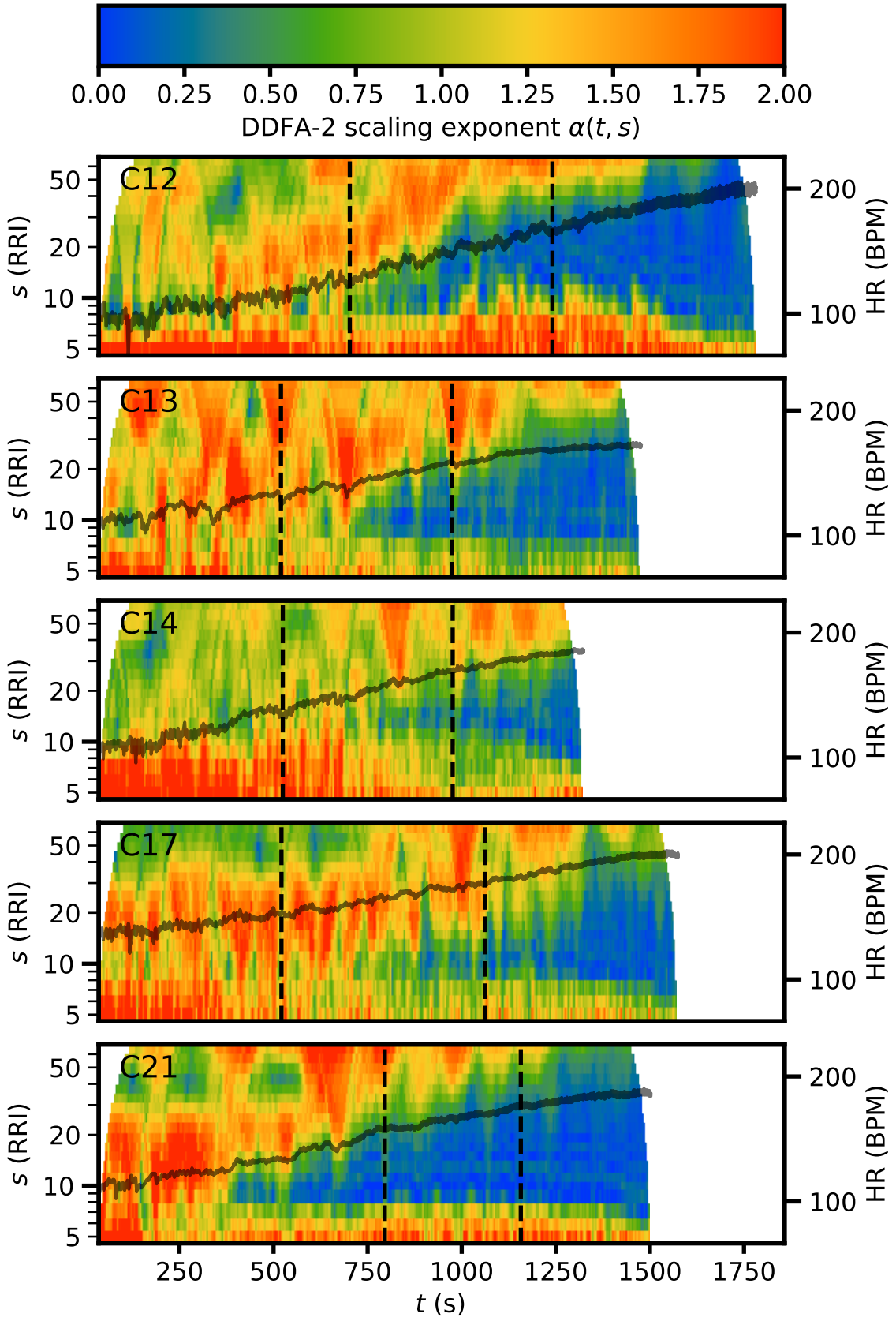

Figure A.2. *DDFA-2 scaling exponents and the heart rate (HR) for cycling subjects C12–C21 as a function of the time t. The aerobic and anaerobic thresholds are shown as vertical dashed lines.*

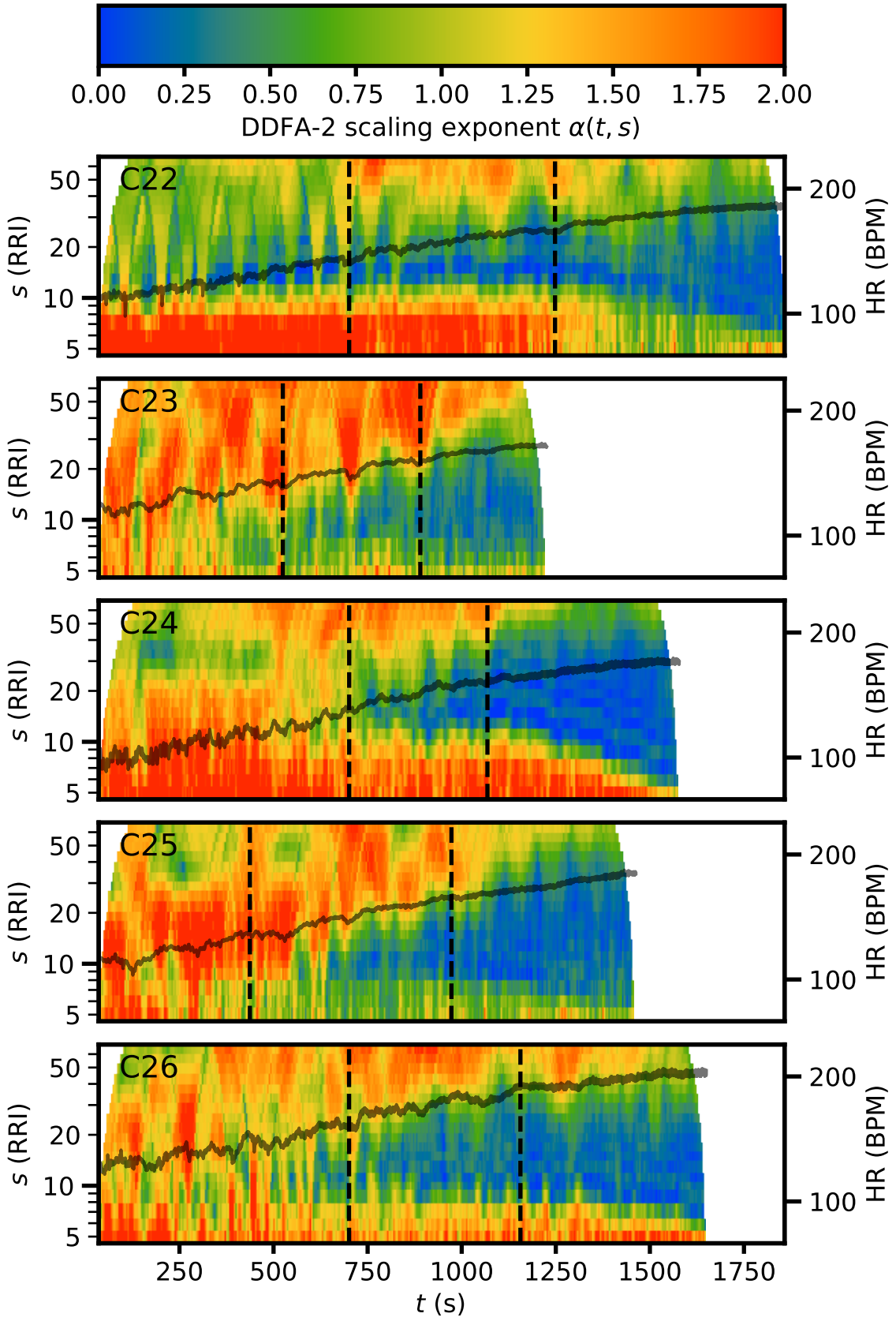

Figure A.3. *DDFA-2 scaling exponents and the heart rate (HR) for cycling subjects C22–C26 as a function of the time t. The aerobic and anaerobic thresholds are shown as vertical dashed lines.*

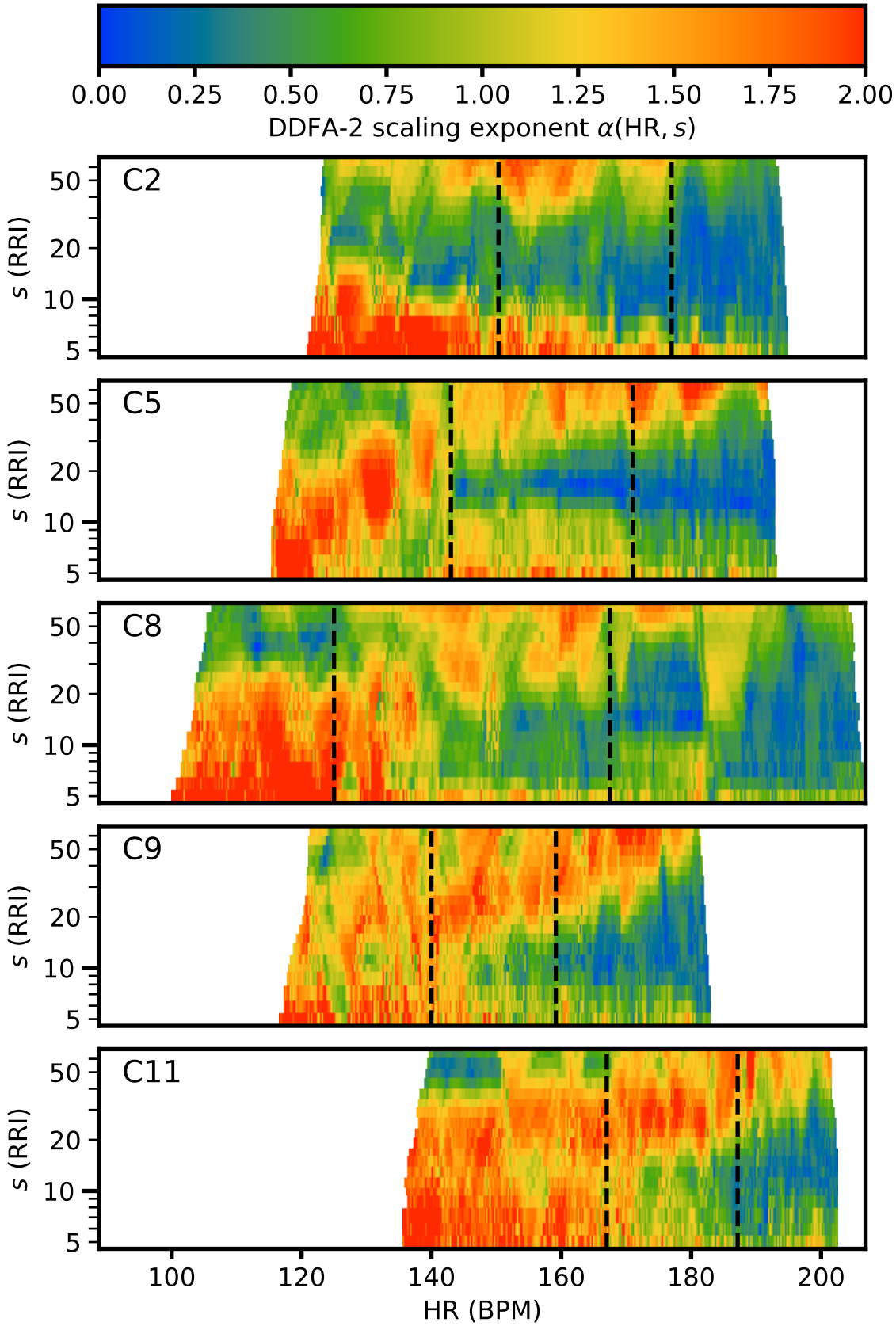

Figure A.4. *DDFA-2 scaling exponents for cycling subjects C2–C11 as a function of the heart rate (HR). The aerobic and anaerobic thresholds are shown as vertical dashed lines.*

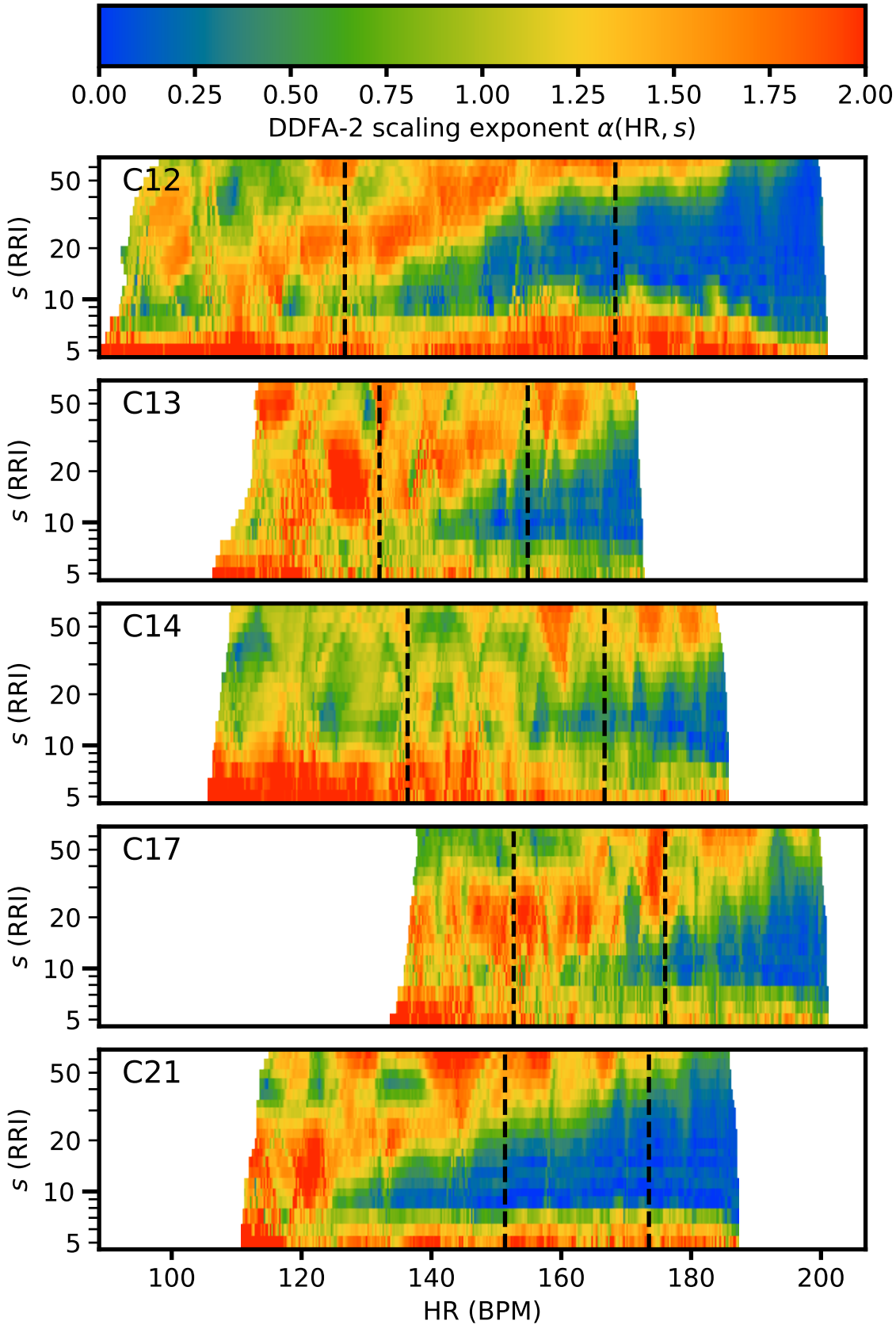

Figure A.5. *DDFA-2 scaling exponents for cycling subjects C12–C21 as a function of the heart rate (HR). The aerobic and anaerobic thresholds are shown as vertical dashed lines.*

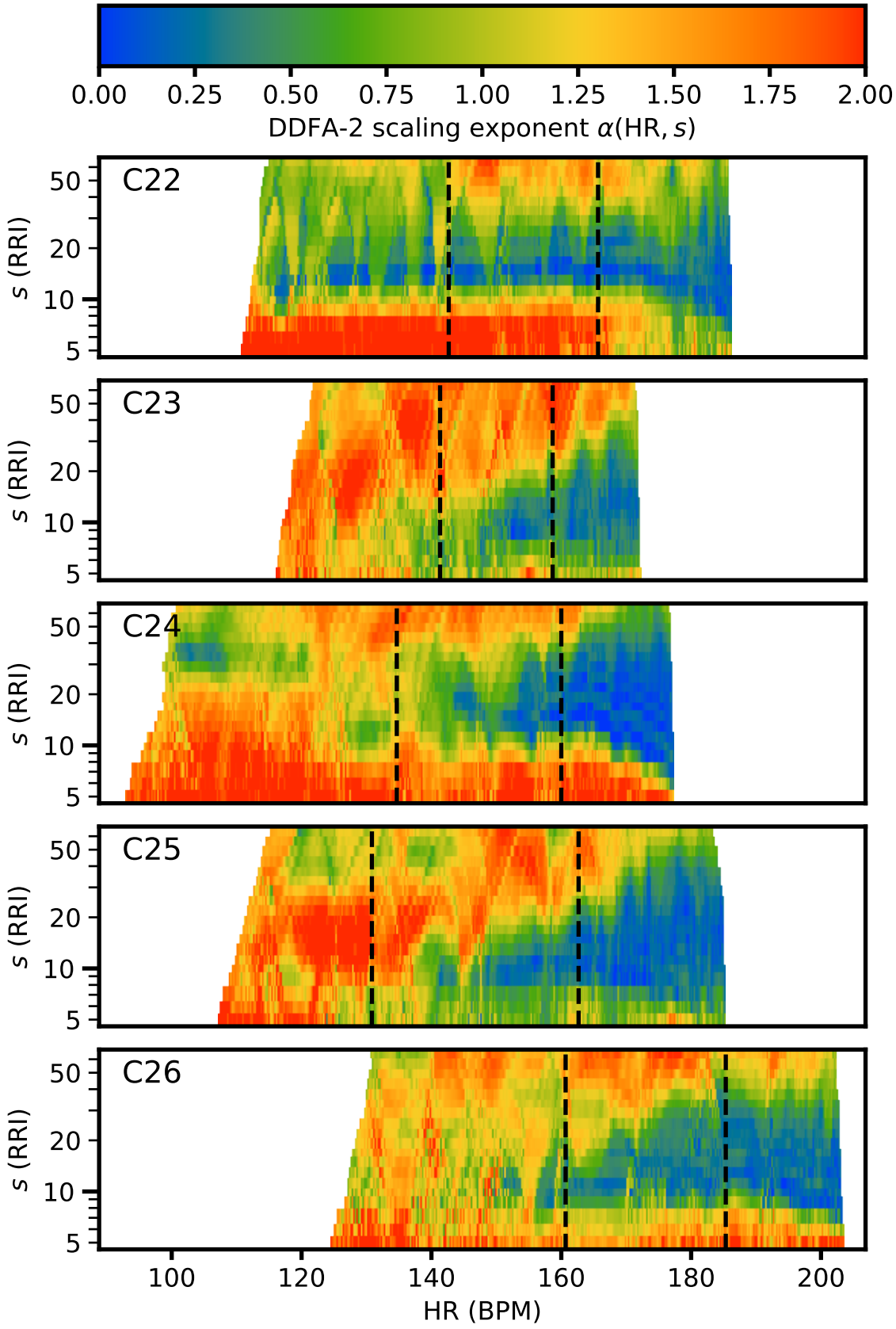

Figure A.6. *DDFA-2 scaling exponents for cycling subjects C22–C26 as a function of the heart rate (HR). The aerobic and anaerobic thresholds are shown as vertical dashed lines.*

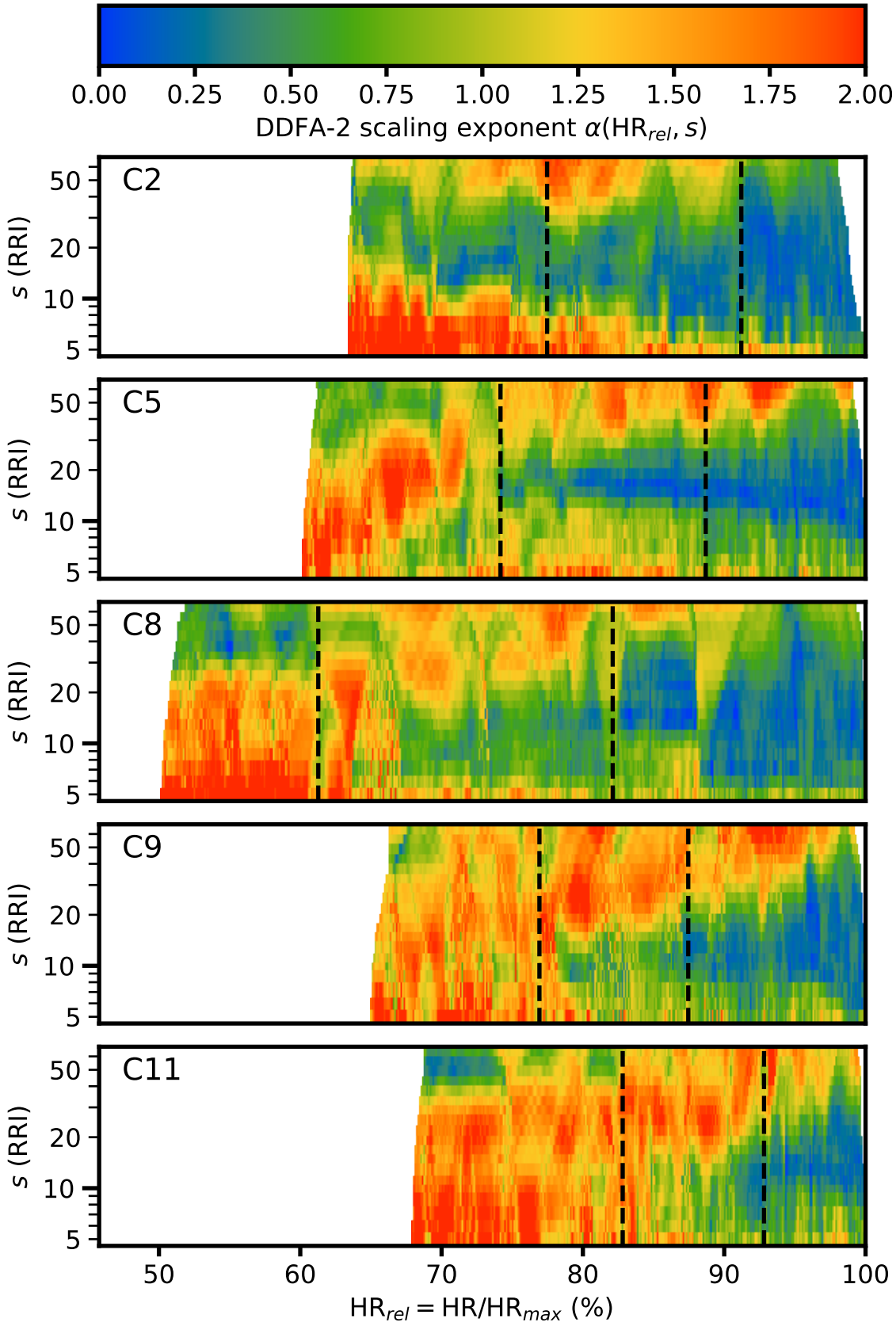

Figure A.7. *DDFA-2 scaling exponents for cycling subjects C2–C11 as a function of the relative heart rate (HR_{rel}). The aerobic and anaerobic thresholds are shown as vertical dashed lines.*

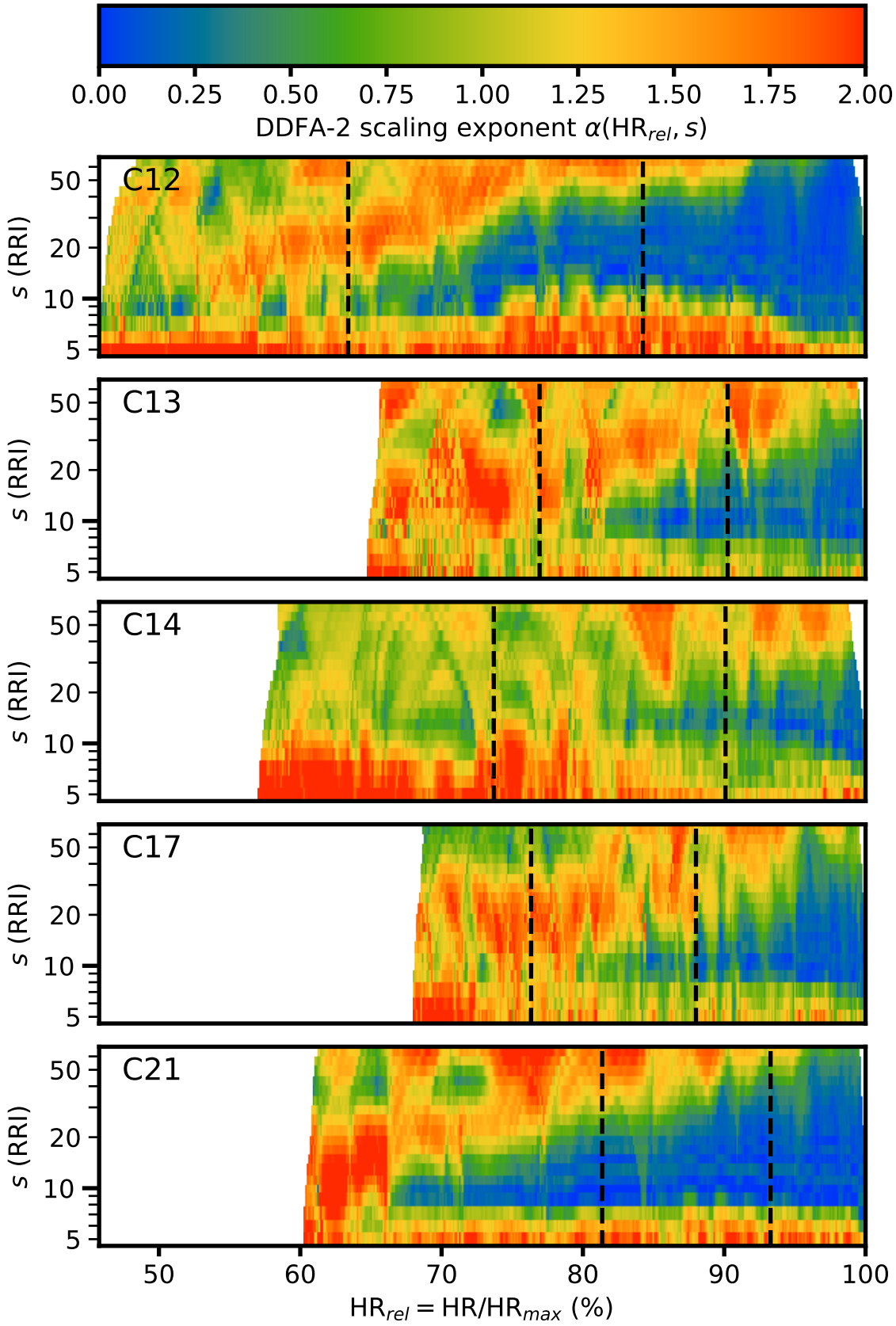

Figure A.8. *DDFA-2 scaling exponents for cycling subjects C12–C21 as a function of the relative heart rate (HR_{rel}). The aerobic and anaerobic thresholds are shown as vertical dashed lines.*

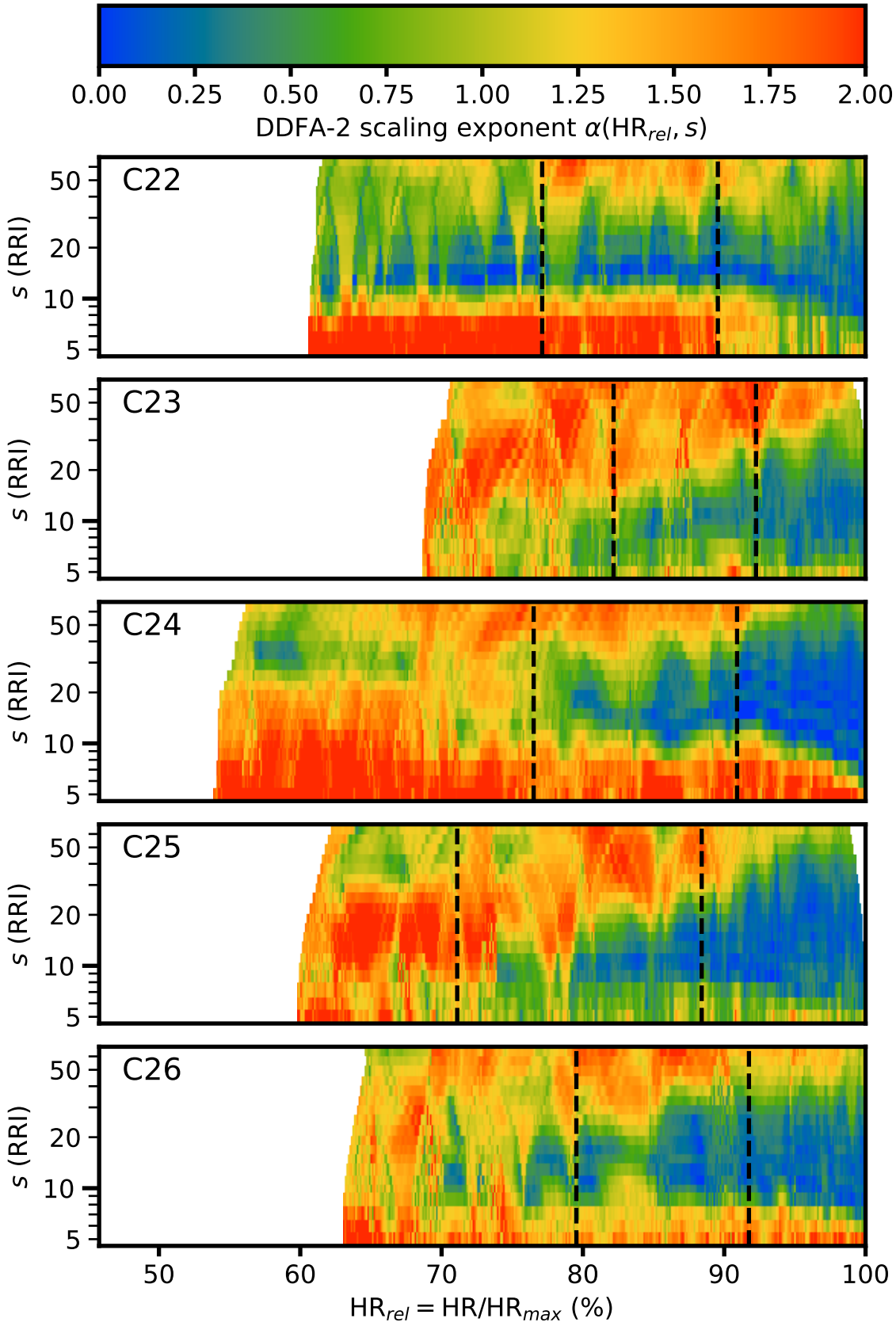

Figure A.9. *DDFA-2 scaling exponents for cycling subjects C22–C26 as a function of the relative heart rate (HR_{rel}). The aerobic and anaerobic thresholds are shown as vertical dashed lines.*

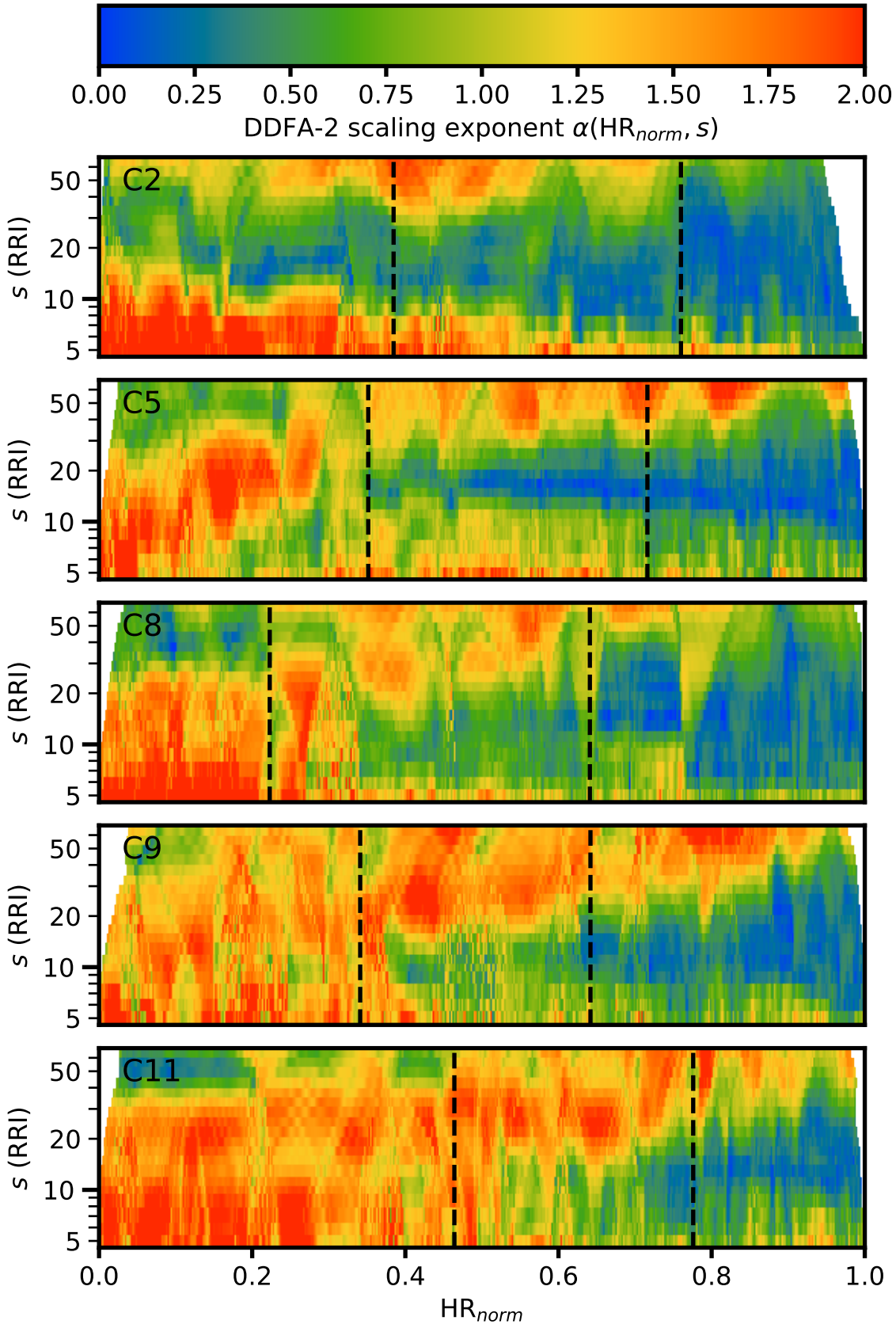

Figure A.10. *DDFA-2 scaling exponents for cycling subjects C2–C11 as a function of the normalized heart rate (HR_{norm}). The aerobic and anaerobic thresholds are shown as vertical dashed lines.*

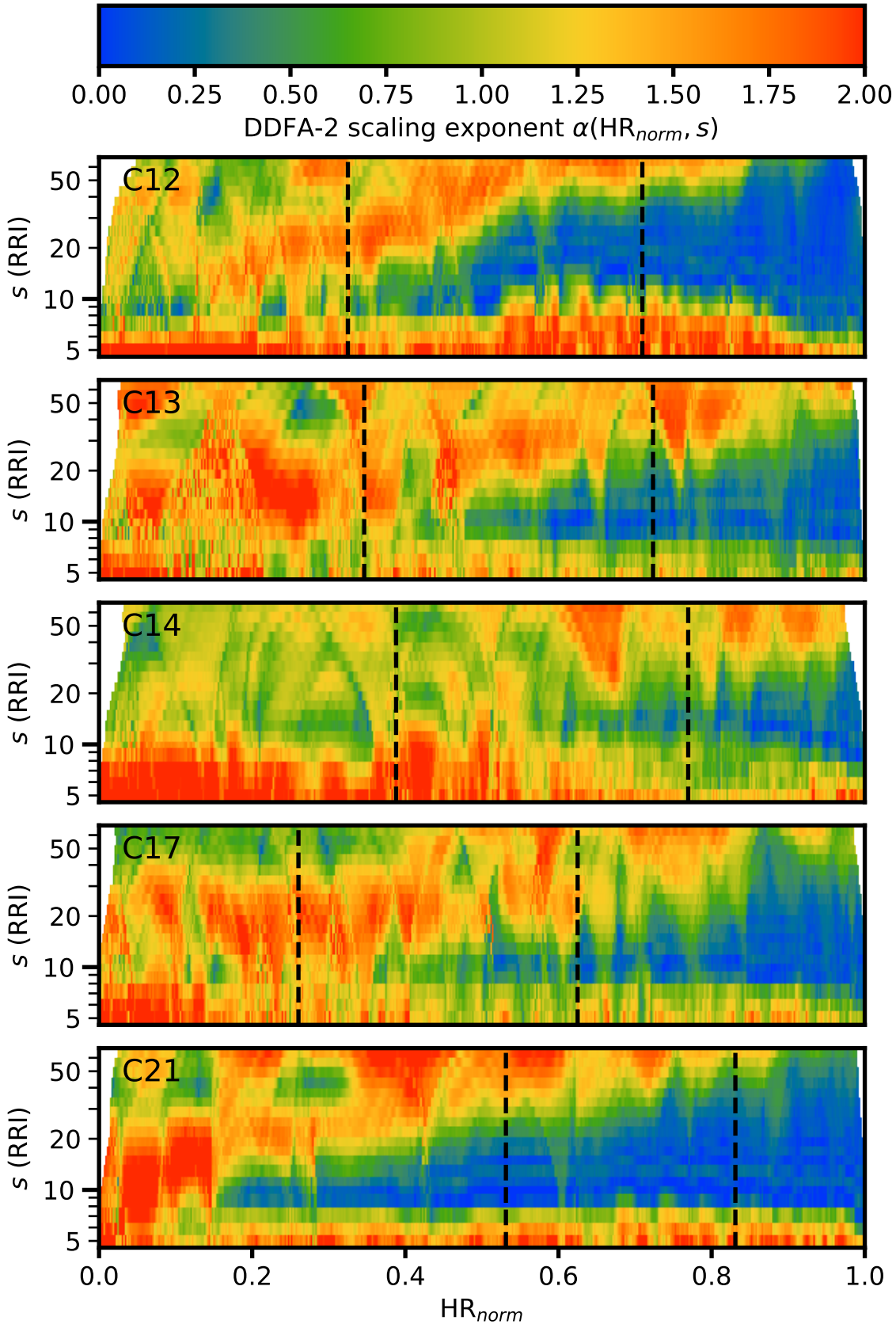

Figure A.11. *DDFA-2 scaling exponents for cycling subjects C12–C21 as a function of the normalized heart rate (HR_{norm}). The aerobic and anaerobic thresholds are shown as vertical dashed lines.*

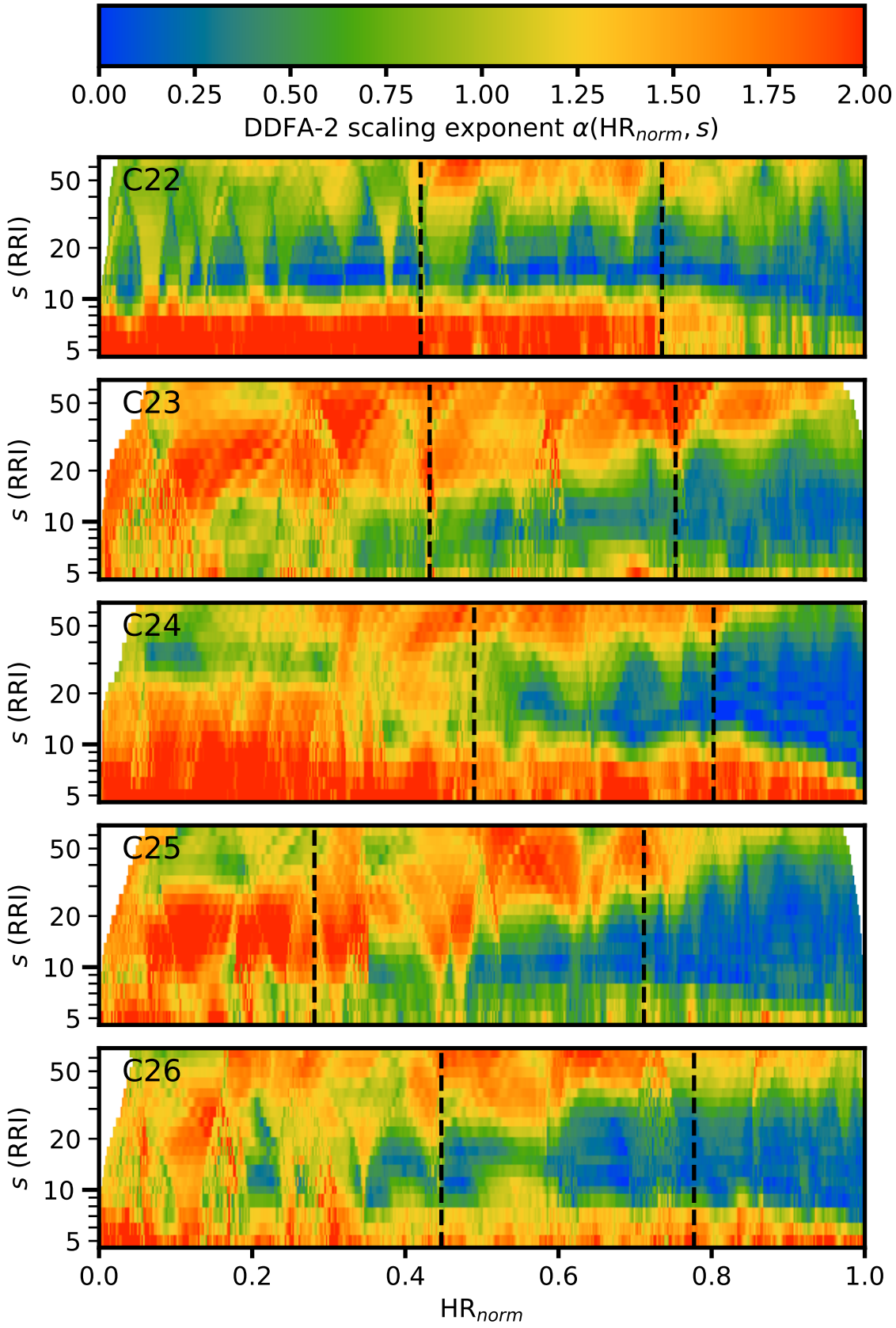

Figure A.12. *DDFA-2 scaling exponents for cycling subjects C22–C26 as a function of the normalized heart rate (HR_{norm}). The aerobic and anaerobic thresholds are shown as vertical dashed lines.*

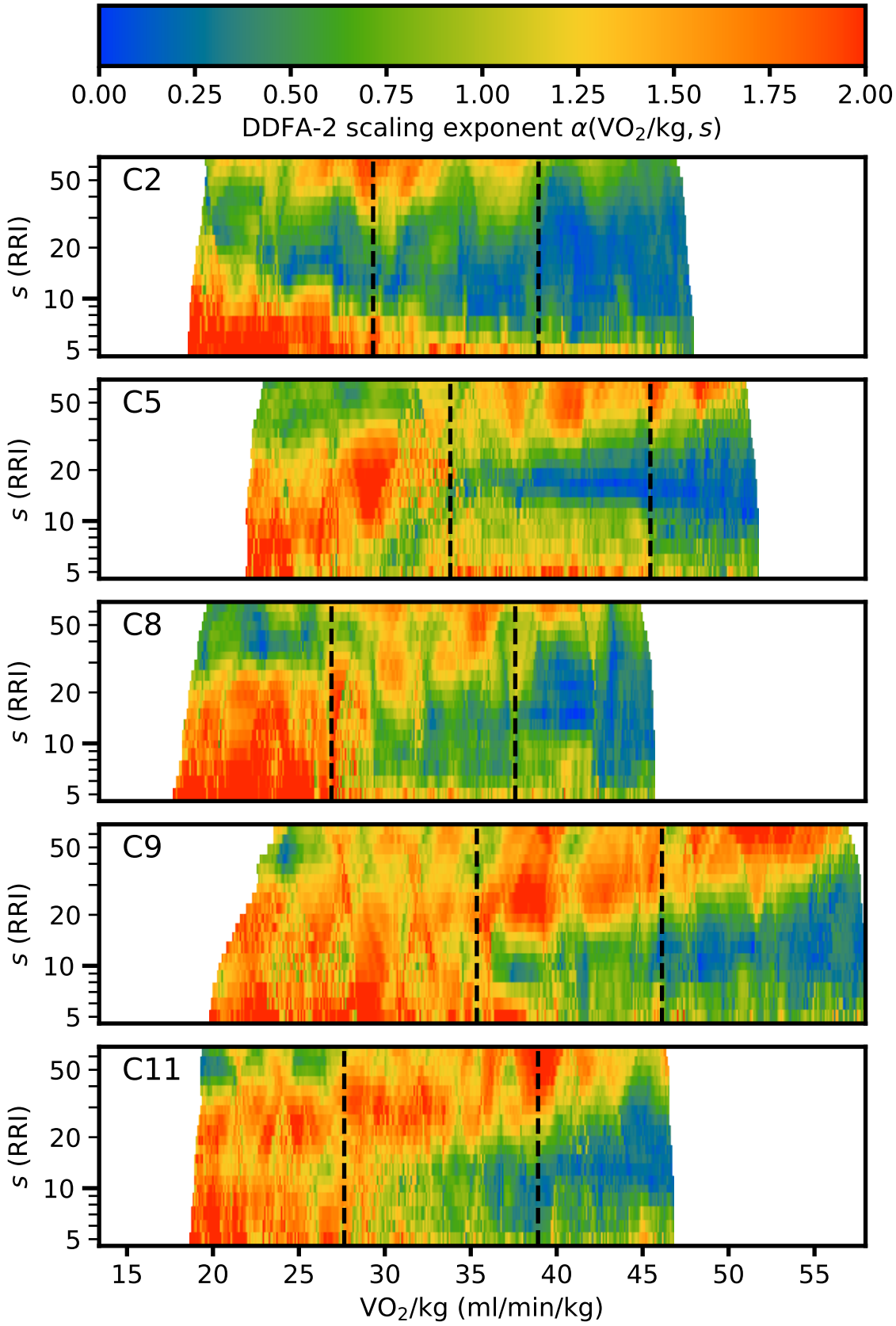

Figure A.13. *DDFA-2 scaling exponents for cycling subjects C2–C11 as a function of the weight-proportional oxygen uptake (VO_2/kg). The aerobic and anaerobic thresholds are shown as vertical dashed lines.*

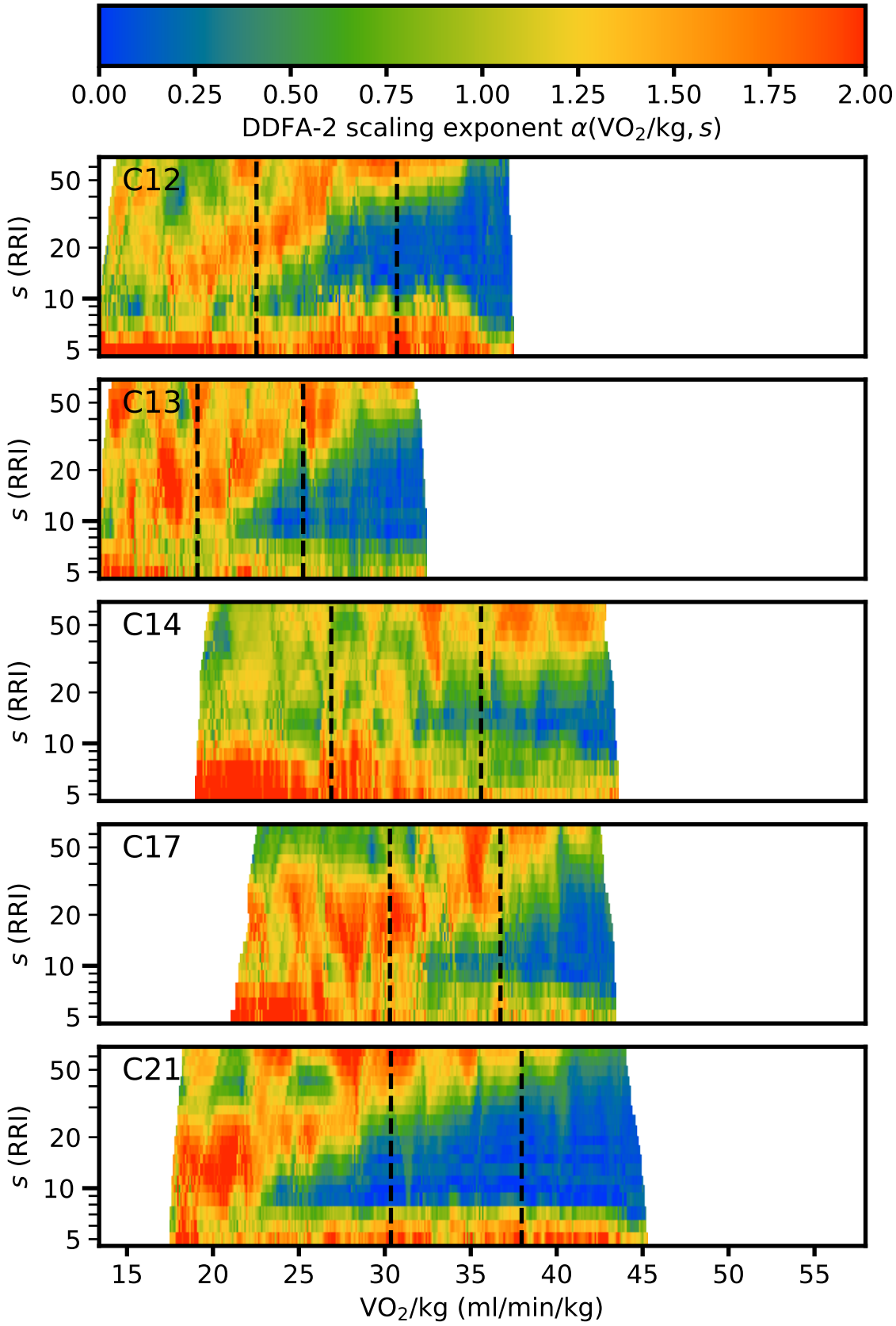

Figure A.14. *DDFA-2 scaling exponents for cycling subjects C12–C21 as a function of the weight-proportional oxygen uptake (VO_2/kg). The aerobic and anaerobic thresholds are shown as vertical dashed lines.*

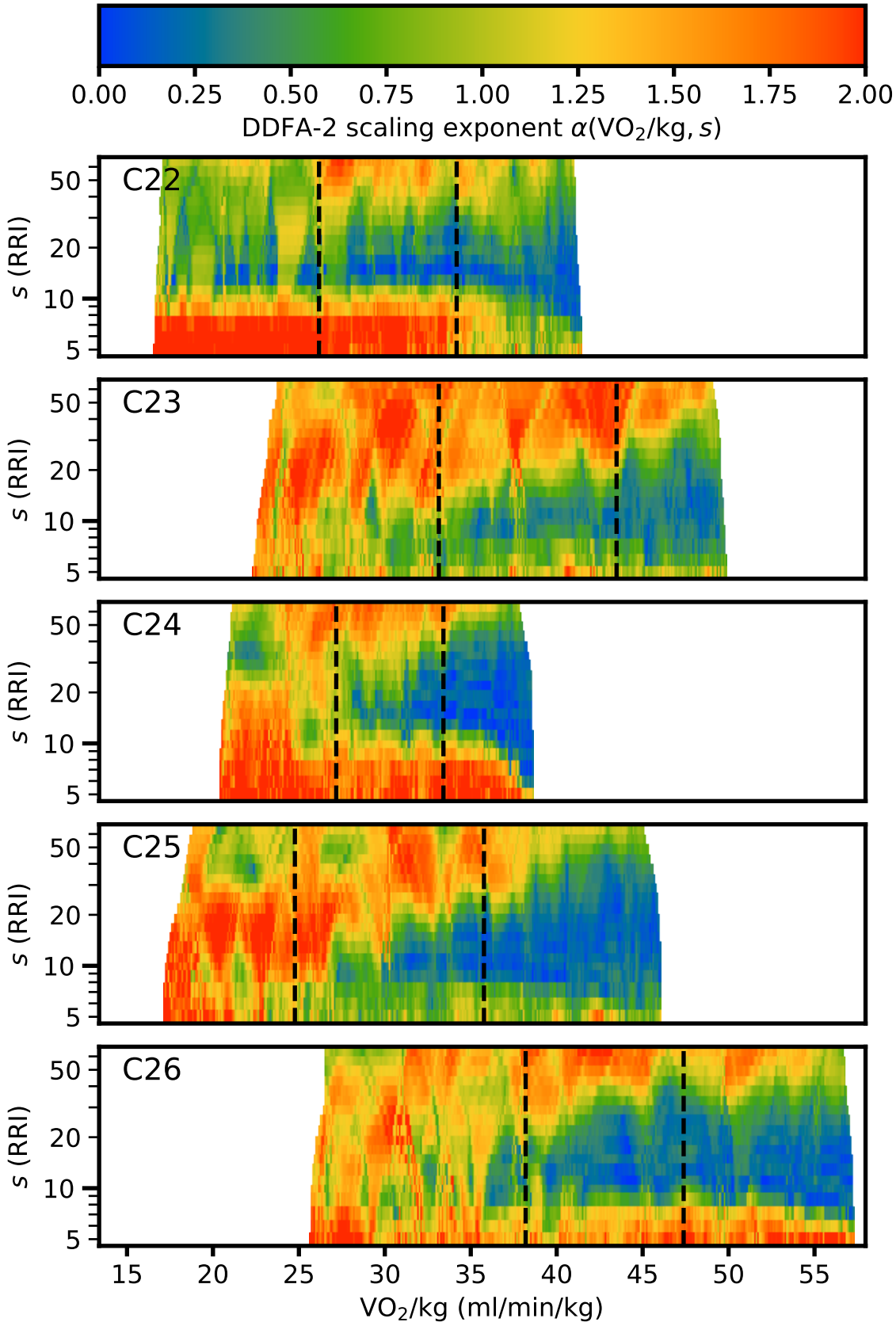

Figure A.15. *DDFA-2 scaling exponents for cycling subjects C22–C26 as a function of the weight-proportional oxygen uptake (VO_2/kg). The aerobic and anaerobic thresholds are shown as vertical dashed lines.*

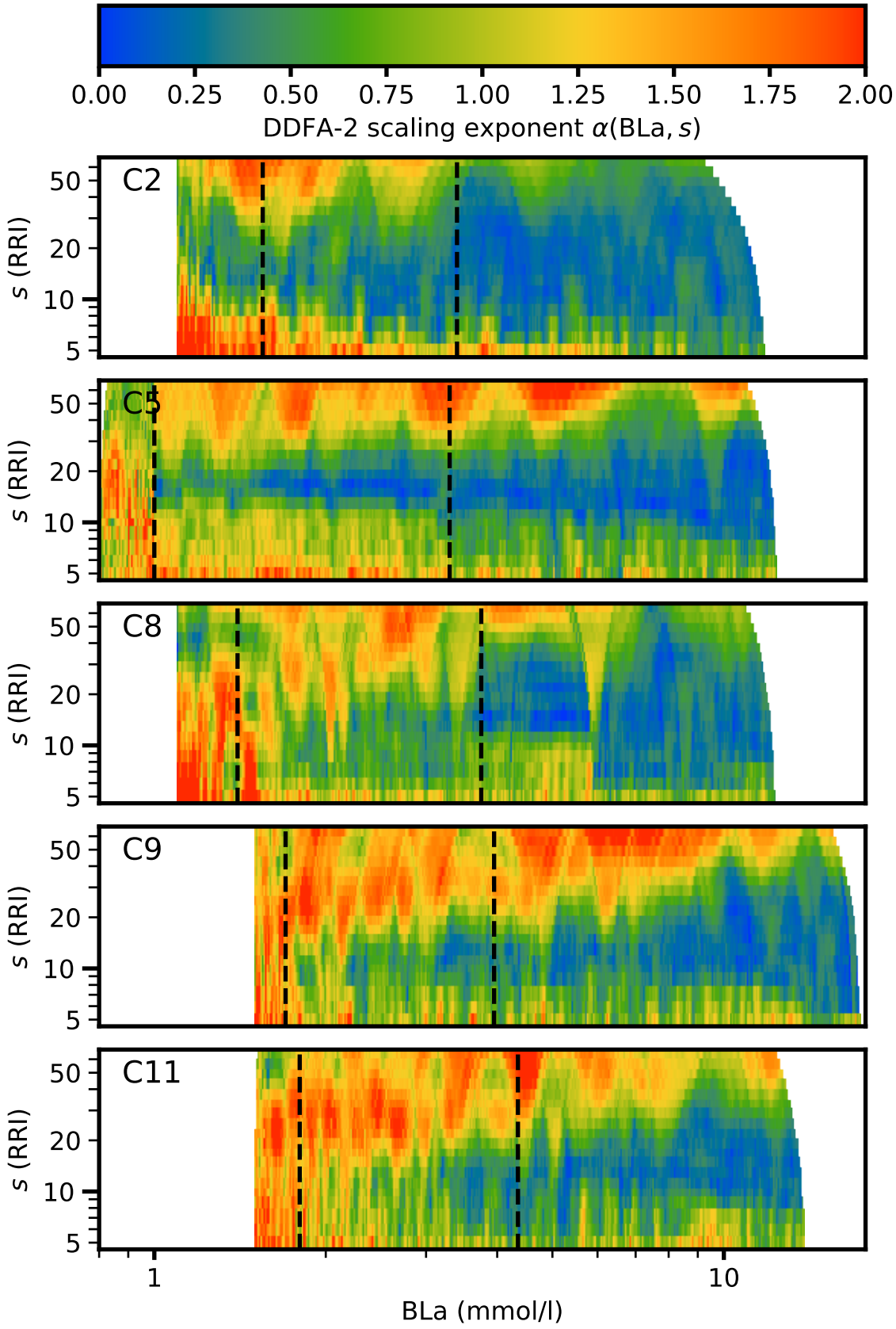

Figure A.16. *DDFA-2 scaling exponents for cycling subjects C2–C11 as a function of the blood lactate concentration (BLa). The aerobic and anaerobic thresholds are shown as vertical dashed lines. Note the logarithmic x-axis.*

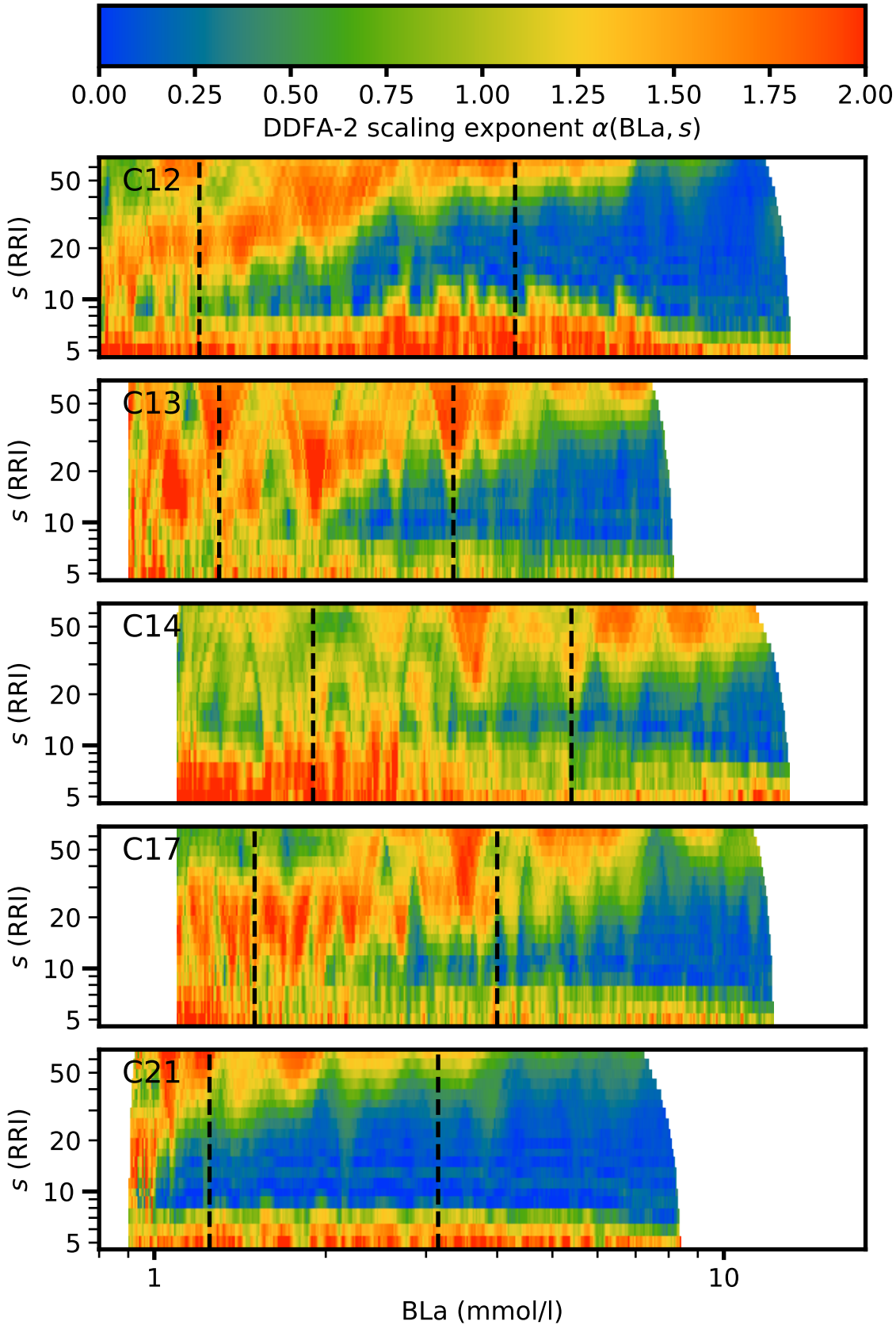

Figure A.17. *DDFA-2 scaling exponents for cycling subjects C12–C21 as a function of the blood lactate concentration (BLa). The aerobic and anaerobic thresholds are shown as vertical dashed lines. Note the logarithmic x-axis.*

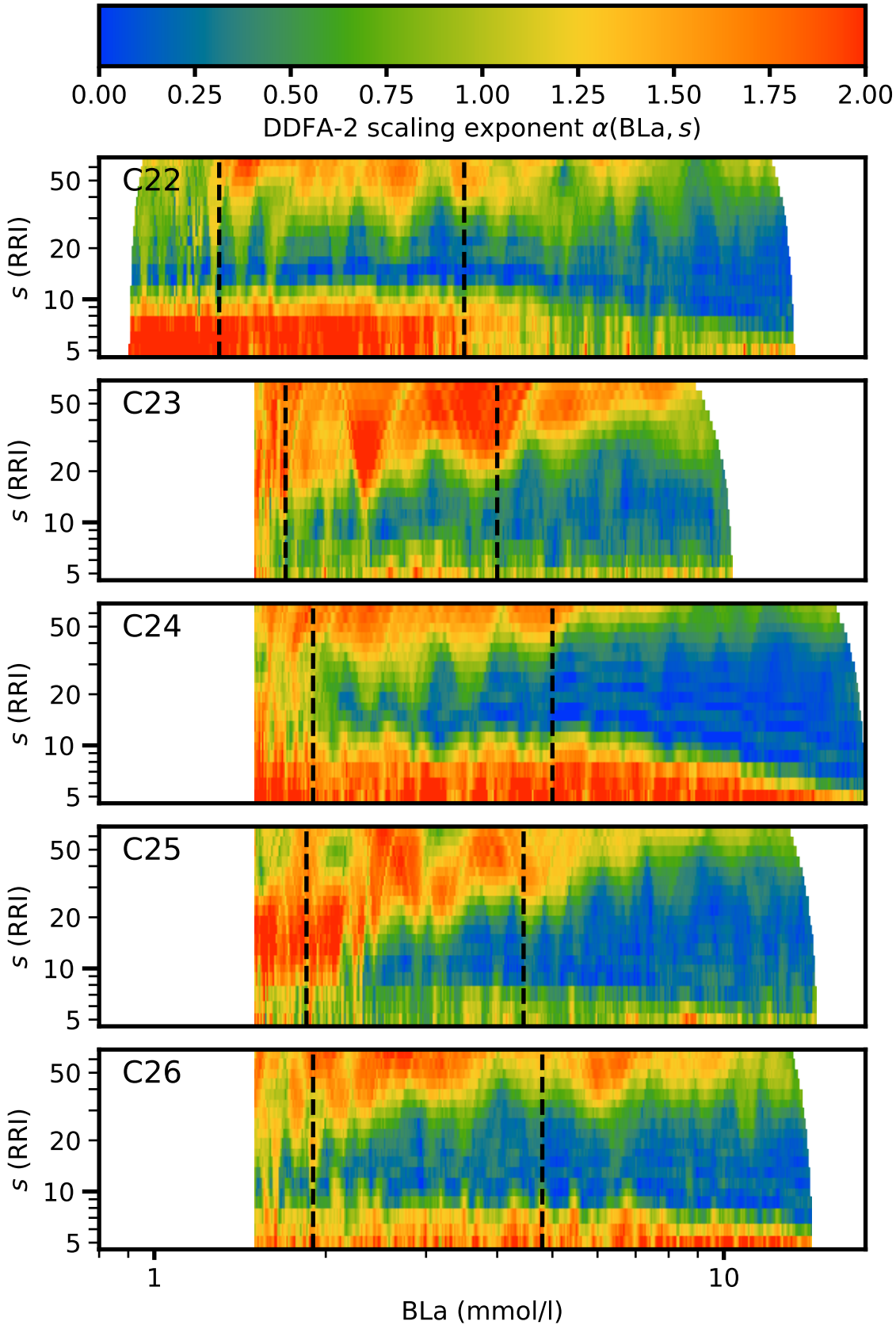

Figure A.18. *DDFA-2 scaling exponents for cycling subjects C22–C26 as a function of the blood lactate concentration (BLa). The aerobic and anaerobic thresholds are shown as vertical dashed lines. Note the logarithmic x-axis.*

APPENDIX B: RUNNING FIGURES

This appendix contains additional pictures of all the subjects who took the test on the treadmill.

List of Figures in Appendix B

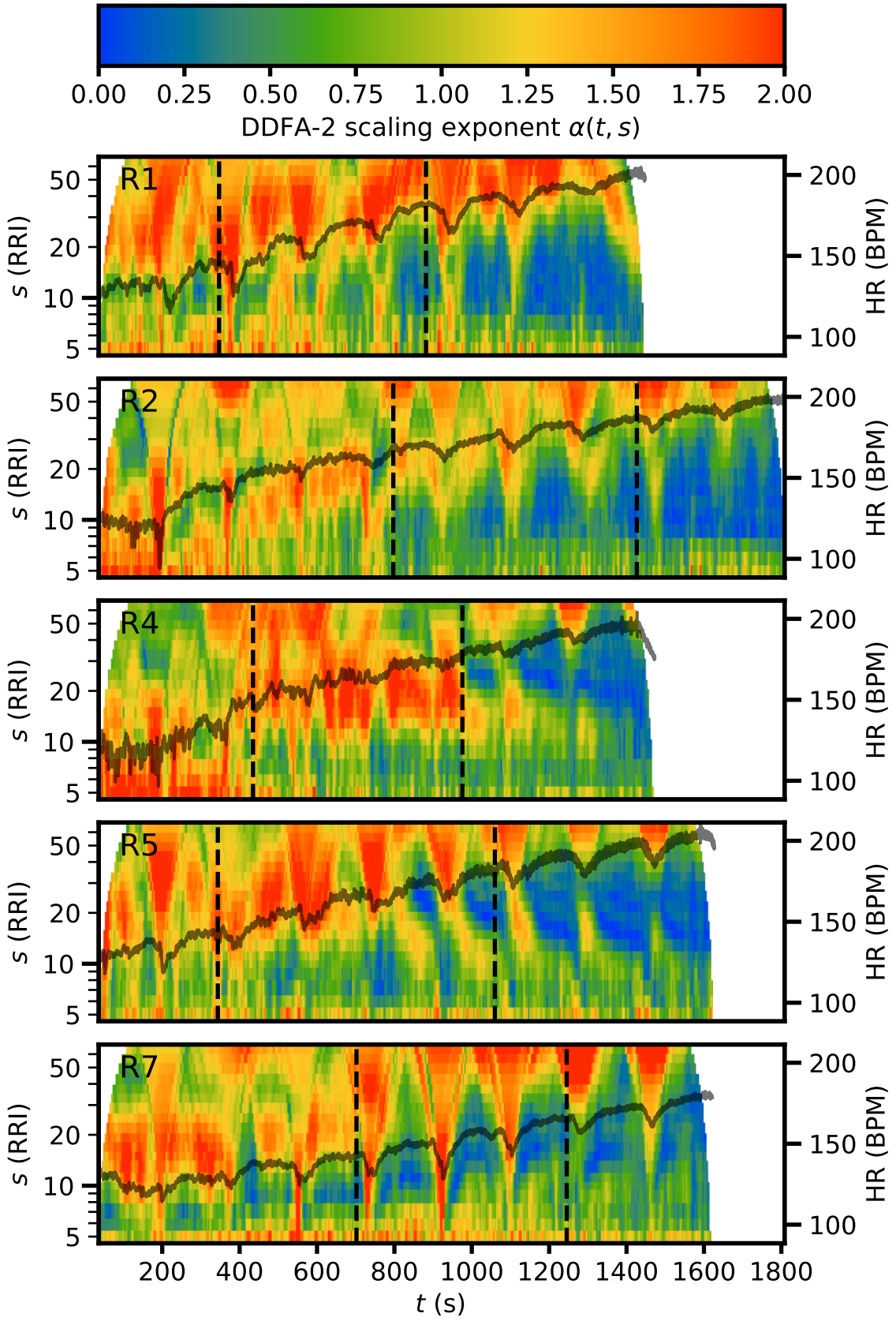

Figure B.1. *DDFA-2 scaling exponents and the heart rate (HR) for running subjects R1–R7 as a function of the time t. The aerobic and anaerobic thresholds are shown as vertical dashed lines.*

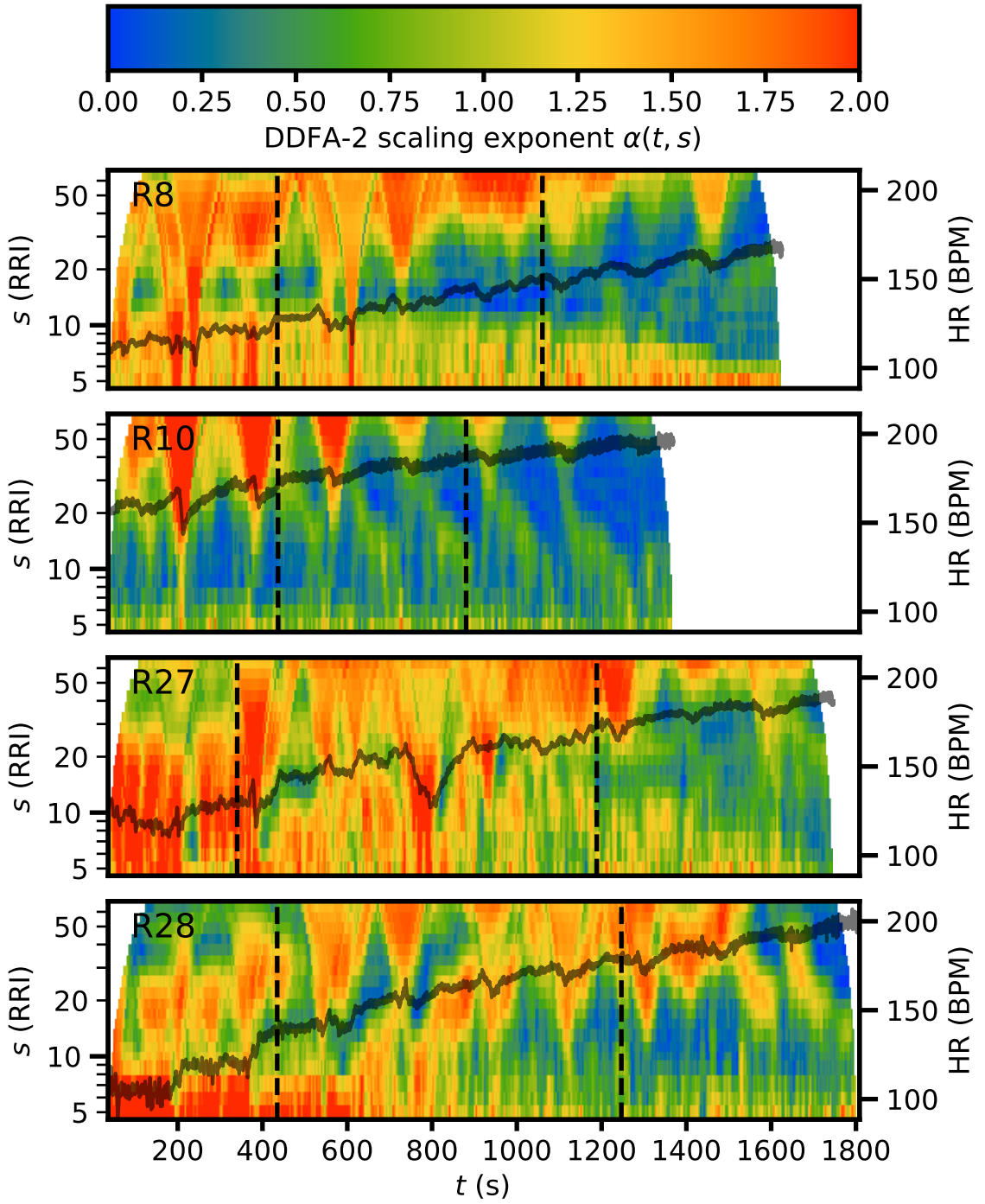

Figure B.2. *DDFA-2 scaling exponents and the heart rate (HR) for running subjects R8–R28 as a function of the time t. The aerobic and anaerobic thresholds are shown as vertical dashed lines.*

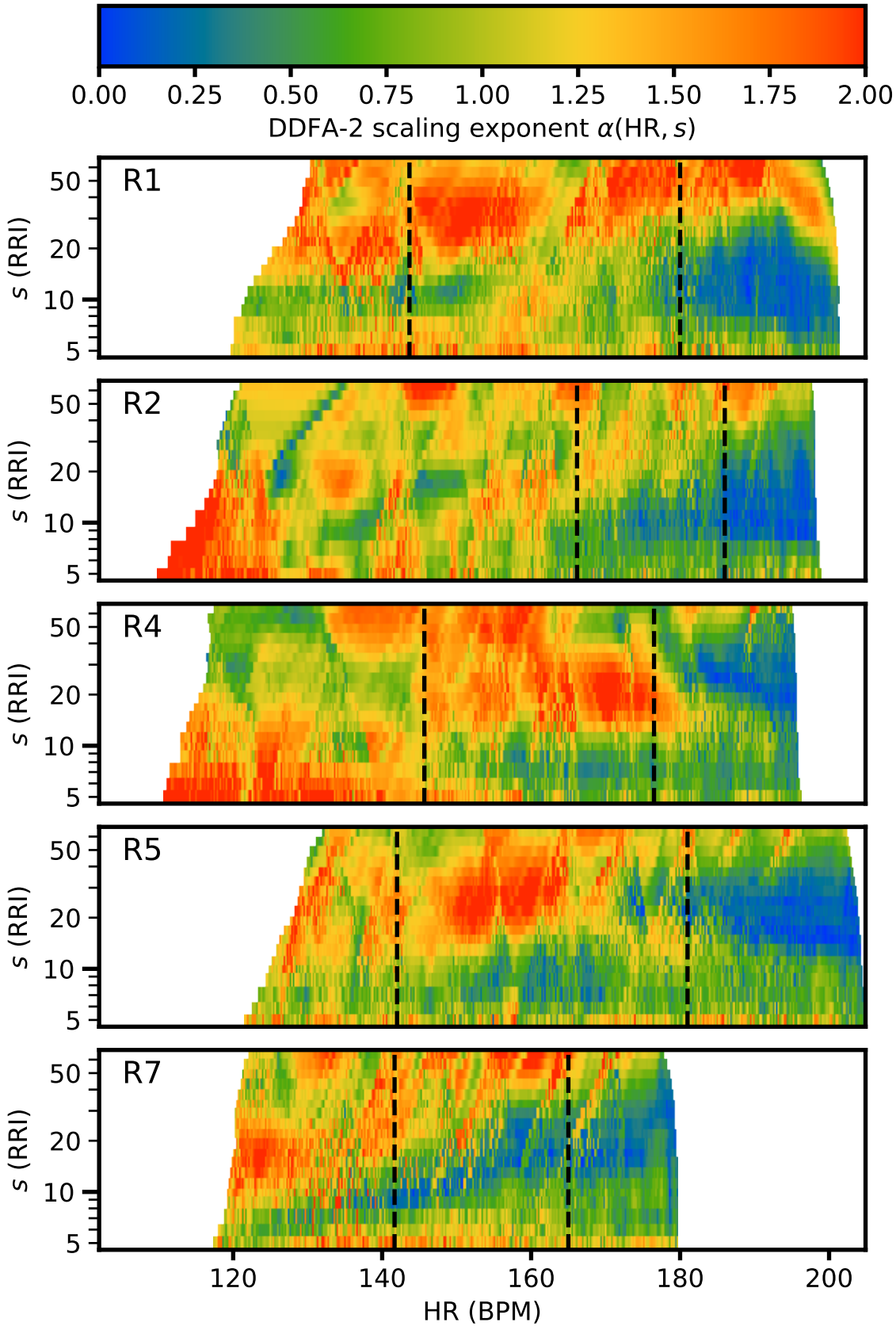

Figure B.3. *DDFA-2 scaling exponents for running subjects R1–R7 as a function of the heart rate (HR). The aerobic and anaerobic thresholds are shown as vertical dashed lines.*

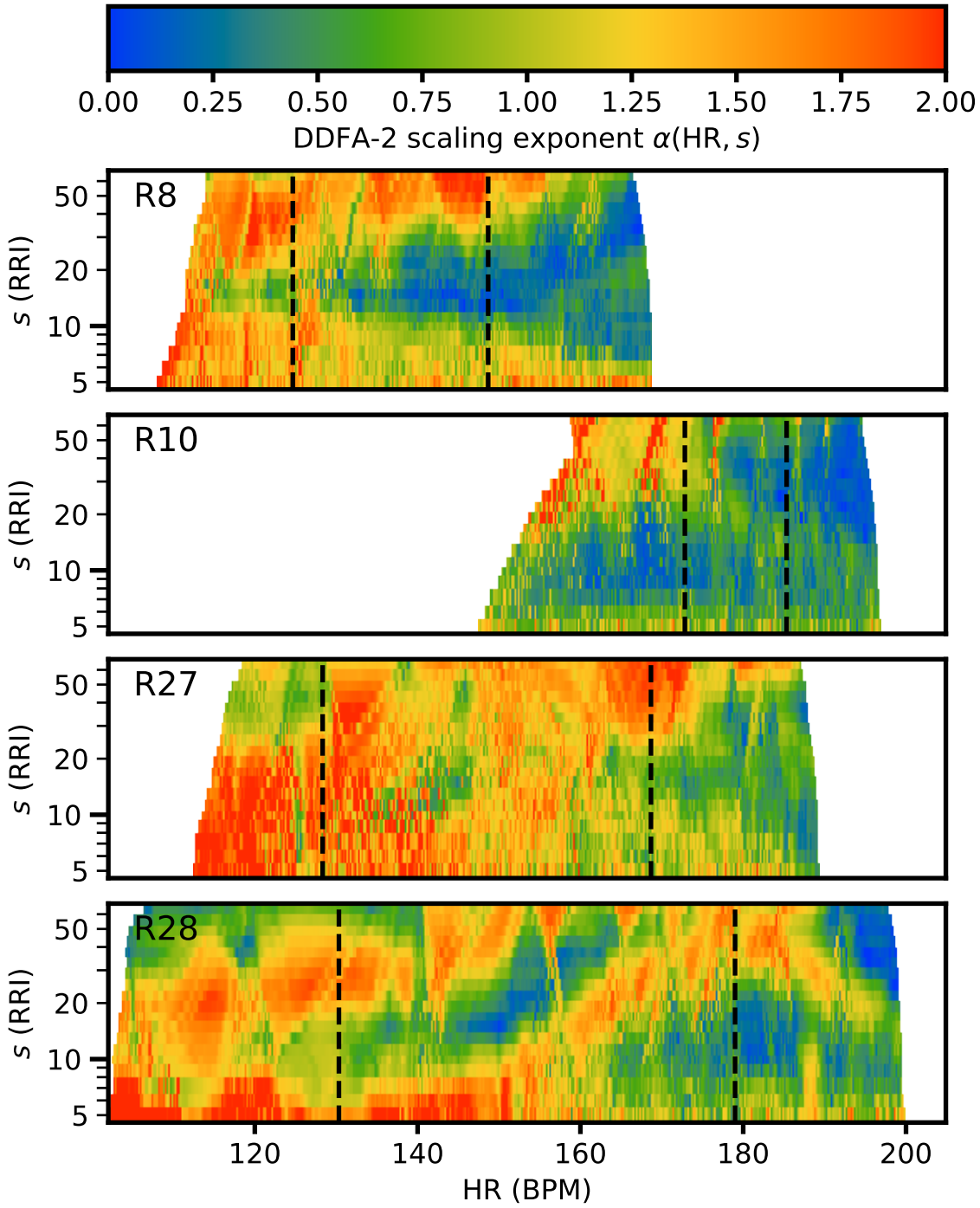

Figure B.4. *DDFA-2 scaling exponents for running subjects R8–R28 as a function of the heart rate (HR). The aerobic and anaerobic thresholds are shown as vertical dashed lines.*

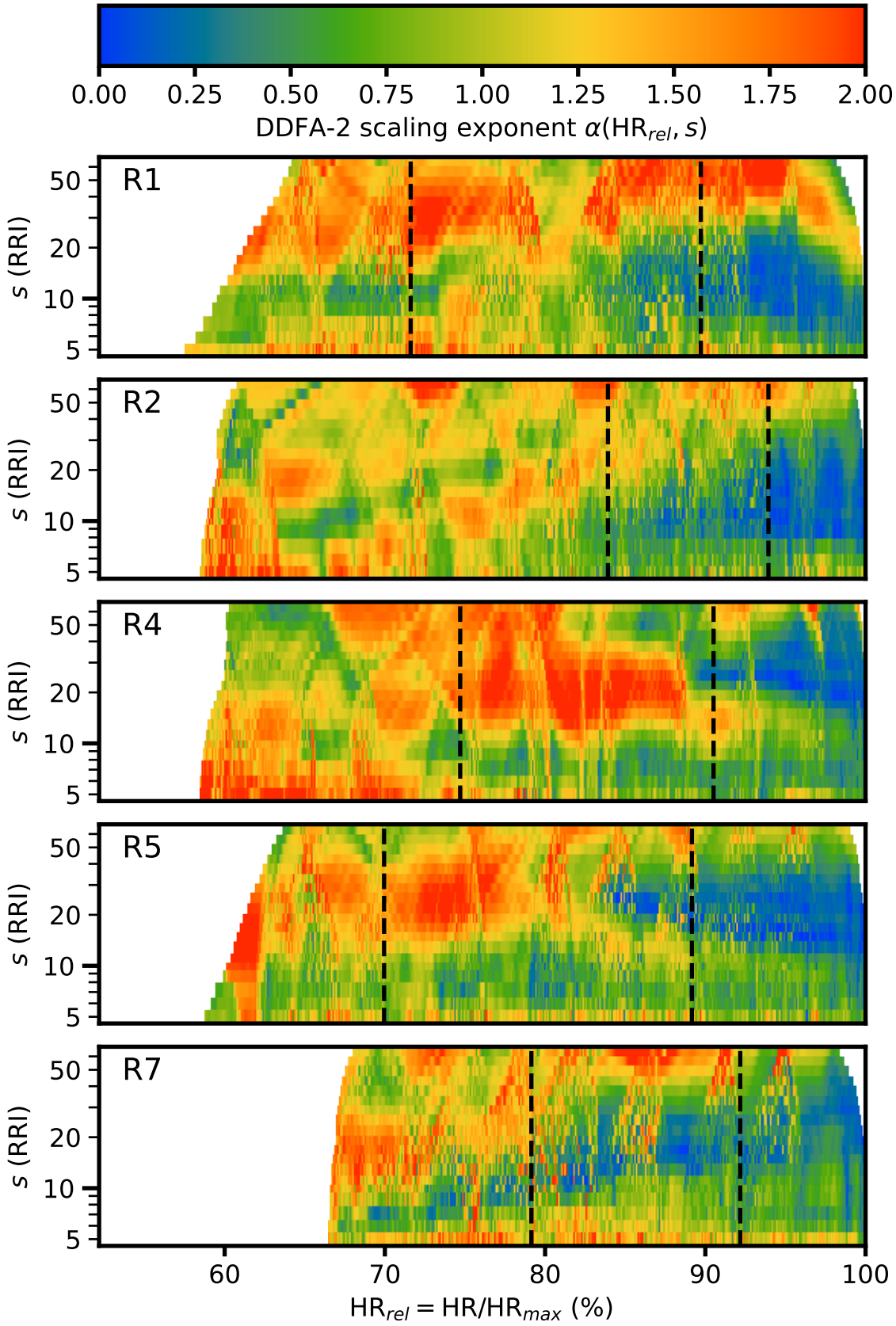

Figure B.5. *DDFA-2 scaling exponents for running subjects R1–R7 as a function of the relative heart rate (HR_{rel}). The aerobic and anaerobic thresholds are shown as vertical dashed lines.*

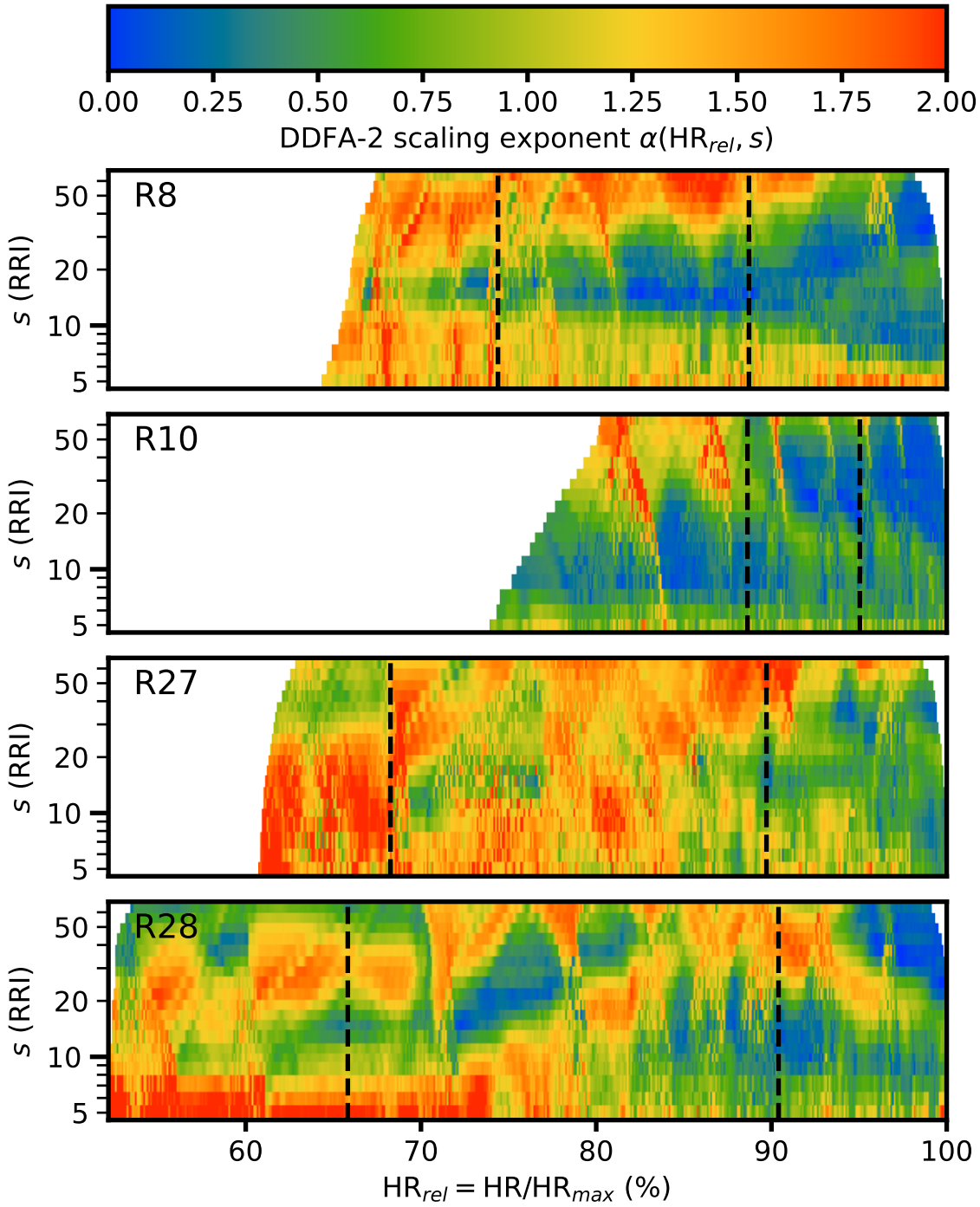

Figure B.6. *DDFA-2 scaling exponents for running subjects R8–R28 as a function of the relative heart rate (HR_{rel}). The aerobic and anaerobic thresholds are shown as vertical dashed lines.*

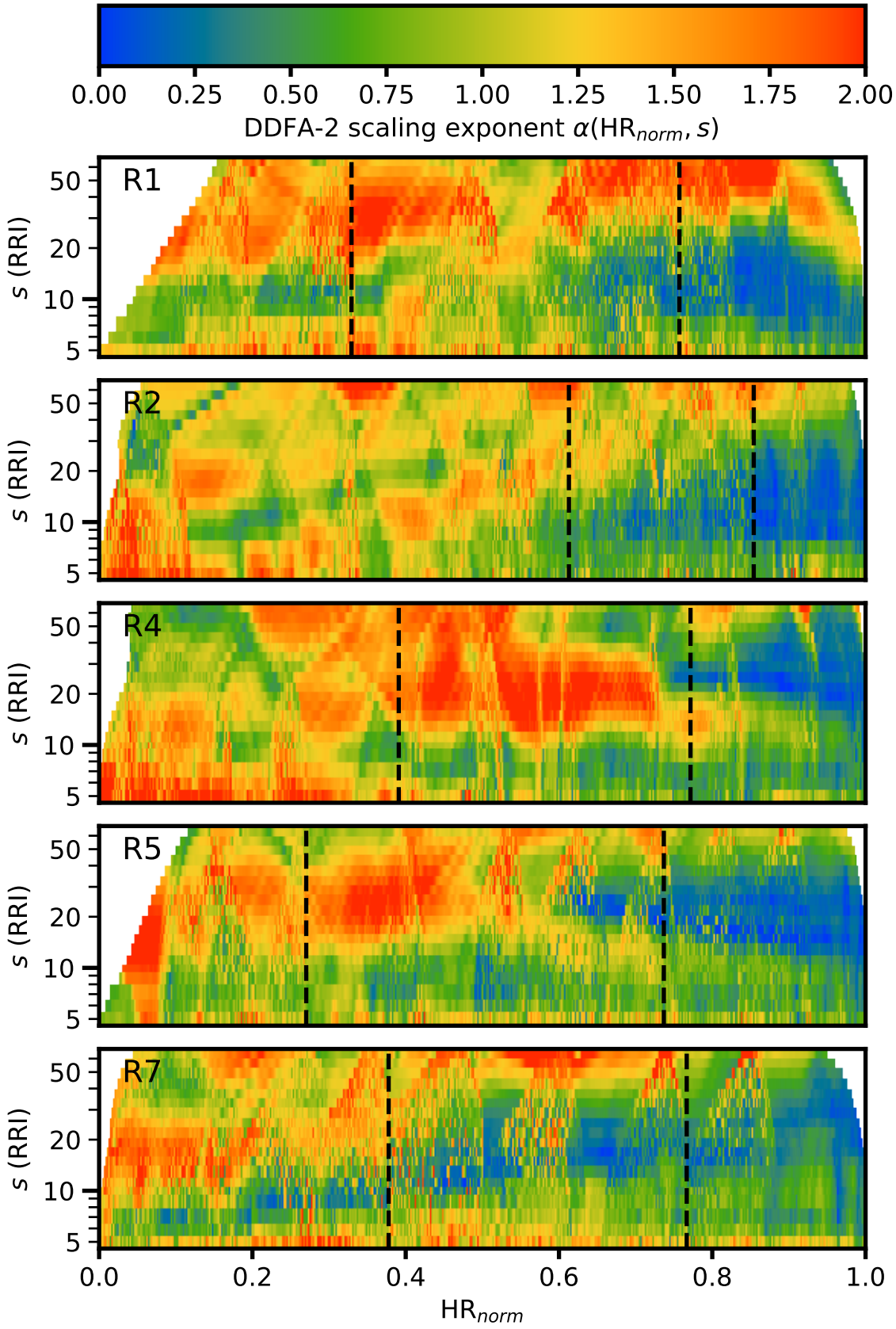

Figure B.7. *DDFA-2 scaling exponents for running subjects R1–R7 as a function of the normalized heart rate (HR_{norm}). The aerobic and anaerobic thresholds are shown as vertical dashed lines.*

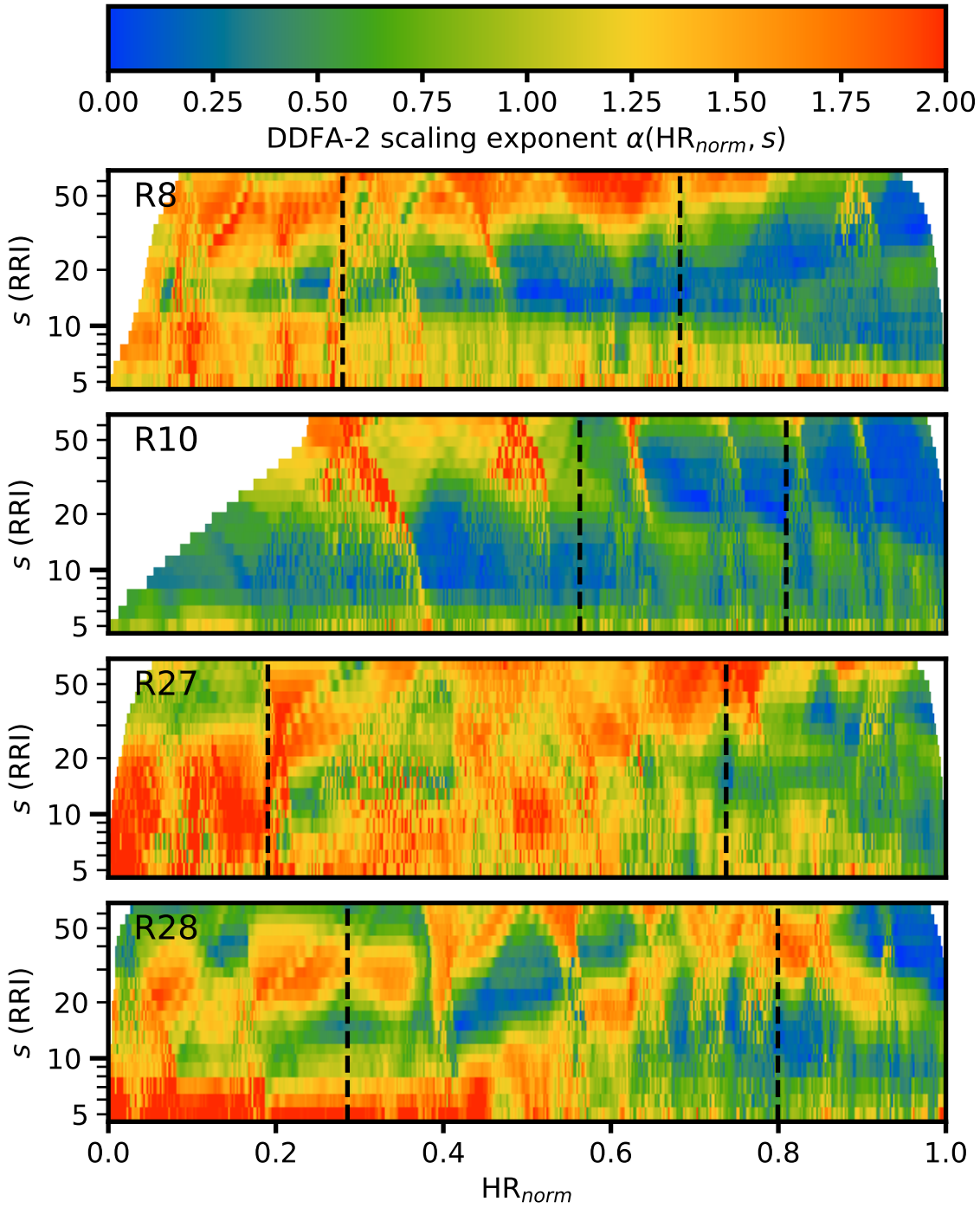

Figure B.8. *DDFA-2 scaling exponents for running subjects R8–R28 as a function of the normalized heart rate (HR_{norm}). The aerobic and anaerobic thresholds are shown as vertical dashed lines.*

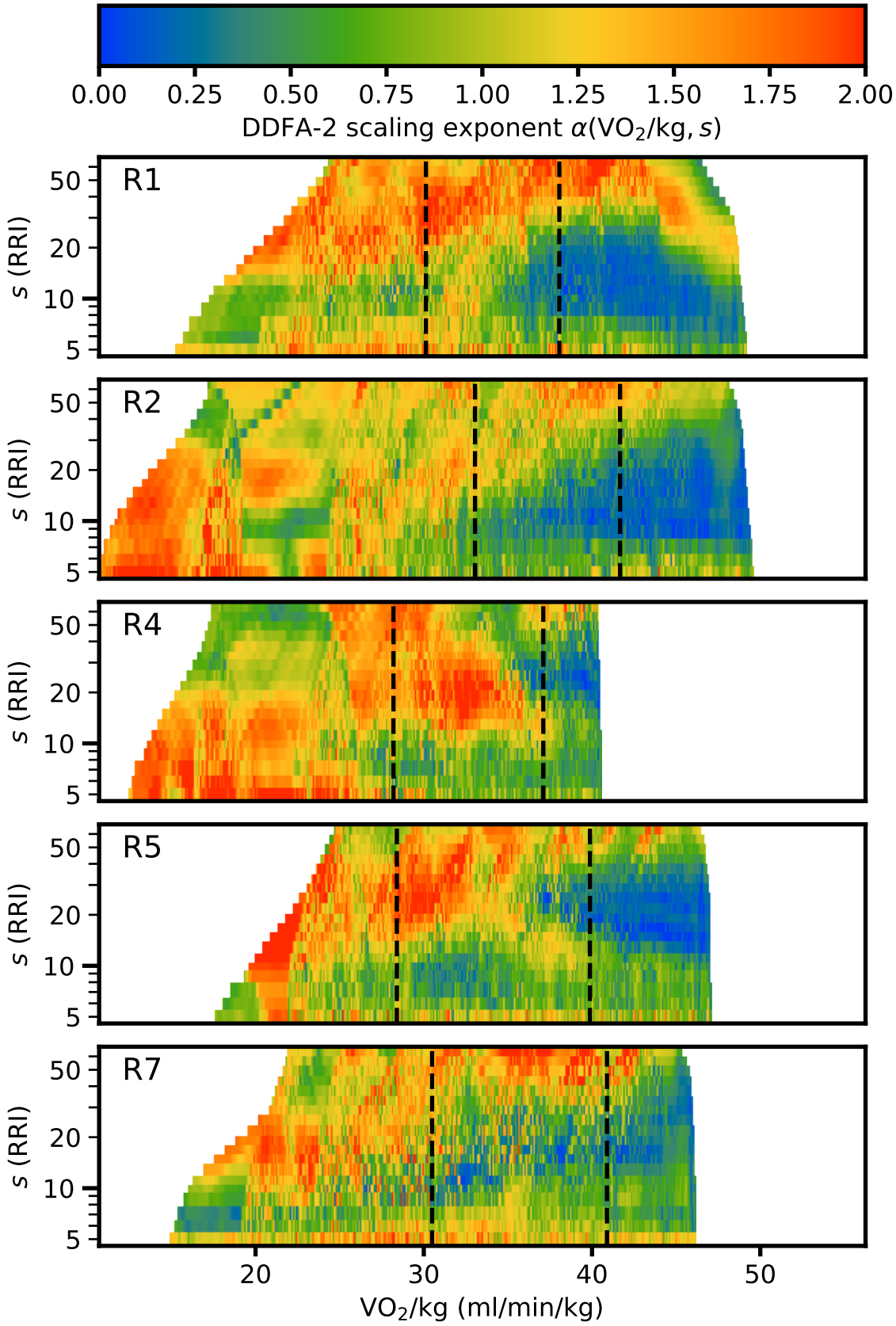

Figure B.9. *DDFA-2 scaling exponents for running subjects R1–R7 as a function of the weight-proportional oxygen uptake (VO_2/kg). The aerobic and anaerobic thresholds are shown as vertical dashed lines.*

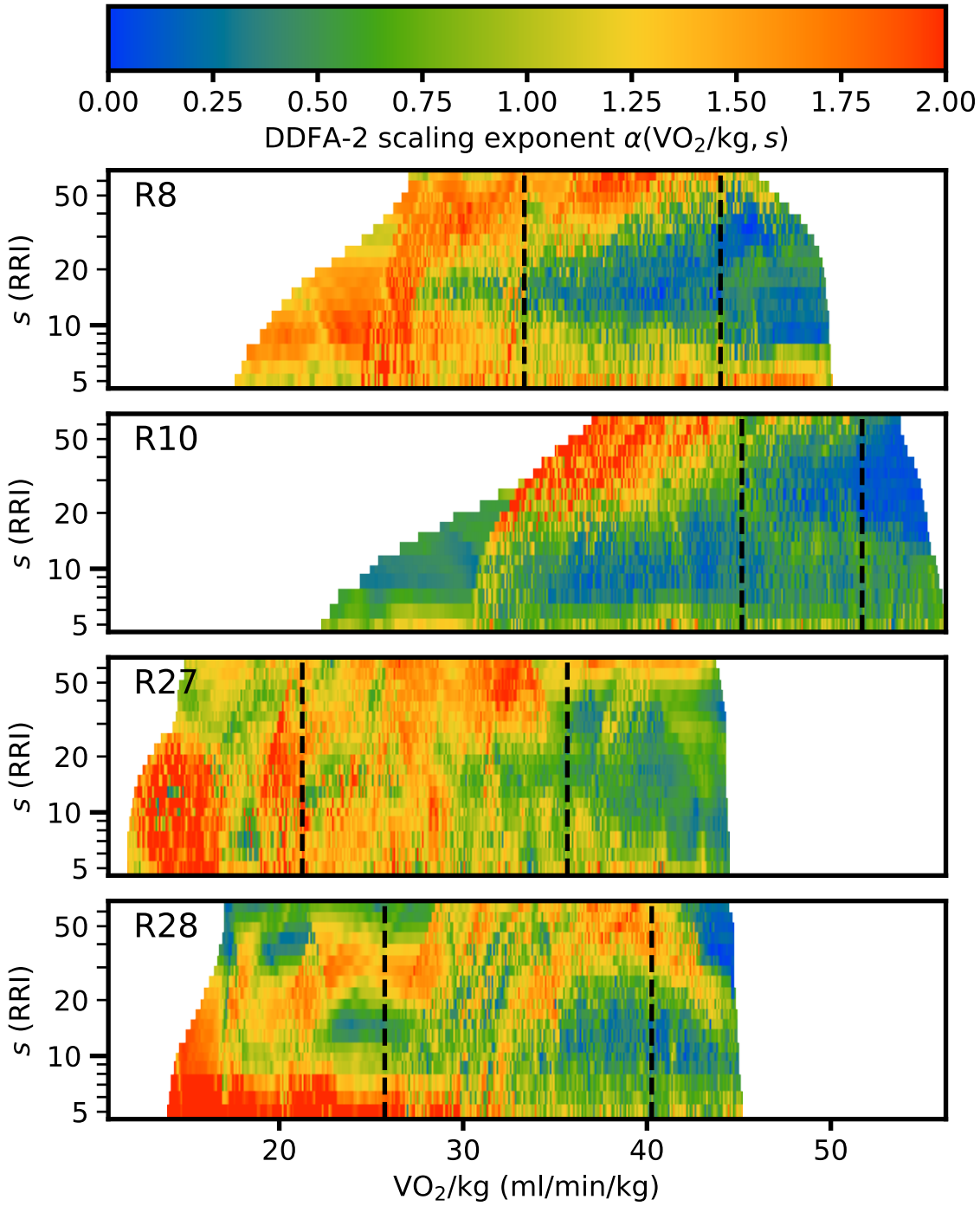

Figure B.10. *DDFA-2 scaling exponents for running subjects R8–R28 as a function of the weight-proportional oxygen uptake (VO_2/kg). The aerobic and anaerobic thresholds are shown as vertical dashed lines.*

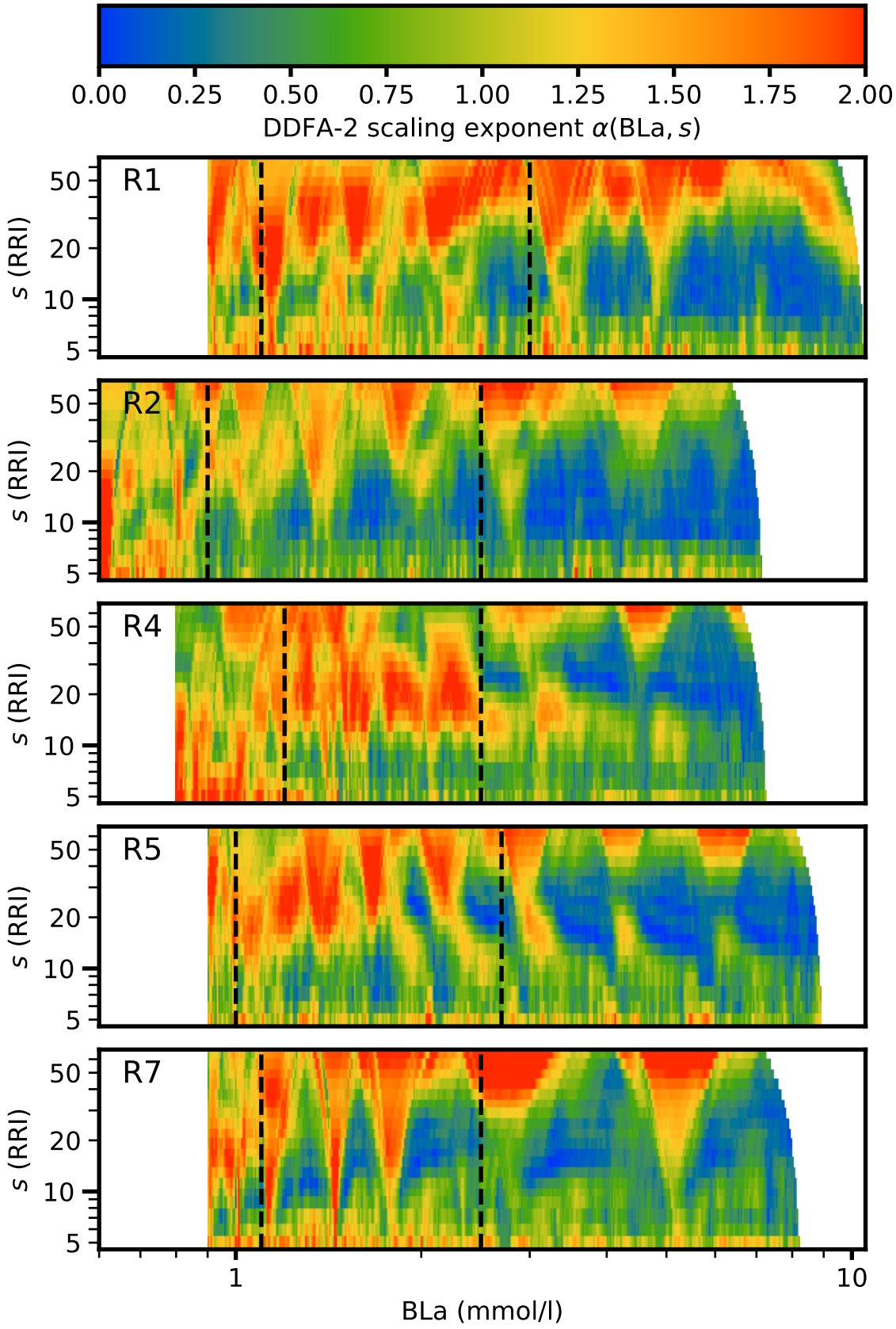

Figure B.11. *DDFA-2 scaling exponents for running subjects R1–R7 as a function of the blood lactate concentration (BLa). The aerobic and anaerobic thresholds are shown as vertical dashed lines. Note the logarithmic x-axis.*

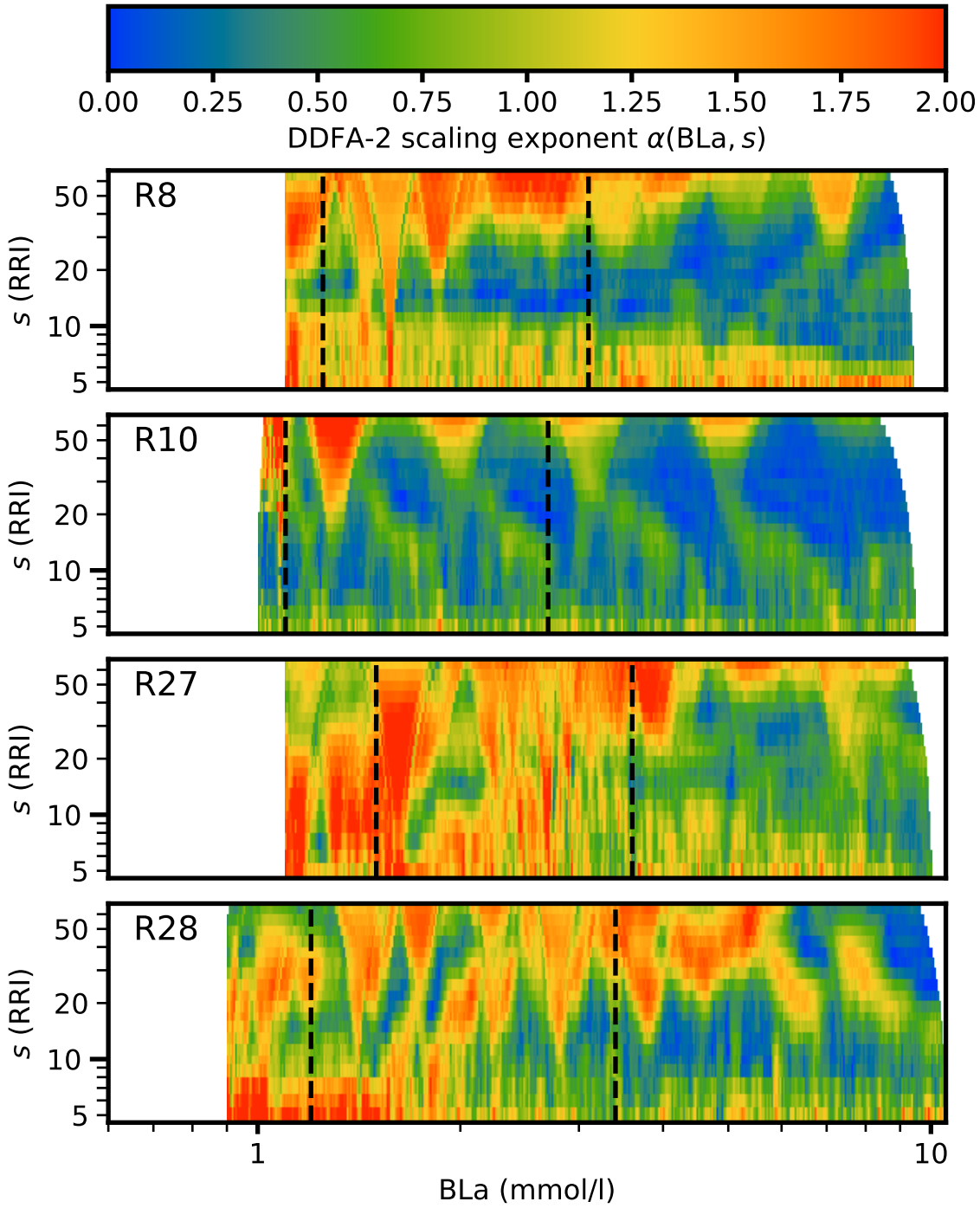

Figure B.12. *DDFA-2 scaling exponents for running subjects R8–R28 as a function of the blood lactate concentration (BLa). The aerobic and anaerobic thresholds are shown as vertical dashed lines. Note the logarithmic x-axis.*